Forschungszentrum Jülich - Institut für Bio-Geo Wissenschaften 3

EFFECT OF SOIL MECHANICAL PROPERTIES, ROOT TIP GEOMETRY, AND MUCILAGE ON PENETRATION RESISTANCE TO ROOT GROWTH

Dissertation

zur Erlangung des Grades

Doktor der Agrarwissenschaften (Dr. agr.)

der Agrar-, Ernährungs- und

Ingenieurwissenschaftlichen Fakultät

der Rheinischen Friedrich-Wilhelms-Universität Bonn

von

Ravi Kumar Mysore Janakiram

aus

Mysore, Indien

Bonn 2026

Referent: Prof. Dr. Harry Vereecken
Koreferent: Prof. Dr. Andrea Carminati

Tag der mündlichen Prüfung: 24.02.2026

Angefertigt mit Genehmigung der Agrar-, Ernährungs- und
Ingenieurwissenschaftlichen Fakultät der Universität Bonn

In memory of my father,

Janakiram Cheluviah (1959-2023)

ನನ್ನ ತಂದೆಯವರ ಸ್ಮರಣಾರ್ಥ,

ಜಾನಕಿರಾಮ್ ಚೆಲುವಯ್ಯ (1959-2023)

ನೀವು ನಮ್ಮ ಹೃದಯದಲ್ಲಿ ಶಾಶ್ವತವಾಗಿ ಜೀವಂತವಾಗಿರುತ್ತೀರಿ

ಎಲ್ಲಾ ತ್ಯಾಗಗಳಿಗೆ ಧನ್ಯವಾದಗಳು

PERSONAL DECLARATION

I hereby affirm that I have prepared the present thesis self-dependently, and without the use of any other tools than the ones indicated. All parts of the text, having been taken over verbatim or analogously from published or not published scripts, are indicated as such. The thesis hasn't yet been submitted in the same or similar form, or in extracts within the context of another examination.

[Place], [Date of submission]

Student's Signature: _____

ACKNOWLEDGEMENTS

This project was funded by the Deutsche Forschungsgemeinschaft (DFG) through the project "How does mucilage alter soil mechanical properties and soil penetration resistance to root growth?" with project number 439374140.

First and foremost, I would like to express my deepest gratitude to my former supervisor, Dr. Eva Kroener, for her invaluable guidance during the initial two years of my PhD and for her role in the proposal writing. Her support laid the foundation for my research journey.

I am especially grateful to my daily supervisor, Prof. Dr. Johan Alexander (Sander) Huisman, for his unwavering support, patience, and mentorship. After the transition in supervision, certain tasks became challenging for me, but his readiness to help, guide, and correct my mistakes made a significant difference. As the topic was new for him as well, he took on the additional responsibility of verifying concepts and providing meticulous guidance, particularly in scientific writing. I vividly remember our intense sessions where he patiently explained how to write clearly, analyse data systematically, and present my results effectively. I truly enjoyed these sessions and learned immensely from him. Beyond academic guidance, he was always considerate of my well-being, checking in on me during difficult times. It has been a privilege to work with him over the past three years.

I would also like to extend my sincere appreciation to Dr. Suil Ruiz, whose work (Ruiz et al., 2016) greatly inspired my research. My research questions closely align with his, and many fundamental ideas stem from his contributions. Beyond inspiration, he generously offered his expertise when I encountered challenges with the cavity expansion model, helping me resolve key issues and gain a clearer understanding of the topic.

My heartfelt gratitude also goes to Prof. Dr. Jan Vanderborght for his insightful guidance and thought-provoking questions during our weekly meetings, which often led me to a deeper understanding of my research. I am also thankful to Prof. Dr. Harry Vereecken for being my PhD supervisor and for his valuable suggestions during my PhD report discussions.

I am profoundly grateful to the administrative staff and my supervisors for facilitating remote work from India during one of the most difficult periods of my life, following the loss of my father. Their support allowed me to continue my research while navigating personal hardships.

A special thanks to Shirin Bagheri for her help in the lab, particularly with mucilage extraction, and for her kindness and support during my hospitalization. I also appreciate the support of Odilia Esser and Claudis Walraf for her prior assistance with materials and processes. I am incredibly grateful to Thomas Töpfer for manufacturing the hollow needle used in Chapter 5. His contribution was instrumental in obtaining highly insightful results, which would not have been possible without his help. I would also like to acknowledge the administrative support of Gaby Pillert, Dr. Marie-Isabel Ludwig, and Dr. Kathrin Vermöhlen, whose assistance made numerous processes smoother.

A warm thank you to my office mates, Chris Poppe and Yikui Zhang, and my fellow PhD colleagues Vishak Shivaprasad, Antonio De Matteis, Jay Carl Cacerez, Adrian Haupenthal, Riffat Rahim, Omid Esmaeelipoor Jahromi and others, for their companionship, encouragement, and support, both academically and personally. Their presence made this journey more enjoyable and helped me through challenging times.

Beyond academia, I found solace in my walks along the path next to the IBG-3 institute, which provided much-needed moments of peace and re-energized me during stressful days.

Finally, my deepest gratitude goes to my mother, my sister, my late father, and Swantje Kasper. Their unwavering love, encouragement, and support carried me through the most difficult moments of my life. I could not have completed this journey without them.

ABSTRACT

Plant root systems are essential for global food security. Their growth, however, is governed by a complex interplay of soil's physical, biological, and chemical properties and is critically limited by soil compaction. In compacted soils, roots face high penetration resistance that forces them to expend considerable energy to push through the soil. This resistance can reduce root elongation by up to 50%, severely restricting plant development. Faced with this challenge, plants have evolved sophisticated adaptive strategies, primarily through the secretion of root mucilage, a gelatinous exudate that acts as a biological lubricant and hydrator to facilitate growth. While recent research has made significant progress in isolating the individual roles of key factors such as soil physical properties (water content, compaction, texture), root tip geometry, and mucilage secretion, the state-of-the-art reveals a fundamental gap. Most studies examine these variables in isolation under controlled conditions, overlooking their dynamic and synergistic interactions within the complex, heterogeneous environment of the natural rhizosphere. Consequently, critical questions remain unanswered: How do root tip geometry and mucilage secretion interact to reduce penetration resistance across different soil types and water content regimes? To what extent does the method of mucilage delivery, mimicking natural exudation patterns, influence its efficacy as a lubricant? This thesis aims to address these pivotal questions by systematically quantifying the coupled effects of soil physical properties, root tip geometry, and mucilage biomechanics on penetration resistance, thereby advancing our understanding of root-soil interactions to inform strategies for enhancing crop resilience.

In a first step, the combined effects of water content, bulk density, root tip geometry (cone shape), and presence of mucilage with various concentrations on penetration resistance to root growth was investigated. This was done using steel needles (penetrometers) with semi-apex angles of 15° (sharp) and 30° (blunt) as a proxy for plant roots with different root tip geometry. Chia seed mucilage was applied at various mass concentrations (0%, 0.1%, 0.3%, and 0.5%) to determine to what extent mucilage concentration affects penetration resistance. Unlike the common method of mixing mucilage with soil, mucilage application in this study follows a unique approach by applying a single 0.1 ml drop of mucilage directly at the injection site,

allowing it to infiltrate into the surrounding soil naturally. Soil samples were compacted using constant mechanical energy for various gravimetric water contents (15%, 20%, 25%, and 30%) to determine the effect of compaction. Penetration resistance was measured by pushing needles to a depth up to 8 mm at a constant velocity of 2.5 mm min^{-1} into the soil samples with known water content, bulk density, and mucilage concentration. Penetration resistance was measured using a rheometer and it was converted to energy for total insertion depth (8 mm) and shaft insertion depth. The experimental results showed that the penetration resistance decreased significantly at very high water content (30%) for both sharp and blunt needles. The blunt needle recorded significantly higher penetration resistance than the sharp needle at low water content and the sharp needle recorded significantly higher penetration resistance than the blunt needle at high water content. Addition of mucilage significantly reduced the penetration resistance for both needle types, especially at low water contents. Different mucilage concentrations showed no significant effect on the penetration resistance. The measured penetration resistance was analyzed using cavity expansion theory based on soil strength parameters (cohesion and elastic modulus), applying spherical cavity models for the blunt needle and cylindrical cavity models for the sharp needle. The cavity expansion models successfully predicted penetration resistance across water contents, with modelling results agreeing particularly well in drier soils (15% - 25% water content). However, significant discrepancies emerged for the higher water content of 30%, where the spherical cavity model overestimated penetration resistance for the blunt needle. The modeling approach highlighted the critical interdependence between soil water content and needle tip geometry in governing penetration dynamics. It was concluded that the amount of water in the soil is a major factor in determining the penetration resistance. Variation in degree of compaction, water content, and bulk density affects the behavior of needles differently. While mucilage plays a vital role in reducing penetration resistance, the magnitude of reduction also depends on soil water content. The model results reveal that current limit pressure cavity expansion theory, while successful in drier soils (15-25% water content), fails to accurately predict penetration resistance for a blunt cone in wet soil (specifically at 30% water content). In these saturated conditions, the theory significantly overestimates resistance for the blunt cone, indicating it does not fully capture the altered soil mechanical behavior. Consequently, the theory must be advanced to better incorporate the combined influence of water content and tip geometry, which is essential for developing accurate predictive models in saturated soils.

In a second step, the effects of soil texture, mucilage type, and mucilage concentration on root penetration resistance were investigated. Loam and sandy loam samples were used as representative soil textures, flax and chia seed mucilage at mass concentrations of 0.1% and 0.5% were used. Soil samples were compacted to a dry bulk density of 1.6 g/cm³ at gravimetric water contents of 9%, 12%, 15%, and 18%. Penetration resistance was determined using a needle with a 1.5 mm shaft diameter and a 30° semi-apex angle that was inserted into soil samples at the rate of 2.5 mm min^{-1}. Similar to the first study, mucilage application was done by applying a single 0.1 ml drop of mucilage directly at the injection site, allowing it to infiltrate into the surrounding soil naturally. Penetration resistance was measured using a rheometer and it was converted to mechanical energy. The results showed that loam consistently required significantly more energy than sand for penetration. An increase in water content decreased the penetration resistance significantly for both soils, especially in loam. The presence of mucilage significantly reduced the required energy in both soil types, with a more substantial effect in loam. No significant difference in penetration resistance was observed between mucilage types for loam, but flax seed mucilage was more effective than chia seed mucilage in reducing penetration resistance for sandy loam. In conclusion, this study demonstrates that soil texture significantly influences root penetration resistance, with loam requiring more energy than sand, especially at lower water contents. Mucilage application effectively reduced penetration resistance in both soil types, more notably in loam. While mucilage type and concentration generally showed limited differences, notable variations were observed in sandy loam, where flax seed mucilage reduced penetration resistance more effectively than chia mucilage.

In a third and final step, the impact of different mucilage application methods on root penetration resistance was investigated. For this, mucilage was extracted from chia and flax seeds and freeze-dried to obtain its pure form. The pure mucilage was then diluted to concentrations of 0.1% and 0.5% by weight. Sandy loam samples were prepared with 9% and 12% gravimetric water content and compacted to a dry bulk density of 1.6 g/cm³. Penetration resistance was determined using a needle with a 1.5 mm shaft diameter and a 30° semi-apex angle inserted into soil samples at the rate of 2.5 mm/min. Three mucilage application methods were investigated and compared to a control measurement without mucilage. In the droplet method, 0.1 ml of mucilage was applied locally onto the soil surface. In the mixing method, the mucilage was thoroughly mixed with the soil sample during preparation by adding the mucilage solution to soil while gradually mixing with a spatula, followed by gentle

stirring for 5 minutes to ensure a homogeneous distribution throughout the sample. Finally, for the injection method, we used a motorized syringe pump connected to a needle. During penetration, mucilage was continuously exuded through the tip of the needle at a controlled rate of 0.03 ml min^{-1}. The insertion took 200 seconds, resulting in a total mucilage volume of 0.1 ml being distributed along the penetration path. The results showed that the injection method, which most closely mimics natural root exudation, consistently resulted in significantly lower penetration resistance compared to the droplet and mixing methods. Complex interactions between mucilage type, concentration, soil water content, and application method were observed, stressing the multifaceted nature of mucilage effects on the physical properties of soil. For chia seed mucilage, the mixing method reduced penetration resistance more effectively than the droplet method across water contents (9% and 12%) for both mucilage concentrations (0.1% and 0.5%). However, in the case of flax seed mucilage, a significant reduction in penetration resistance for the mixing method compared to the droplet method was only observed at 12% water content. It was concluded that the mucilage application technique needs to be carefully considered in future root-soil-mucilage interaction studies.

This thesis demonstrates that root penetration resistance is governed by a hierarchy of factors, with soil water content, texture, and compaction as primary determinants, while mucilage and root tip geometry modulate penetration resistance in context-dependent ways. Notably, mucilage serves as a key biological factor influencing soil mechanical properties, but its effectiveness is highly dependent on the mucilage concentration, type, and prevailing soil conditions. The findings emphasize the critical role of mimicking natural exudation processes in experimental studies and highlight the broader implications for plant-soil interactions.

ZUSAMMENFASSUNG

Das Wurzelsystem von Pflanzen ist für die globale Ernährungssicherheit von entscheidender Bedeutung. Sein Wachstum wird jedoch durch ein komplexes Zusammenspiel der physikalischen, biologischen und chemischen Eigenschaften des Bodens gesteuert und durch Bodenverdichtung erheblich eingeschränkt. In verdichteten Böden stoßen Wurzeln auf einen hohen Eindringwiderstand, wodurch sie enorme Energie aufwenden müssen, um sich durch den Boden zu drängen. Dieser Widerstand kann das Wurzelwachstum um bis zu 50 % verringern und die Pflanzenentwicklung stark einschränken. Angesichts dieser Herausforderung haben Pflanzen ausgefeilte Anpassungsstrategien entwickelt, vor allem durch die Sekretion von Wurzelschleim, einem gelartigen Exsudat, das als biologisches Schmiermittel und Feuchtigkeitsspender wirkt und das Wachstum fördert. Während die jüngste Forschung bedeutende Fortschritte bei der Isolierung der individuellen Rollen von Schlüsselfaktoren wie den physikalischen Eigenschaften des Bodens (Wassergehalt, Verdichtung, Textur), der Geometrie der Wurzelspitzen und der Schleimsekretion erzielt hat, zeigt der aktuelle Stand der Technik eine grundlegende Lücke auf. Die meisten Studien untersuchen diese Variablen isoliert unter kontrollierten Bedingungen und übersehen dabei ihre dynamischen und synergistischen Wechselwirkungen innerhalb der komplexen, heterogenen Umgebung der natürlichen Rhizosphäre. Folglich bleiben wichtige Fragen unbeantwortet: Wie wirken die Geometrie der Wurzelspitzen und die Schleimsekretion zusammen, um den Eindringwiderstand in verschiedenen Bodentypen und bei unterschiedlichen Wassergehalten zu verringern? Inwieweit beeinflusst die Art und Weise der Schleimabgabe, die natürliche Ausscheidungsmuster nachahmt, dessen Wirksamkeit als Schmiermittel? Diese Arbeit zielt darauf ab, diese zentralen Fragen zu beantworten, indem sie die gekoppelten Auswirkungen der physikalischen Eigenschaften des Bodens, der Geometrie der Wurzelspitzen und der Biomechanik des Schleims auf den Eindringwiderstand systematisch quantifiziert und damit unser Verständnis der Wechselwirkungen zwischen Wurzeln und Boden verbessert, um Strategien zur Erhöhung der Widerstandsfähigkeit von Nutzpflanzen zu entwickeln.

In einem ersten Schritt wurden die kombinierten Auswirkungen von Wassergehalt, Schüttdichte, Wurzelspitzengeometrie (Kegelform) und Vorhandensein von Schleim in

verschiedenen Konzentrationen auf den Eindringwiderstand für das Wurzelwachstum untersucht. Dazu wurden Stahlnadeln (Penetrometer) mit Halbspitzenwinkeln von 15° (scharf) und 30° (stumpf) als Ersatz für Pflanzenwurzeln mit unterschiedlicher Wurzelspitzengeometrie verwendet. Chia-Samen-Schleim wurde in verschiedenen Massenkonzentrationen (0%, 0,1%, 0,3% und 0,5%) aufgetragen, um festzustellen, inwieweit die Schleimkonzentration den Eindringwiderstand beeinflusst. Im Gegensatz zur üblichen Methode, Schleim mit Erde zu mischen, wurde in dieser Studie ein einzigartiger Ansatz verfolgt, bei dem ein einzelner Tropfen Schleim (0,1 ml) direkt an der Injektionsstelle aufgetragen wurde, sodass er auf natürliche Weise in den umgebenden Boden eindringen konnte. Die Bodenproben wurden unter Verwendung konstanter mechanischer Energie für verschiedene gravimetrische Wassergehalte (15%, 20%, 25% und 30%) verdichtet, um die Auswirkung der Verdichtung zu bestimmen. Der Eindringwiderstand wurde gemessen, indem Nadeln mit einer konstanten Geschwindigkeit von 2,5 mm min-1 bis zu einer Tiefe von 8 mm in die Bodenproben mit bekanntem Wassergehalt, bekannter Schüttdichte und bekanntem Schleimkonzentration gedrückt wurden. Der Eindringwiderstand wurde mit einem Rheometer gemessen und in Energie für die Gesamteinsetztiefe (8 mm) und die Schafteinsetztiefe umgerechnet. Die Versuchsergebnisse zeigten, dass der Eindringwiderstand sowohl bei scharfen als auch bei stumpfen Nadeln bei sehr hohem Wassergehalt (30%) deutlich abnahm. Die stumpfe Nadel wies bei niedrigem Wassergehalt einen deutlich höheren Eindringwiderstand auf als die scharfe Nadel, während die scharfe Nadel bei hohem Wassergehalt einen deutlich höheren Eindringwiderstand aufwies als die stumpfe Nadel. Die Zugabe von Schleim reduzierte den Eindringwiderstand für beide Nadeltypen deutlich, insbesondere bei niedrigem Wassergehalt. Unterschiedliche Schleimkonzentrationen zeigten keinen signifikanten Einfluss auf den Eindringwiderstand. Der gemessene Eindringwiderstand wurde anhand der Hohlraumausdehnungstheorie auf der Grundlage von Bodenfestigkeitsparametern (Kohäsion und Elastizitätsmodul) analysiert, wobei für die stumpfe Nadel sphärische Hohlraummodelle und für die scharfe Nadel zylindrische Hohlraummodelle verwendet wurden. Die Hohlraumausdehnungsmodelle sagten den Eindringwiderstand über den gesamten Wassergehalt erfolgreich voraus, wobei die Modellierungsergebnisse insbesondere bei trockeneren Böden (15% – 25% Wassergehalt) sehr gut übereinstimmten. Bei einem höheren Wassergehalt von 30% traten jedoch erhebliche Abweichungen auf, wobei das sphärische Hohlraummodell den Eindringwiderstand für die stumpfe Nadel überschätzte. Der Modellierungsansatz hob die kritische Wechselbeziehung zwischen dem Wassergehalt des Bodens und der Geometrie der Nadelspitze bei der Steuerung

der Eindringdynamik hervor. Es wurde der Schluss gezogen, dass die Wassermenge im Boden ein wichtiger Faktor für die Bestimmung des Eindringwiderstands ist. Schwankungen im Verdichtungsgrad, Wassergehalt und Schüttdichte beeinflussen das Verhalten der Nadeln unterschiedlich. Während Schleimstoffe eine wichtige Rolle bei der Verringerung des Eindringwiderstands spielen, hängt das Ausmaß der Verringerung auch vom Wassergehalt des Bodens ab. Die Modellergebnisse zeigen, dass die aktuelle Theorie der Grenzspannungshohlraumerweiterung zwar in trockeneren Böden (15% – 25% Wassergehalt) erfolgreich ist, jedoch den Eindringwiderstand für einen stumpfen Kegel in feuchten Böden (insbesondere bei einem Wassergehalt von 30 %) nicht genau vorhersagen kann. Unter diesen gesättigten Bedingungen überschätzt die Theorie den Widerstand des stumpfen Kegels erheblich, was darauf hindeutet, dass sie das veränderte mechanische Verhalten des Bodens nicht vollständig erfasst. Folglich muss die Theorie weiterentwickelt werden, um den kombinierten Einfluss von Wassergehalt und Spitzengeometrie besser zu berücksichtigen, was für die Entwicklung genauer Vorhersagemodelle in gesättigten Böden unerlässlich ist.

In einem zweiten Schritt wurden die Auswirkungen der Bodenbeschaffenheit, der Schleimart und der Schleimkonzentration auf den Widerstand gegen das Eindringen von Wurzeln untersucht. Als repräsentative Bodenbeschaffenheiten wurden Lehm- und sandige Lehmproben verwendet, wobei Flachs- und Chiasamen-Schleim in Massenkonzentrationen von 0,1% und 0,5% zum Einsatz kamen. Die Bodenproben wurden bei gravimetrischen Wassergehalten von 9%, 12%, 15% und 18% auf eine Trockenrohdichte von 1,6 g/cm³ verdichtet. Der Penetrationswiderstand wurde mit einer Nadel mit einem Schaftdurchmesser von 1,5 mm und einem Halbspitzenwinkel von 30° bestimmt, die mit einer Geschwindigkeit von 2,5 mm min^{-1} in die Bodenproben eingeführt wurde. Ähnlich wie in der ersten Studie erfolgte die Schleimzugabe durch Auftragen eines einzelnen 0,1-ml-Tropfens Schleim direkt an der Injektionsstelle, sodass dieser auf natürliche Weise in den umgebenden Boden eindringen konnte. Der Penetrationswiderstand wurde mit einem Rheometer gemessen und in mechanische Energie umgerechnet. Die Ergebnisse zeigten, dass Lehm durchweg deutlich mehr Energie für die Penetration benötigte als Sand. Ein Anstieg des Wassergehalts verringerte den Eindringwiderstand bei beiden Böden erheblich, insbesondere bei Lehm. Das Vorhandensein von Schleim reduzierte die erforderliche Energie bei beiden Bodentypen erheblich, wobei der Effekt bei Lehm stärker war. Bei Lehm wurde kein signifikanter Unterschied im Eindringwiderstand zwischen den Schleimtypen beobachtet, aber Flachssamen-Schleim war bei der Verringerung des Eindringwiderstands bei sandigem Lehm

wirksamer als Chia-Samen-Schleim. Zusammenfassend zeigt diese Studie, dass die Bodenbeschaffenheit den Eindringwiderstand der Wurzeln erheblich beeinflusst, wobei Lehm mehr Energie erfordert als Sand, insbesondere bei geringerem Wassergehalt. Die Anwendung von Schleimstoffen reduzierte den Eindringwiderstand bei beiden Bodenarten wirksam, insbesondere bei Lehm. Während die Schleimstoffart und -konzentration im Allgemeinen nur geringe Unterschiede aufwiesen, wurden bei sandigem Lehm deutliche Unterschiede beobachtet, wo Flachssamen-Schleim den Eindringwiderstand wirksamer reduzierte als Chia-Schleim.

In einem dritten und letzten Schritt wurde der Einfluss verschiedener Methoden zur Anwendung von Schleimstoffen auf den Widerstand gegen das Eindringen von Wurzeln untersucht. Dazu wurde Schleimstoff aus Chia- und Leinsamen extrahiert und gefriergetrocknet, um ihn in seiner reinen Form zu erhalten. Der reine Schleimstoff wurde dann auf Konzentrationen von 0,1% und 0,5% (Gewichtsprozent) verdünnt. Es wurden sandige Lehmproben mit einem gravimetrischen Wassergehalt von 9% und 12% vorbereitet und auf eine Trockenrohdichte von 1,6 g/cm³ verdichtet. Der Penetrationswiderstand wurde mit einer Nadel mit einem Schaftdurchmesser von 1,5 mm und einem Halbspitzenwinkel von 30° bestimmt, die mit einer Geschwindigkeit von 2,5 mm/min in die Bodenproben eingeführt wurde. Es wurden drei Methoden zur Anwendung des Schleims untersucht und mit einer Kontrollmessung ohne Schleim verglichen. Bei der Tropfenmethode wurden 0,1 ml Schleim lokal auf die Bodenoberfläche aufgetragen. Bei der Mischmethode wurde der Schleim während der Vorbereitung gründlich mit der Bodenprobe vermischt, indem die Schleimlösung unter allmählichem Mischen mit einem Spatel zum Boden hinzugefügt und anschließend 5 Minuten lang vorsichtig gerührt wurde, um eine homogene Verteilung in der gesamten Probe sicherzustellen. Bei der Injektionsmethode schließlich wurde eine motorbetriebene Spritzenpumpe verwendet, die mit einer Nadel verbunden war. Während der Penetration wurde Schleim mit einer kontrollierten Geschwindigkeit von 0,03 ml min^{-1} kontinuierlich durch die Nadelspitze abgegeben. Die Einführung dauerte 200 Sekunden, wodurch insgesamt 0,1 ml Schleim entlang des Penetrationsweges verteilt wurden. Die Ergebnisse zeigten, dass die Injektionsmethode, die die natürliche Wurzelausscheidung am besten nachahmt, im Vergleich zur Tropfen- und Mischmethode durchweg zu einem deutlich geringeren Eindringwiderstand führte. Es wurden komplexe Wechselwirkungen zwischen Schleimtyp, Konzentration, Bodenwassergehalt und Anwendungsmethode beobachtet, was die Vielschichtigkeit der Auswirkungen von Schleim auf die physikalischen Eigenschaften des

Bodens unterstreicht. Bei Chia-Samen-Schleim reduzierte die Mischmethode den Penetrationswiderstand bei beiden Schleimkonzentrationen (0,1% und 0,5%) über den gesamten Wassergehalt (9% und 12%) hinweg wirksamer als die Tropfenmethode. Bei Flachssamen-Schleim wurde jedoch nur bei einem Wassergehalt von 12% eine signifikante Verringerung des Penetrationswiderstands bei der Mischmethode im Vergleich zur Tropfenmethode beobachtet. Es wurde der Schluss gezogen, dass die Technik der Schleimapplikation in zukünftigen Studien zur Wechselwirkung zwischen Wurzeln, Boden und Schleim sorgfältig berücksichtigt werden muss.

Diese Arbeit zeigt, dass der Penetrationswiderstand von Wurzeln durch eine Hierarchie von Faktoren bestimmt wird, wobei der Wassergehalt, die Textur und die Verdichtung des Bodens die primären Determinanten sind, während Schleim und die Geometrie der Wurzelspitzen den Penetrationswiderstand in kontextabhängiger Weise modulieren. Insbesondere dient Schleim als wichtiger biologischer Faktor, der die mechanischen Eigenschaften des Bodens beeinflusst, aber seine Wirksamkeit hängt stark von der Schleimkonzentration, der Art und den vorherrschenden Bodenbedingungen ab. Die Ergebnisse unterstreichen die entscheidende Rolle der Nachahmung natürlicher Ausscheidungsprozesse in experimentellen Studien und heben die weiterreichenden Auswirkungen auf die Wechselwirkungen zwischen Pflanzen und Boden hervor.

CONTENTS

LIST OF FIGURES

LIST OF TABLES

LIST OF ABBREVIATIONS

CPT	Cone penetration testing
CET	Cavity expansion theory
X-ray CT	X-ray computed tomography
MCR	Modular compass rheometer
EPFM	Elastic-plastic fracture mechanics
DEM	Discrete element method
EPS	Extracellular polymeric substances

LIST OF SYMBOLS

σ_1	Maximum compressive stress
σ_3	Minimum compressive stress
τ	Shear stress
θ	Inclination angle
φ	Angle of internal friction
C	Cohesion
σ	Normal stress
r	Radial co-ordinate
θ	Circumferential co-ordinate
$\Delta\sigma_r$	Change in radial stress
$\Delta\sigma_\theta$	Change in circumferential stress
k	Shape factor
R_C	Cavity radius
R_{C_0}	Initial radius
R_P	Plastic radius
γ	Poisson's ratio
ϵ_r	Radial strain
ϵ_θ	Circumferential strain
E	Elastic modulus
u	Total radial displacement
A	Integration constant
σ_r	Radial stress

p_0	Initial internal pressure
Δp	Change in pressure
p	Total pressure
u_{R_P}	Elastic displacement
p_L	Limit pressure
$F_{Z,T}$	Total axial force
F_Z	Axial force
μ	Coefficient of friction
α	Semi-apex angle of the cone
F_r	Radial force
$F_{f,s}$	Shaft frictional forces
$F_{n,s}$	Normal force
Z	Total depth of needle insertion
S_u	Soil strength
l_c	Length of the needle cone
U	Mechanical energy
U_T	Total energy
U_{F_C}	Cone energy
U_{F_R}	Shaft energy
F_{dz}	Total axial penetration resistance
F_{dl_c}	Force at the cone length
N	Penetration resistance

CHAPTER 1

INTRODUCTION

1.1 Motivation

Root systems serve as the primary interface between plants and their soil environment, performing essential functions in water and nutrient acquisition, mechanical anchorage, and environmental sensing (Gregory, 2006; Lynch, 2013). However, their growth and function are fundamentally constrained by soil penetration resistance - the mechanical impedance roots encounter as they extend through the soil matrix (Bengough et al., 2011). This resistance arises from the need to displace and compact soil particles, creating a physical barrier that can reduce root elongation rates by up to 50% in compacted soils (Clark et al., 2003). The challenge of soil penetration is particularly acute in agricultural systems, where over 60% of arable land experiences some degree of compaction (Hamza and Anderson, 2005), and is expected to worsen under climate change scenarios featuring more frequent droughts and intensive rainfall events (Colombi et al., 2018).

Plants have evolved remarkable adaptations to overcome this mechanical challenge, most notably through the secretion of root mucilage - a gelatinous exudate produced by the root cap that modifies the soil-root interface (Carminati et al., 2016). This complex mixture of polysaccharides, proteins, and lipids serves multiple functions: acting as a biological lubricant to reduce frictional resistance (Kroener et al., 2018), maintaining hydraulic connectivity in drying soils (Ahmed et al., 2014), and modifying soil structure through its unique physicochemical properties (Zickenrott et al., 2016). Recent studies demonstrate that mucilage can reduce penetration resistance by up to 40% in dry, compacted soils (Colombi et al., 2017), highlighting its crucial role in facilitating root growth under mechanical stress.

Despite the growing body of research on individual factors affecting root penetration, such as soil compaction, water availability, root exudation, and root tip geometry, there remains a significant gap in understanding how these elements interact simultaneously within real soil environments (Carminati et al., 2010; Ruiz et al., 2015; Valentine et al., 2012). Most studies have isolated one or two variables under controlled conditions, but the natural rhizosphere is

a highly dynamic system where multiple physical, chemical, and biological processes interact. This complexity is particularly relevant for agricultural soils that experience cycles of drying, wetting, and mechanical disturbances, which continually alter the conditions roots must overcome to grow (Oleghe et al., 2017). For example, Koebernick et al. (2017) highlighted the spatial heterogeneity of soil mechanical resistance in field conditions and how roots must continuously adapt to changing stress patterns. Moreover, as climate change intensifies, fluctuating rainfall patterns and prolonged droughts will exacerbate the mechanical challenges of soil penetration, making it increasingly important to identify strategies that support root growth in suboptimal conditions. Gaining insight into how root tip geometry and mucilage function together under different soil strength may offer a significant breakthrough in developing crops that are more resilient to compacted and dry soils. Such knowledge is especially valuable as global agricultural systems shift towards reduced tillage and no-till practices to improve soil health, which may result in higher bulk density and increased penetration resistance in the upper soil layers (Mooney and Drake, 2012). Furthermore, insights into how different plant species optimize root tip structure to counteract mechanical impedance could inform breeding programs aiming to develop resilient crop varieties with improved rooting depth and water use efficiency.

Recent advances in imaging technologies, such as x-ray computed tomography and magnetic resonance imaging, have provided unprecedented opportunities to observe root-soil interactions in situ (Mooney and Drake, 2012), allowing researchers to capture how roots deform soil, distribute mucilage, and alter pore structures during penetration. These tools can now be used to link microscale processes to entire plant performance, contributing to a more mechanistic understanding of root growth under physical stress. Ultimately, by integrating knowledge of soil mechanics, root biology, and plant physiology, this study aims to address critical agricultural challenges, such as improving crop yield in compacted soils, enhancing water uptake under drought, and sustaining yields on marginal lands. This research is motivated not only by the need to close yield gaps in existing agricultural systems but also by the broader goal of promoting sustainable soil management and resilient food production in the face of global environmental change. Thus, exploring the coupled effects of root tip geometry, mucilage secretion, and soil mechanical properties is essential to unlock new strategies that enhance plant performance under mechanical stress, ensuring food security for a growing population in an era of increasing climatic uncertainty.

1.2 Mechanical interactions between plant roots and soil in rhizosphere

The rhizosphere, defined as the narrow zone of soil directly influenced by root activity, represents a complex and highly dynamic environment where biological, chemical, and physical processes converge to facilitate plant growth. Plant roots are active structures within this zone. They modify their surrounding soil environment through exudation of organic compounds, water uptake, and mechanical displacement, influencing both the physical architecture and microbial composition of the rhizosphere (Philippot et al., 2013).

One of the primary physical interactions between roots and the rhizosphere involves mechanical displacement of soil particles or aggregates as roots grow. Root elongation requires the application of axial and radial forces to overcome soil mechanical resistance, which depends on bulk density, texture, water content, and shear strength (Bengough et al., 2011). As roots advance, they locally compact the soil at the root-soil interface while simultaneously creating zones of loosening behind the elongation zone, modifying pore connectivity and influencing water and gas exchange (Dexter, 1987; White and Kirkegaard, 2010). This dynamic alteration of the soil's physical structure feeds back into the rhizosphere environment, as it affects not only the ease of further root penetration but also the movement of nutrients and water to the root surface (Lehmann et al., 2020; Oswald et al., 2008; Prosser and Martiny, 2020).

Recent research has further revealed the complexity of these mechanical interactions, revealing that root growth through heterogeneous soil environments requires continuous adaptation to localized variations in mechanical impedance, moisture levels, and particle arrangement (Correa et al., 2019). The axial force generated at the root tip is essential for penetrating denser soil regions, while radial forces laterally displace particles, easing resistance in the elongation zone (Kolb et al., 2017). These actions not only enable the immediate advancement of the root but also create persistent structural modifications in the surrounding soil, such as enlarged bio-pores and preferential flow paths, which can facilitate the penetration of subsequent roots and the migration of microorganisms (Lucas et al., 2019).

The mechanical impact of roots on soil structure also varies depending on root architecture and growth patterns. Plants with thicker, stronger roots generate greater axial force to penetrate compacted layers, while finer roots exploit smaller pores, enhancing the connectivity of pore networks (Bengough et al., 2016). Moreover, root hairs play a crucial role in binding soil particles together and reinforcing aggregate stability, thereby enhancing

the structural cohesion of the rhizosphere (Brown et al., 2017; Hallett et al., 2022). Root plasticity plays a critical role in navigating mechanical resistance, as plants adjust growth angles, branching patterns, and elongation rates to avoid highly resistant zones (Colombi et al., 2022; Lee et al., 2013).

The role of soil moisture in modulating these mechanical interactions is profound. Moist soils have lower friction and penetration resistance, while dry soils show an increased cohesion between particles that amplifies mechanical impedance (Bengough and Mullins, 1990; Valentine et al., 2012). Under these conditions, mucilage secretion becomes vital, hydrating the rhizosphere and modifying its viscoelastic properties to ease root movement and prevent the loss of hydraulic continuity (Naveed et al., 2018; Zickenrott et al., 2016).

Imaging methods such as x-ray computed tomography and neutron radiography have greatly expanded the understanding of these root-soil mechanical processes (Koebernick et al., 2014; Mooney and Drake, 2012). It showed how roots reshape their surrounding soil matrix, influence pore architecture, and affect water distribution patterns on both the micro and the macroscale. Combined with modelling, these insights have been used to predict root behaviour under varying mechanical constraints and to design strategies for improving plant performance in challenging soils (Wang et al., 2021).

The study of root penetration resistance has employed various mechanical theories to describe soil deformation and stress distribution during root growth. Among these, fracture mechanics has been used to model crack propagation in brittle soils, while plasticity theory describes permanent soil deformation around penetrating roots. Cone penetration models, adapted from geotechnical engineering, relate probe measurements to root resistance, though they often oversimplify biological factors. The cavity expansion theory has emerged as a particularly relevant framework, as it mathematically describes how cylindrical or spherical objects expand within an elasto-plastic medium—analogous to root tips displacing soil (Yu, 2000). This theory, detailed in Chapter 2, quantifies the stress fields around penetrating roots, linking soil properties (cohesion, friction angle, elastic modulus) to resistance forces (Houlsby and Wroth, 1984). It also incorporates root tip geometry and confining pressures, providing a mechanistic basis for predicting penetration resistance in variably compacted or hydrated soils (Mckenzie et al., 2013). While other models offer partial insights, cavity expansion theory uniquely bridges geotechnical principles with root-soil interactions, making it a cornerstone for understanding mechanical impedance in plant roots.

Altogether, the mechanical displacement of soil by roots is a dynamic process that shapes the rhizosphere environment and feeds back into the mechanical and hydraulic challenges roots must overcome. By modifying soil structure, roots influence water retention, nutrient mobility, and microbial habitat formation. The establishment of this complex network of interactions is critical for plant health and productivity.

1.3 Biochemical interactions in the rhizosphere: The role of mucilage in modifying rheological properties

The rhizosphere is a chemically dynamic interface where biochemical interactions are essential for modifying the physical properties of soil and enhancing plant survival under diverse environmental conditions. Root exudation is central to these processes, comprising a complex suite of organic molecules such as sugars, amino acids, organic acids, phenolics, and high-molecular-weight polysaccharides like mucilage (Jones et al., 2009; Zhang et al., 2019). These exudates perform critical ecological functions, including nutrient mobilization, modulation of microbial activity, and alteration of soil structural and hydraulic properties. Among these compounds, mucilage has emerged as a particularly influential component due to its unique physico-chemical properties and multifaceted interactions with the soil matrix and microbial communities.

Mucilage is primarily composed of polysaccharides with varying proportions of neutral sugars, uronic acids, and proteins, which give it high viscosity, water retention capacity, and adhesive properties (Carminati et al., 2016; Naveed et al., 2018). Upon secretion from the root cap and border cells, mucilage rapidly hydrates upon contact with soil water, expanding to occupy pore spaces and encapsulating soil particles within a cohesive gel matrix. This creates a transitional zone between the root surface and bulk soil known as the rhizosheath, where mucilage mediates both physical and biochemical interactions (Holz et al., 2018). An important feature of this interaction stabilizes soil around the root and can enhance hydraulic connectivity, especially under conditions of limited moisture (Carminati and Javaux, 2020; Delory et al., 2018). This zone regulates water and gas exchange by altering pore continuity and creating microenvironments that balance oxygen supply and carbon dioxide diffusion, which are essential for root respiration and microbial activity (Koebernick et al., 2017). One of the critical roles of mucilage is the regulation of rhizosphere water dynamics, particularly under drought conditions. Due to its hydrophilic nature, mucilage can delay desiccation at the root-soil interface by retaining water and maintaining liquid connectivity in otherwise fragmented pore networks (Ahmed et al., 2014; Carminati et al., 2010). This hydraulic

buffering effect supports sustained water uptake, even when the surrounding bulk soil is dry, thereby postponing the onset of drought stress.

The importance of mucilage for the rhizosphere extends beyond hydration. Recent research has demonstrated that mucilage alters the rheological properties of the soil, reducing mechanical resistance and facilitating root penetration in compacted or dry soils (Rosskopf et al., 2022; Watt et al., 1994; Zickenrott et al., 2016). By reducing interparticle friction and decreasing the shear strength of the soil near the root tip, mucilage serves as a biological lubricant, easing root elongation under high-impedance conditions (Kroener et al., 2018). In fine-textured soils with high clay content, where capillary forces and particle cohesion are substantial, mucilage can effectively disrupt particle bonding, allowing roots to exploit pore spaces that would otherwise be inaccessible (Naveed et al., 2018). These effects are highly dependent on mucilage composition, concentration, and its interaction with specific soil textures, highlighting the need for species-specific studies that examine mucilage chemistry in detail (Nazari et al., 2022).

Mucilage also modulates chemical gradients in the rhizosphere that influence nutrient mobility and microbial dynamics. Organic acids present within mucilage can chelate micronutrients such as iron and mobilize phosphate from mineral surfaces through acidification and ligand exchange (Chen and Liao, 2016; Dakora and Sinclair, 2002; Oburger et al., 2013). These processes are crucial in nutrient-limited environments, where direct uptake from soil solution is insufficient. Moreover, mucilage provides a carbon-rich substrate that fuels microbial activity within the rhizosphere, effectively creating localized hotspots of microbial proliferation (Carvalhais et al., 2011; Dennis et al., 2010; Sher et al., 2020). These microbial communities, in turn, contribute to nutrient cycling, organic matter turnover, and the production of phytohormones such as auxins and cytokinins that feed back on root growth and architecture (Vacheron et al., 2013).

The symbiotic relationships fostered within mucilage-enriched rhizospheres are particularly evident in the context of biofilm formation. Bacteria and fungi exploit the hydrated, polysaccharide-rich environment of mucilage to establish stable biofilms on root surfaces, enhancing microbial resilience against desiccation and enabling collective metabolic activity (Rüger et al., 2023). These biofilms contribute to the stabilization of mucilage structures and can further modify the rheological properties of the rhizosphere by producing extracellular polymeric substances (EPS), which reinforce the gel-like matrix surrounding roots (Coyago-Cruz et al., 2025; Silva et al., 2022). This synergistic interaction between mucilage and

microbial EPS has been proposed as a key mechanism in sustaining root function during prolonged periods of water scarcity, as the combined polymers enhance water retention and protect roots from mechanical stress (Ghezelbash et al., 2025).

Environmental stressors, such as compaction and drought, have been shown to induce changes in the quantity and composition of mucilage exuded by roots. Holz et al. (2018) demonstrated that under mechanical stress, plants increase the exudation of high-viscosity polysaccharides, likely as an adaptive response to lubricate the soil and reduce impedance. Similarly, in arid conditions, drought-tolerant species produce mucilage with higher uronic acid content, which enhances water-binding capacity and delays the loss of hydraulic continuity between the root surface and surrounding soil (Nazari et al., 2022). Such plasticity in mucilage production suggests that plants modulate biochemical exudation as part of a coordinated strategy to overcome combined mechanical and hydraulic constraints.

Several modelling studies have sought to integrate mucilage dynamics into mechanistic descriptions of root water uptake and soil mechanics. Carminati and Vetterlein (2013) proposed conceptual models in which mucilage mediates the transition between liquid and vapor-phase water transport, maintaining hydraulic connectivity in drying soils. More recently, Naveed et al. (2018) developed rheological models to predict how mucilage modifies soil strength and flow behaviour under different moisture regimes. These models are instrumental in predicting plant performance under field conditions, especially as climate change intensifies the prevalence of compacted and drought-affected soils.

Despite extensive research, key gaps remain in understanding root penetration resistance due to oversimplified experimental approaches. Most studies examine isolated factors (e.g., soil compaction or mucilage secretion) under controlled conditions, neglecting the dynamic interactions between root morphology, soil heterogeneity, and environmental stresses. A major limitation is the lack of realistic experimental systems that simulate field-like soil conditions including natural texture variations, pore structures, and wetting-drying cycles while measuring root responses.

Additionally, the interplay between root tip geometry and soil mechanical properties remains poorly quantified. While root tip traits influence penetration efficiency, their effectiveness likely varies across soil types (e.g., sand vs. clay) and compaction levels, yet most studies assume idealized root shapes and homogeneous soils. Similarly, although mucilage is known

to reduce friction, its role in real-world scenarios—where soil moisture, microbial activity, and repeated root growth alter its lubricating effects—is unclear.

Most critically, current methods fail to bridge microscale root-soil interactions with whole-root system behaviour. Advanced imaging techniques (e.g., X-ray CT) have improved observations of soil deformation, but integrating these with root biomechanics and hydraulic processes remains challenging. Furthermore, standardized methodologies for measuring penetration resistance are lacking, limiting comparisons across studies. Addressing these gaps requires experiments that combine realistic soil environments, dynamic stress conditions, and multi-scale analyses to better predict root growth in agricultural systems.

1.4 Objectives and outline of the thesis

The primary aim of this thesis is to investigate the complex mechanical interactions occurring in the rhizosphere, focusing on how soil physical properties, root tip geometry, and root exudates (mucilage) govern penetration resistance and, consequently, root elongation under varying environmental conditions. Specifically, this thesis seeks to quantify how mechanical constraints and mucilage dynamics collectively influence root penetration mechanics through controlled laboratory experiments and theoretical analysis. The following chapters systematically develop the theoretical foundation and experimental investigations necessary to advance our understanding of root-soil interactions.

Chapter 2 provides the theoretical framework for understanding the mechanics of root penetration into soil, focusing on cavity expansion theory. I first review the key formulations of cavity expansion theory, its adaptations for biological analogues like roots, and recent applications in plant science that provide a basis for interpreting experimental penetration resistance data (Dexter, 1987; Kirby and Bengough, 2002). By establishing this theoretical foundation, the thesis contextualizes the subsequent experimental results within a robust mechanical framework, helping to understand how soil cohesion and elastic modulus alter the energy demands for root growth.

In Chapter 3, the focus is on understanding how soil physical properties and root biological traits interact to influence mechanical impedance to penetration in the rhizosphere. Specifically, the research addresses how variations in water content, degree of compaction, bulk density, root tip geometry, and mucilage exudation affect penetration resistance. For this, a controlled experimental setup using artificial root analogues (steel needles) with different tip geometries to simulate sharp and blunt root tips was used. Soil samples were prepared at

multiple water contents and subjected to standardized compaction with constant energy that resulted in varying bulk densities. Chia seed mucilage was applied at controlled concentrations to evaluate its role in reducing or increasing penetration resistance under different soil conditions. Using a rheometer to record penetration forces over standardized depths and velocity of the needle (penetrometer), this experimental framework allows us to systematically investigate how mechanical and biochemical factors interact to affect root penetration resistance.

Chapter 4 expands the core research question and focuses on whether different soil textures (loamy sand and loam), combined with variations in mucilage properties, influence the mechanical environment encountered by roots during elongation. To address this, an experimental setup was used where standardized soil samples of loamy sand and loam were prepared at distinct water contents and compacted to a uniform bulk density. Mucilage extracted from flax and chia seeds was applied at different concentrations using a localized droplet method to better replicate natural exudation patterns. Penetration was simulated using a steel needle with a fixed geometry (1.5 mm shaft diameter and a 30° semi-apex angle) inserted into the samples under controlled conditions. The penetration forces were recorded and analysed to evaluate the mechanical responses across different soil and mucilage treatments. This experimental design enables a systematic examination of how textural differences in soil and biochemical variations in mucilage jointly influence penetration resistance, contributing to a better understanding of root-soil interactions in various environmental contexts.

In Chapter 5, the focus shifts to investigating how different mucilage application methods affect penetration resistance in loamy sand soils. The primary research question explores whether the mode of mucilage delivery; applied as a droplet, mixed uniformly with soil, or injected during penetration, modulates the mechanical environment encountered by real roots. To address this, a standardized experimental setup using sandy soil compacted at different water contents and a fixed bulk density was used. Mucilage from chia and flax seeds was prepared at mass concentrations of 0.1% and 0.5%, and three application methods were implemented: (1) droplet application on the soil surface, (2) uniform mixing throughout the soil matrix, and (3) continuous injection along the penetration path using a motorized syringe pump. The penetration process was simulated using a hollow steel needle with openings at the tip and monitored with a rheometer to quantify penetration resistance under each treatment. This experimental design provides critical insights into how the spatial dynamics

of mucilage delivery affect soil mechanical behaviour, enabling better replication of natural exudation processes.

Chapter 6 synthesizes the findings of the thesis and reflects on the broader implications of the work for understanding root-soil interactions. This chapter summarizes the key contributions of the theoretical and experimental investigations, emphasizing how soil physical properties, root tip geometry, mucilage composition, and application methods together shape mechanical resistance to root growth. Finally, the thesis concludes with an outline of potential directions for future research.

CHAPTER 2

THEORY AND BACKGROUND

2.1 Introduction

Understanding the mechanical interactions between soil and plant roots is crucial for advancing agricultural and ecological research. This chapter provides the theoretical foundation necessary to explore these interactions, with a particular focus on penetration resistance—a key factor influencing root growth. Penetration resistance refers to the force required for roots to elongate through soil, and it is influenced by soil properties such as compaction, moisture content, and texture. To study this phenomenon, researchers have adapted geotechnical methods, such as cone penetration testing (CPT), and used theoretical frameworks like cavity expansion theory (CET) to describe root-soil interactions.

This chapter explores how cone penetration testing and cavity expansion theory have been adapted from geotechnical engineering to study root penetration in agricultural and ecological contexts. It also introduces the role of failure criteria, such as the Mohr-Coulomb failure criterion, in modelling soil deformation and root penetration. Understanding how soils transition from elastic to plastic behaviour under stress is essential for predicting root growth and soil displacement. The chapter further delves into the theoretical foundations of cavity expansion theory, which provides a critical framework for understanding the mechanics of root penetration and soil deformation.

By integrating concepts from geotechnical engineering with biological processes, this chapter aims to provide a comprehensive understanding of the mechanical interactions between roots and soil. This knowledge is vital for developing sustainable agricultural practices, particularly in challenging soil conditions where mechanical resistance significantly impacts plant productivity.

2.2 Cone penetration testing

Cone Penetration Testing (CPT), a well-established geotechnical method for assessing soil strength and compaction, has been increasingly adapted to study root-soil interactions in the rhizosphere. This adaptation stems from the need to quantify the mechanical impedance that roots encounter as they grow through soil, a factor that significantly influences root elongation, morphology, and overall plant productivity. The rhizosphere, the region of soil directly influenced by root secretions and microbial activity, presents unique challenges due to its dynamic and heterogeneous nature. CPT provides a quantitative measure of soil penetration resistance, which is critical for understanding the mechanical barriers roots face in different soil conditions.

The adaptation of CPT to rhizosphere research draws parallels between the penetration of cone penetrometers in geotechnical engineering and the growth of plant roots through soil. In both cases, the penetrating object (cone or root) must overcome the mechanical resistance of the soil. The primary parameter measured in CPT, cone resistance, is analogous to the resistance experienced by roots as they push through soil. This resistance is influenced by soil properties such as bulk density, moisture content, and particle arrangement, which are also critical factors in root growth (Bengough et al., 2011). Bengough and Mullins (1990) were among the first to explicitly link CPT measurements to root penetration resistance. They demonstrated that the force required for root elongation could be estimated using principles derived from CPT, particularly in cohesive soils. Their work highlighted the importance of soil strength, root tip geometry, and soil-root friction in determining penetration resistance. By simulating root growth using controlled penetration experiments, researchers have been able to quantify resistance forces under diverse soil conditions, providing a mechanistic framework for understanding root-soil interactions (Bengough, 1997).

Root penetration through soil is governed by the interplay of matric potential, structural rigidity, and particle size distribution, all of which influence mechanical impedance (Ruiz et al., 2016). Herrick and Jones (2002) investigated the effects of soil compaction and moisture on root growth, using CPT-derived methods to measure soil strength. They found that increased soil compaction significantly raised penetration resistance, thereby limiting root elongation. This research underscored the utility of CPT in predicting root growth limitations in compacted soils, which is particularly relevant for agricultural practices aimed at improving crop yields in marginal soils.

In addition to soil properties, biological factors such as root exudates and mucilage also influence penetration resistance. Bengough and McKenzie (1997) explored the role of mucilage in reducing soil-root friction, thereby facilitating root growth. They used CPT to measure the mechanical impedance of soils treated with mucilage and found that mucilage significantly reduced penetration resistance, particularly in dry and compacted soils. This finding has important implications for understanding how root exudates modify the rhizosphere environment to enhance root growth.

The integration of cone penetration testing (CPT) into rhizosphere research has significantly advanced our mechanistic understanding of root-soil interactions. By providing precise, quantitative measurements of penetration resistance, CPT has revealed how soil mechanical properties—including compaction, moisture-dependent strength, and particle arrangement—interact with biological processes such as mucilage exudation to govern root growth dynamics. Recent studies leveraging CPT methodologies have further demonstrated that root tip geometry and soil-structure feedback critically modulate penetration resistance (Colombi et al., 2022; Ruiz et al., 2021). These advances not only bridge geotechnical engineering and plant physiology but also inform innovative soil management practices. For instance, CPT-derived metrics are now being used to optimize tillage regimes and develop crop varieties with root architectures tailored to overcome soil physical limitations (Bengough et al., 2000). As research extends to heterogeneous field conditions, CPT remains a pivotal tool for unravelling the complex interplay between soil biomechanics and root functionality.

2.3 Stress redistribution and soil deformation patterns during root penetration

Root penetration into soils induces complex three-dimensional stress fields and soil deformation patterns that govern the mechanical impedance experienced by growing roots. These processes involve intricate interactions between root geometry, soil mechanical properties, and biological factors such as mucilage exudation (Bengough et al., 2011). Understanding these patterns is essential for predicting root growth responses to soil physical conditions and developing strategies to mitigate penetration resistance.

The stress distribution during root penetration can be described using principles adapted from cavity expansion theory, where the root tip acts as a penetrometer expanding a cylindrical or spherical cavity in the soil matrix (Yu, 2000). As the root advances, it generates radial stresses that displace soil particles while simultaneously creating zones of compression ahead of the tip and tension behind the elongation zone (Greacen et al., 1968). These stress patterns vary

significantly depending on root tip geometry (Figure 2.1) - sharp-tipped roots produce more localized stress concentrations compared to blunt tips, which distribute stresses over a wider area (Kirby and Bengough, 2002).

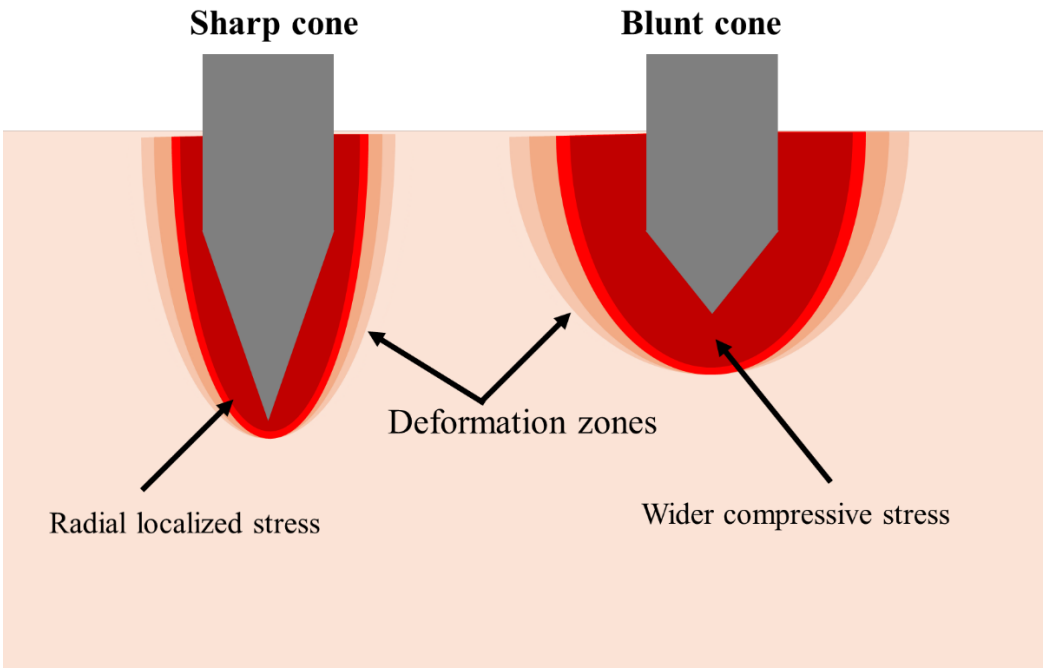

Figure 2.1 Deformation zones during sharp and blunt cone tip penetration into elasto-plastic soil

Soil deformation during root penetration occurs through several distinct mechanisms. Immediately ahead of the root tip, particles undergo compressive deformation and densification, while adjacent zones experience shear deformation along curved failure planes (Kolb et al., 2022). The thickness and geometry of these shear zones depend on soil texture and moisture content, with wetter soils typically developing thicker plastic zones (Bengough, 1997). Mucilage exudation at the root tip modifies these deformation patterns by reducing interfacial friction between the root and soil particles, effectively lubricating the penetration pathway (Kroener et al., 2018).

The transition from elastic to plastic soil behaviour during root penetration follows the Mohr-Coulomb failure criterion but is complicated by biological factors. Root exudates can reduce soil cohesion (c) by up to 35% while simultaneously increasing the angle of internal friction (φ) through particle binding effects (Naveed et al., 2018). This creates a unique failure envelope for rhizosphere soil that differs substantially from bulk soil behaviour (Carminati et

al., 2016). The resulting deformation patterns show pronounced hysteresis, with stress-strain relationships during root advancement differing from those during static loading (Kolb et al., 2017).

Microscale computed tomography (CT) studies have revealed that root penetration creates persistent bio-pores surrounded by a compacted sleeve of soil particles (Koebernick et al., 2019). These bio-pores typically measure 1.2-1.5 times the root diameter and exhibit altered hydraulic properties due to mucilage deposition on pore walls (Lucas et al., 2023). The stability of these pores depends on soil texture, with mucilage playing a critical role in stabilizing pores in sandy soils while having less effect in clay-rich soils (Zickenrott et al., 2016).

The energy requirements for root penetration are strongly influenced by these deformation patterns. Approximately 60-70% of the total penetration energy is dissipated in plastic work deforming the soil, while 30-40% overcomes frictional resistance along the root-soil interface (Bengough and Mullins, 1990). Mucilage secretion can reduce the frictional component by up to 50%, significantly lowering the total energy requirement (Colombi et al., 2017). However, these benefits are highly dependent on soil moisture content, with mucilage being most effective at intermediate water contents (Ahmed et al., 2014).

Recent advances in x-ray CT and digital image correlation techniques have enabled quantification of three-dimensional strain fields around penetrating roots (Mooney and Drake, 2012). These studies show that soil deformation extends 5-8 root diameters radially from the penetration axis, with strain magnitudes decaying exponentially with distance (Fan and Su, 2009). The strain fields are strongly anisotropic, with vertical strains dominating directly ahead of the root tip and radial strains becoming more significant along the sides (Kirby and Bengough, 2002).

Theoretical models combining cavity expansion theory with biofilm rheology have also begun to incorporate biological effects (Peng et al., 2023). These hybrid approaches treat mucilage as a viscoelastic fluid that modifies the boundary conditions at the root-soil interface, providing better predictions of penetration resistance in biologically active soils (Carminati and Vetterlein, 2013). However, challenges remain in accounting for time-dependent changes in mucilage properties and soil-microbe interactions (Naveed et al., 2018).

2.4 Mohr-Coulomb failure criterion

In soil mechanics, failure criteria define the conditions under which soil transitions from an elastic state, where it deforms but is able to return to its original shape, to a plastic state, where permanent deformation or failure occurs. Understanding these criteria is essential for modelling how roots penetrate and displace soil, as root growth is fundamentally a process of progressive failure of the surrounding soil matrix. Several failure criteria have been developed to predict when soils will yield under applied stresses. The choice of an appropriate failure criterion depends on the nature of the soil (cohesive, frictional, or both) and the loading conditions.

The Tresca, von Mises, Drucker-Prager, and Mohr-Coulomb failure criteria form an evolutionary progression in modelling material failure, with increasing sophistication for geotechnical applications. While the yield and failure criteria are typically expressed in three-dimensional principal stress space, where their surfaces form polyhedra, cones, and cylinders, the two-dimensional projections (Figures 2.2 and Figure 2.3) provide a clearer illustration of their relative shapes and underlying assumptions. These simplified views are especially useful for visualizing the differences between smooth criteria (von Mises, Drucker–Prager) and piecewise linear ones (Tresca, Mohr–Coulomb), which directly influence how materials are modeled under multiaxial loading conditions.

The Tresca criterion, representing a hexagonal prism in principal stress space (a 3D representation of stress states), serves as the simplest shear-based model and is mathematically equivalent to Mohr-Coulomb criterion when soil friction is neglected. While the von Mises failure criterion offers a circular cylindrical yield surface in deviatoric stress space (considering only distortional stresses), making it ideal for metals, its lack of pressure-sensitivity renders it inadequate for soils where confinement pressure significantly affects strength. The Drucker-Prager failure criterion bridges this gap by introducing a conical yield surface that accounts for pressure-dependence, effectively providing a smooth mathematical approximation of Mohr-Coulomb's more complex irregular hexagonal pyramid. Ultimately, the Mohr-Coulomb failure criterion emerges as the most comprehensive criterion, explicitly incorporating both cohesive and frictional strength components through its characteristic linear envelope in shear-normal stress space, making it the standard for geotechnical analysis where accurate representation of soil behaviour under various stress conditions is paramount. This hierarchy of criteria - from Tresca's simplicity to Mohr-Coulomb's completeness -

reflects the trade-offs between computational convenience and physical accuracy in geo-mechanical modelling.

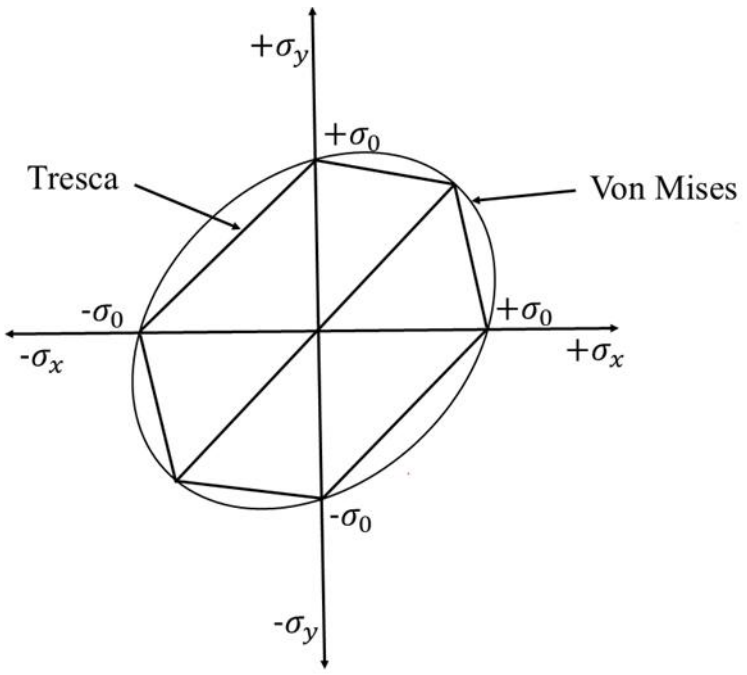

Figure 2.2 Failure surfaces in principal stress space for ductile materials: Comparison between two–dimensional representation of the Tresca and von Mises yield criteria. Uniaxial yield stress of the material (σ_y) and uniaxial applied stress (σ_x).

The Mohr-Coulomb failure criterion is a fundamental model extensively utilized in geotechnical engineering and soil mechanics to characterize the shear strength of soils and rocks. This criterion is named after Charles-Augustin de Coulomb, who initially introduced the concept of shear strength in 1776, and Otto Mohr, who subsequently developed the graphical representation of stress states. Typically, a soil mass experiences a three-dimensional stress system. However, in many soil engineering applications, the stresses in the third dimension are often negligible, allowing the system to be simplified to two dimensions. Under these conditions, plane strain assumptions are commonly applied, where the strain in the third dimension is considered to be zero. At any point within a stressed body, there exist three principal planes where shear stresses are zero. The plane experiencing the maximum compressive stress (σ_1) is referred to as the major principal plane, while the plane with the

minimum compressive stress (σ_3) is known as the minor principal plane. The third plane, subjected to a stress value between σ_1 and σ_3, is termed the intermediate principal plane.

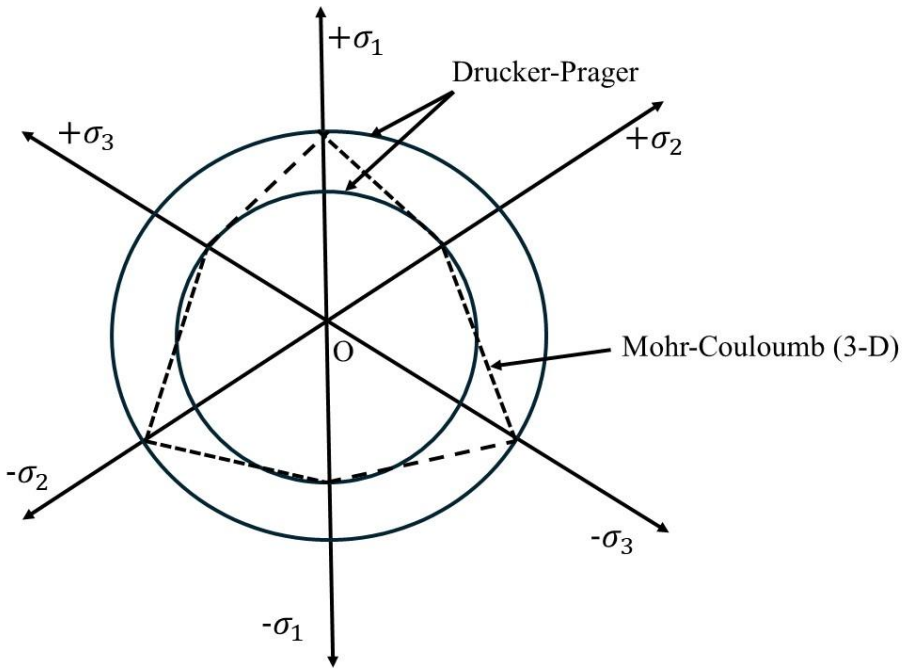

Figure 2.3 Failure surfaces in principal stress space for pressure-dependent materials: Comparison between two–dimensional representation of the Mohr–Coulomb and the Drucker–Prager criteria. σ_1, σ_2, and σ_3 are major, intermediate, and minor principal stresses.

In Figure 2.4, a plane perpendicular to the intermediate principal plane is depicted, illustrating the major and minor principal stresses acting upon it. Here, the major principal plane is oriented horizontally, and the minor principal plane is oriented vertically. The stress on the failure plane can be determined using the Mohr-Coulomb criterion, which relates the shear strength of the material to the normal stress and the material's inherent properties, such as cohesion (c) and the angle of internal friction (φ).

The Mohr circle (Figure 2.5) is a fundamental graphical tool in mechanics used to analyse the state of stress at a point within a material, particularly for determining principal stresses and their orientation. The circle is constructed by plotting normal stress (σ) on the horizontal axis

and shear stress (τ) on the vertical axis (Figure 2.5). The centre of the circle is given by (σ_1 + σ_3)/2 and represents the average of the major (σ_1) and the minor principal stresses (σ_3).

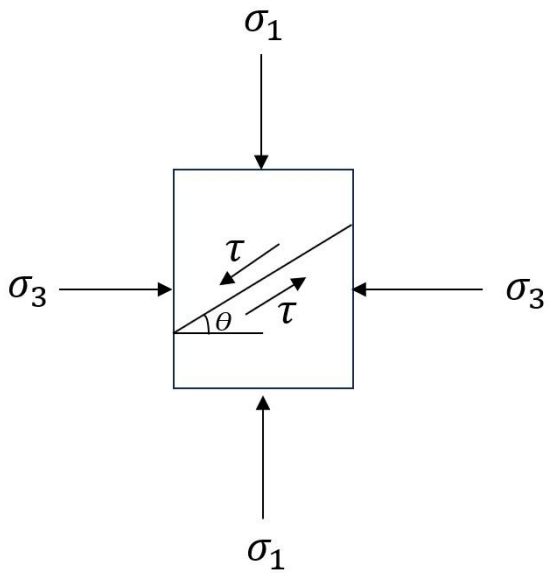

Figure 2.4 Stress state on a plane perpendicular to the intermediate principal stress axis, showing major ($\boldsymbol{\sigma_1}$) and minor ($\boldsymbol{\sigma_3}$) principal stresses. Shear stress (τ) acts on a plane inclined at angle θ to the major principal plane (horizontal).

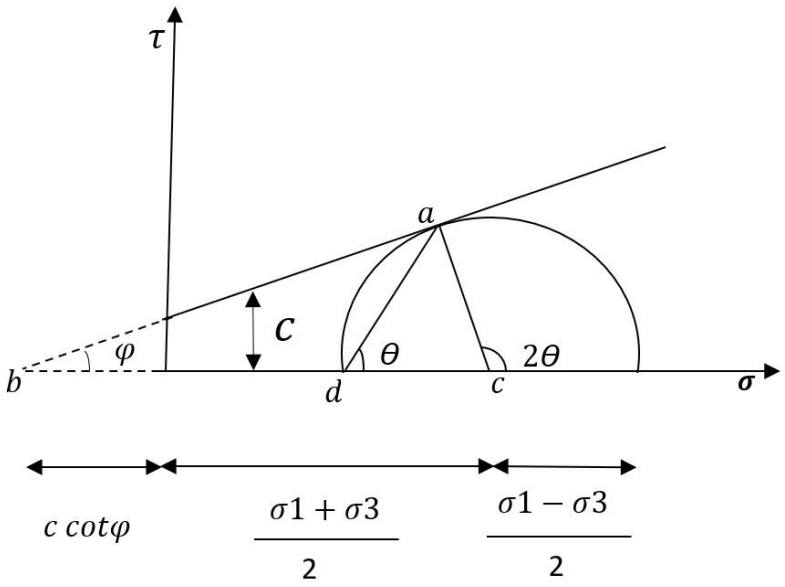

Figure 2.5 Mohr's Circle diagram showing stress conditions at a point in soil. The horizontal axis (σ) represents normal stresses, while the vertical axis (τ) shows shear stresses. The circle spans between the largest (σ_1) and smallest (σ_3) principal stresses. The angle θ represents the orientation of a specific plane relative to the major principal stress direction (σ_1). The failure envelope (straight line) indicates when soil fails - its steepness shows frictional strength, and its τ-intercept shows cohesive strength (c).

The radius of the circle is $(\sigma_1 - \sigma_3)/2$ and corresponds to the maximum shear stress experienced by the material. The Mohr circle extends from σ_3 to σ_1 on the normal stress axis, with any point on its circumference representing the stress state on a specific plane. The stress on the failure plane is given by:

$$(\sigma_1 - \sigma_3) = 2\,c\cos\varphi + (\sigma_1 - \sigma_3)\sin\varphi \quad (1)$$

The angle from the centre to a point on the circle is twice the angle of the corresponding plane in the physical material due to the 2θ relationship inherent in the Mohr circle. Additionally, the term $c\cot\varphi$ is significant in soil mechanics, where c represents cohesion and φ is the angle of internal friction, both of which are critical for determining the shear strength (τ) of the soil. The shear strength is given as:

$$\tau = c + \sigma \tan\varphi \quad (2)$$

To determine the Mohr-Coulomb failure criterion for a given soil, laboratory shear tests such as triaxial compression tests or direct shear tests are performed. These tests investigate the behaviour of soil under controlled stress conditions and identify the stress levels at which shear failure occurs. In direct shear tests, the soil specimen is placed within a shear box, which consists of two stacked halves—an upper and a lower section—that enclose the sample. The specimen is typically thin and either square or circular in top-down view to promote shear failure along the horizontal plane between the two halves. A normal stress is applied vertically to simulate in-situ loading, and a horizontal force is gradually applied to the upper half while the lower half remains fixed. This causes the soil to shear along the pre-defined horizontal plane. Direct shear tests do not provide the full principal stress state and are thus less comprehensive. However, shear stress (τ) is directly calculated from the applied horizontal force divided by the area of the failure surface, and the normal stress (σ) is determined from the applied vertical load. By conducting multiple tests under varying normal stresses, a series of (σ, τ) pairs are obtained. Plotting these on a shear stress versus normal stress graph enables the empirical determination of the Mohr-Coulomb failure envelope. A best-fit straight line through the data points is used to derive the parameters of the failure criterion, described by

equation (2). This method provides a practical means of estimating shear strength parameters, even though it does not capture the complete stress state.

In the triaxial compression test, a cylindrical soil sample is subjected to an all-around confining pressure (σ_3) and then loaded axially until failure, at which point the major principal stress (σ_1) is recorded. The minor principal stress (σ_3) is the applied confining pressure, which remains constant during the test. Once several sets of principal stresses (σ_1 and σ_3) are obtained from different test conditions, Mohr's circles can be constructed for each failure state. Each circle represents the state of stress at failure for a specific test. To draw a Mohr's circle, the center is calculated as the average of the principal stresses, and the radius is half the difference between them. The circle is drawn in a two-dimensional stress space where the horizontal axis represents normal stress (σ) and the vertical axis represents shear stress (τ). By plotting several Mohr's circles corresponding to different normal stresses, the Mohr-Coulomb failure envelope can be constructed. This is a straight line that forms a common tangent to all the Mohr's circles at their point of failure. The envelope represents the shear strength of the soil as a function of normal stress and is described by equation (2). To validate the failure criterion, it is essential that all experimentally obtained Mohr circles are either tangent to or lie below the failure envelope. If any circle exceeds the envelope, it suggests the soil would have failed at a lower stress state than predicted, indicating a discrepancy in the data or a violation of the assumption of linear behaviour. This triaxial testing methodology provides a robust framework for predicting shear failure in soils and is widely used in both laboratory research and practical engineering design.

2.5 Evolution of cavity expansion theory

Cavity expansion theory originated in the context of metal indentation studies (Bishop et al., 1945; Hill, 1950). Subsequent adaptations to geotechnical engineering problems (e.g., Anderson et al. (1972)) were followed by significant theoretical refinements over the next two decades. The theory has since evolved into a robust framework for analysing soil-structure interaction problems, with particular emphasis on its application to cylindrical and spherical cavity expansion scenarios.

Cavity expansion theory provides a powerful analytical framework for understanding soil and rock behaviour under radial loading, with spherical and cylindrical configurations serving distinct but complementary roles in geotechnical analysis. Spherical cavity expansion models the growth of a spherical void in an infinite medium, finding application in deep foundation

design, cone penetrometer analysis, and blast loading scenarios. In contrast, cylindrical cavity expansion describes the radial deformation of a long cylindrical cavity, making it particularly relevant for pile installation and tunnelling applications. The fundamental difference between these approaches lies in their stress-strain distributions: spherical expansion produces truly axisymmetric conditions with uniform radial and circumferential strains, while cylindrical expansion assumes plane-strain conditions better suited to elongated geo-structures.

Cylindrical cavity expansion theory has been extensively applied in geotechnical engineering, particularly in the interpretation of pressuremeter tests (Anderson et al., 1972; Houlsby et al., 1986; Houlsby and Withers, 1988; Palmer, 1972). Pressuremeter tests are in-situ geotechnical tests used to evaluate soil deformation and strength characteristics by radially expanding a cylindrical probe in a borehole. The test measures the pressure-expansion relationship, which is interpreted using cylindrical cavity expansion theory to derive key soil parameters such as shear modulus, undrained shear strength (for clays), and horizontal stress (for sands). These applications enable the direct correlation between pressure-expansion curves and soil properties, providing critical insights into soil behaviour under loading. Randolph and Houlsby (1986) conducted a comprehensive study on the application of cylindrical cavity expansion theory to the modelling of driven-pile installation, highlighting its utility in predicting soil displacement and stress fields during pile driving. Sagaseta (1987) further advanced the theory by investigating the effects of longitudinal shaft friction in expanding cylindrical cavities, a critical factor in assessing pile bearing capacity and shaft resistance.

The development of spherical cavity expansion solutions has progressed significantly since Hill's (1950) foundational work on finite expansion in Tresca materials - idealized perfectly plastic solids that yield when maximum shear stress reaches a critical value. Chadwick (1959) advanced this theory by presenting comprehensive solutions for elastic-plastic materials governed by the associated Mohr-Coulomb flow rule. This flow rule - which may be associated or non-associated - governs the direction of plastic strain increments. An associated flow rule assumes plastic strains develop normal to the yield surface, implying predictable dilatancy effects, whereas non-associated flow rules employ separate plastic potential functions to better capture realistic soil behaviour where volume changes during shearing may deviate from theoretical predictions. Chadwick's (1959) analytical framework also yielded closed-form solutions for limit pressures in purely cohesive, incompressible materials. Vesić (1972) subsequently expanded this work by incorporating soil compressibility through non-

zero volumetric strains, developing approximate limit pressure solutions that proved particularly valuable for deriving bearing capacity factors in deep foundation design.

Recent advancements in cavity expansion theory include the work of Carter et al. (1986), who developed an analytical solution for limit pressures in modified or non-associated Mohr-Coulomb materials under the assumption of steady-state deformation at large strains. However, their analysis contains certain approximations that limit the accuracy of their limit pressure solution, suggesting that it should be regarded as an approximate rather than definitive result. Bigoni and Laudiero, (1989) emphasized the importance of accounting for elastic deformations within the plastic zone during cavity expansion. Their approach combined analytical methods with numerical integration techniques, adopting the non-associated Mohr-Coulomb criterion. For cylindrical cavity expansion, they assumed that the longitudinal normal stress equalled the mean of the other two principal stresses. However, this assumption introduces inconsistencies with the flow rule governing plastic strains in the axial direction, highlighting a limitation in their methodology.

The adaptation of cavity expansion theory to root penetration resistance emerged from the understanding that root growth through soil involves the creation and expansion of a cylindrical cavity, akin to the expansion of a cavity in a soil mass under external pressure. This analogy was first explicitly explored by Greacen et al. (1968), who applied cavity expansion principles to model the forces required for root elongation through soil. The study demonstrated that the pressure needed for root penetration could be estimated using solutions derived from cylindrical cavity expansion theory, particularly in cohesive soils. Subsequent studies refined this approach by incorporating soil-specific properties and root morphological characteristics. Bengough and Mullins (1990) extended the theory to account for the effects of soil strength, root tip geometry, and soil-root friction on penetration resistance. They highlighted the importance of soil dilatancy and compressibility in determining the resistance encountered by roots, drawing parallels to the large-strain cavity expansion problems studied in geotechnical engineering (Carter and Yeung, 1985; Yu and Houlsby, 1991). Further advancements were made by Kirby and Bengough (2002), who integrated cavity expansion theory with root growth models to predict the influence of soil compaction on root penetration resistance. The study emphasized the role of soil stress in understanding root-soil interactions. This approach allowed to predict root penetration resistance in both loose and compacted soils, providing a mechanistic basis for evaluating the impact of soil management practices on root growth.

Kolb et al. (2017) applied cavity expansion theory to investigate the effects of soil texture and moisture content on root penetration resistance. The study demonstrated that the theory could be effectively used to predict root growth limitations in different soil types, particularly in arid and semi-arid regions where soil mechanical resistance is a major constraint on plant productivity. This work underscored the utility of cavity expansion theory in agronomic and ecological studies, particularly in understanding the mechanical barriers to root growth in heterogeneous soils.

Ruiz et al. (2016) extended the classical cavity expansion theory by incorporating the concept of limit pressure, marking an important advancement in predicting penetration forces during cone insertion. The limit pressure, defined in geotechnical studies as the pressure required to push a penetrometer tip into the soil until steady penetration occurs (Houlsby and Wroth, 1991; Ruiz et al., 2016), provides a more realistic basis for formulating penetration force compared with the earlier use of cavity pressure alone. Importantly, penetration resistance curves derived from limit pressure clearly distinguish between the insertion of the penetrometer tip (cone) and the subsequent advance of the penetrometer shaft, thereby capturing the two stages of penetration more precisely. Ruiz et al. (2016) also showed that tip geometry exerts a major influence on deformation zones: blunt and sharp needles exhibit significant differences in penetration resistance, particularly at cone depth, where the stress field around the tip controls the ease of entry. For root biology, this distinction is crucial, since sharp tips tend to concentrate stresses locally, lowering the penetration resistance but making roots more sensitive to soil heterogeneity, whereas blunt tips distribute stresses more widely, leading to higher penetration forces but a more stable advancement. Building on this framework, the use of limit pressure cavity expansion theory in the present study allows to more accurately quantify the mechanical constraints imposed by soil on root elongation and provides a robust basis for comparing penetration resistance across different root tip morphologies and soil conditions, thereby setting the stage for the analyses that follow.

2.6 Modeling penetration resistance using limit pressure cavity expansion theory

Previous studies have used models based on cavity expansion theory to describe penetration resistance. In this theory, homogenous, isotropic, elastic, and perfectly plastic soils are typically assumed in which a spherical cavity is expanded. Most often, a spherical system with radial (r) and circumferential (θ) coordinates are used, and the self-weight of the soil (body forces) is assumed to be negligible. In the absence of body forces, the stress equilibrium

on a soil element at a distance r from the center of a spherical cavity is given by (Figure 2.6, Carter et al., 1986):

$$\frac{\partial \sigma_r}{\partial r} + \frac{k(\Delta\sigma_r - \Delta\sigma_\theta)}{r} = 0 \quad (3)$$

where $\Delta\sigma_r$ is the change in radial stress and $\Delta\sigma_\theta$ is the change in circumferential stress acting on the soil element. The shape factor (k) is 2 for a spherical cavity. The cavity with a radius R_C (and an initial radius R_{C_0}) is surrounded by a plastic deformation region extending up to radius R_P. The Mohr-Coulomb failure criterion is used to describe the yield behavior of the soil and is given by Equation (1).

In this study, I assume that the soil is purely cohesive ($\emptyset = 0$) (Ruiz et al., 2015), in which case Equation (1) reduces to:

$$\Delta\sigma_r - \Delta\sigma_\theta = 2c \quad (4)$$

The constitutive equations for a purely cohesive and elastic soil (Poisson's ration $\gamma = 0.5$) for the radial strain $\left(\epsilon_r = \frac{du}{dr};\ \text{where } u \text{ is the total radial displacement}\right)$ and circumferential strain $\left(\epsilon_\theta = \frac{u}{r}\right)$, are given by (Elder et al., 1985):

$$E\frac{du}{dr} = \Delta\sigma_r - \Delta\sigma_\theta \quad (5)$$

$$E\frac{u}{r} = -\frac{1}{2}\Delta\sigma_r + \frac{1}{2}\Delta\sigma_\theta \quad (6)$$

where E is the elastic modulus of the soil. From equations (5) and (6), it can be seen that:

$$\frac{du}{dr} = -2\frac{u}{r} \quad (7)$$

Integrating for u (total radial displacement) using $u = 0$ at $r \to \infty$ implies $u = \frac{A}{r^2}$, where A is the integration constant. Using $\epsilon_r = -2\epsilon_\theta$ and substituting for u with $\sigma_r = p_0$ (p_0 is the initial internal pressure) at $r \to \infty$ gives:

$$\Delta\sigma_r = \sigma_r - p_0 = \frac{4EA}{3r^3}. \quad (8)$$

At the cavity surface, $r = R_C$, $\Delta\sigma_r = \Delta p$ (Δp is the change in pressure) gives the integration constant $A = \frac{3\Delta p {R_C}^3}{4E}$. Substituting A in equation (8) and using $\epsilon_r = -2\epsilon_\theta$ results in:

$$\frac{u}{R_C} = \frac{3\Delta p}{4E}\left(\frac{{R_C}^2}{r^2}\right) \quad (9)$$

$$\frac{\Delta\sigma_r}{\Delta p} = \left(\frac{{R_C}^2}{r^2}\right) \quad (10)$$

$$\frac{\Delta\sigma_\theta}{\Delta p} = -\frac{1}{2}\left(\frac{{R_C}^3}{r^3}\right) \tag{11}$$

Yield occurs initially at $r = R_C$ when $\Delta\sigma_r - \Delta\sigma_\theta = 2c$. By using equations (9), (10), and (11), the change in pressure and radius of cavity are given as:

$$\Delta p = \frac{4c}{3} \tag{12}$$

$$R_C = \frac{R_{C0}}{\left(1-\frac{C}{E}\right)} \tag{13}$$

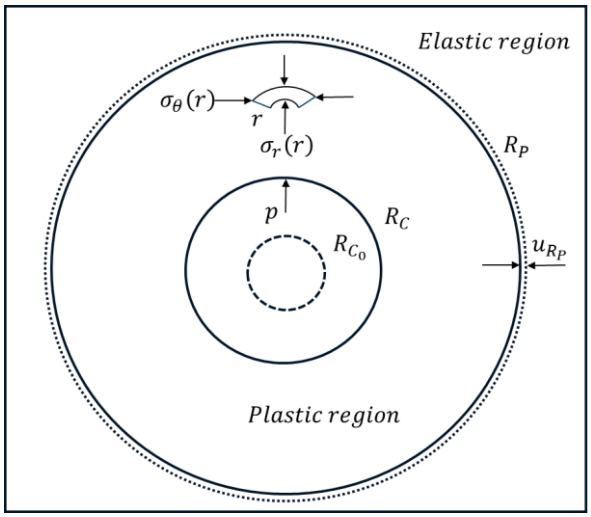

Figure 2.6 Conceptual model to describe cavity expansion in a homogenous and isotropic elasto-plastic medium. The initial radius of the cavity is denoted by R_{C_0}. The final cavity radius and corresponding pressure is denoted by R_C and p, respectively. R_P indicates the radius of the plastic region, and u_{R_P} represents the elastic displacement at the plastic-elastic interface.

In the plastic region, the radial stress can be determined by using equations (3) and (13) with the boundary condition $\sigma_r = p$ (p is the total pressure at the radius of the cavity) at $r = R_C$:

$$\sigma_r = p - 4cln\left(\frac{r}{R_C}\right) \tag{14}$$

The elastic displacement at $r = R_P$ is obtained using equation (9), and it is given as:

$$u_{R_P} = \frac{3R_P}{4E}\left(\Delta p - 4cln\left(\frac{R_P}{R_C}\right)\right) \tag{15}$$

Using equations (12), (13), and (14) at $r = R_P$, the change in radial stress is given as:

$$\Delta\sigma_r = \Delta p - 4c\ ln\left(\frac{R_P}{R_C}\right) = \frac{4c}{3} \tag{16}$$

Thus, the elastic displacement at yielding can be expressed as:

$$u_{R_P} = R_P\left(\frac{c}{E}\right) \tag{17}$$

Equation (16) is used to express $\left(\frac{R_P}{R_C}\right)$ as cavity radius (R_C), so that the change in radial stress and total cavity pressure is expressed as a function of cavity radius (R_C) alone. This is done by equating the volume of the plastic region $R_C \leq r \leq R_P$ to its original volume $R_{C_0} \leq r \leq R_P - u_{R_P}$, which links cavity radius (R_C) to the total cavity pressure (p) and it results in:

$$\left(\frac{R_P}{R_C}\right) = \frac{R_P\left(1-\frac{{R_{C_0}}^3}{R_C}\right)}{3u\left(1-\frac{u_{R_P}}{R_P}+\frac{{u_{R_P}}^2}{3{R_P}^2}\right)} \tag{18}$$

Substituting for u_{R_P} in equation (18) using equation (17) and substituting $\frac{R_P}{R_C}$ in equation (16) gives the relationship between the total cavity pressure (p) and the cavity radius (R_C). The cavity pressure (p) can be expressed as, $p = p_0 + \Delta p$ and it is observed within 1% of the limit pressure (p_L) when $R_C \geq 4R_{C_0}$. Thus, we can approximate the limit pressure (p_L) with the total cavity pressure (p). Assuming the soil is incompressible $\left(\frac{E}{c}>>1\right)$, the limit pressure reduces to (Carter et al., 1986):

$$p_L = p_0 + \frac{4c}{3}\left(1 + ln\frac{E}{3c}\right) \tag{19}$$

Assuming that deformation is mainly in the plastic region, the radial stress on the soil element at distance r from the center of the cavity is obtained by combining equations (3), (1), and (19):

$$\sigma_r(r) = p_L - 4cln\left(\frac{r}{R_C}\right) \tag{20}$$

Ruiz et al. (2016) showed that the total axial force at cone insertion can be calculated as:

$$F_{Z,T} = F_Z\left(\mu cot(\alpha) + 1\right) \tag{21}$$

where μ is the coefficient of friction, α is the semi-apex angle of the cone (needle tip), F_Z is the axial force of the cone that can be calculated using $F_Z = F_r\, tan(\alpha)$, and F_r is the radial force exerted by the cone (needle tip) given as:

$$F_r = \pi r^2 cot(\alpha)\sigma_r(r) \tag{22}$$

After complete insertion of the cone (needle tip), the additional penetration resistance is mainly due to the frictional forces experienced by the shaft. These forces are interfacial

frictional forces associated with the friction between the surface of the needle and the soil particles. To calculate the overall force experienced by the needle, both shaft frictional forces and cone forces should be considered. The shaft frictional forces can be calculated as (Ruiz et al., 2016):

$$F_{f,s} = F_{n,s}\,(\mu) \tag{23}$$

where μ is the interfacial coefficient of friction between the shaft and the soil, and $F_{n,s}$ is the normal force acting on the shaft and is given as (Ruiz et al., 2016):

$$F_{n,s} = 2S_u\big(2\pi r(z - l_c)\big) \tag{24}$$

where S_u is the strength of the soil, z is the total depth of needle insertion, and l_c is the length of the needle cone (needle tip).

2.7 Energy-based analysis of soil penetration

To better understand the mechanical processes involved in root penetration, an energy-based analysis approach that quantifies the work required for soil penetration is used. Figure 2.3 illustrates the components of penetration resistance during soil penetration testing, emphasizing the relationship between the geometry of the needle and the energy requirements for penetration. The schematic representation of the needle highlights its two main sections: the conical tip, with a length defined as cone length (l_c), and the cylindrical shaft, with a length equal to the total depth (Z) minus the cone length ($Z - l_c$).

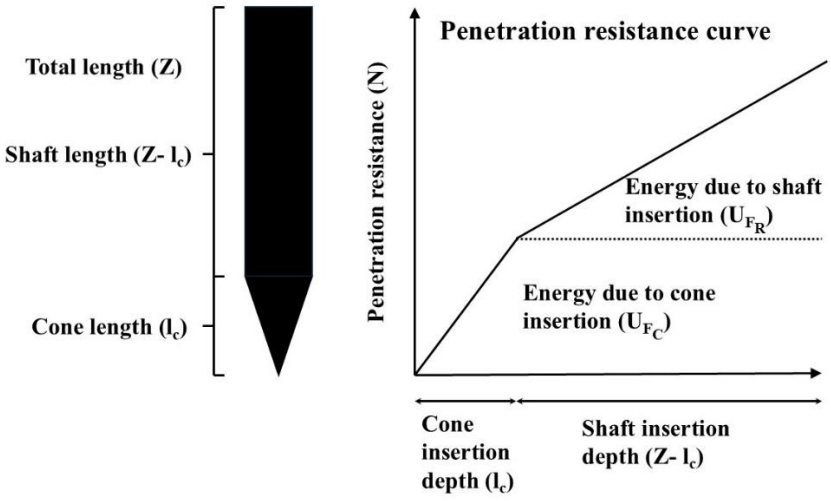

Figure 2.7 Components of penetration resistance and energy partitioning in soil penetration dynamics.

The mechanical energy (U) required for insertion was obtained from the area below the penetration resistance curve as a function of insertion depth following Ruiz et al. (2016):

$$U_T = \left(\int_0^Z F_{dz}\, dz \right) \tag{25}$$

where U_T denotes the total energy required to insert the entire needle up to the total depth, F_{dz} is the total axial penetration resistance as a function of insertion depth, and Z is the total depth of needle.

Figure 2.7 demonstrates how penetration resistance (N) varies with insertion depth (m), dividing the penetration process into two distinct phases. During the cone insertion phase (l_c), resistance increases sharply due to localized soil deformation, with the area under the curve representing the energy required for cone insertion U_{F_C}, and it is given as:

$$U_{F_C} = \left(\int_0^{l_c} F_{dl_c}\, dz + \int_{l_c}^{Z} F_{dl_c}\, dz \right) \tag{26}$$

U_{F_C} is the energy required to insert up to cone insertion depth, l_c is the length of the cone, and F_{dl_c} is the force at the cone length (l_c). In the subsequent shaft insertion phase $(Z - l_c)$, resistance increases linearly, reflecting the frictional forces acting on the shaft, with the corresponding energy denoted as U_{F_R}.

$$U_{F_R} = \left(U_T - U_{F_C} \right) \tag{27}$$

where U_{F_R} is the energy only due to the insertion of the shaft (frictional forces). The total energy (U_T) required for penetration is the sum of two components (U_{F_R} and U_{F_C}), highlighting the distinct contributions of the cone and shaft sections. This representation provides a framework for analysing soil penetration tests by linking needle tip geometry (root tip) and penetration resistance to the mechanical properties of the soil. By incorporating both geometric and mechanical factors, the energy-based approach offers a more biologically relevant analysis method, particularly for understanding root growth dynamics in the rhizosphere where complex interactions between roots, soil, and exudates occur.

CHAPTER 3

EFFECT OF SOIL MECHANICAL PROPERTIES, ROOT TIP GEOMETRY, AND MUCILAGE ON THE PENETRATION RESISTANCE TO ROOT GROWTH

3.1 Introduction

This chapter examines how root tip geometry, mucilage concentration, and soil water content collectively influence root penetration resistance. Soil samples with varying water content and bulk density were prepared using a mini-compaction apparatus with constant compaction energy, and different mucilage concentrations were incorporated to study their effects on penetration resistance. Penetration resistance was measured using needles with two distinct tip geometries: a sharp tip (semi-apex angle 15°) and a blunt tip (semi-apex angle 30°), driven at a constant velocity. The theoretical foundation for interpreting these results was provided in Chapter 2.

This study builds on the experimental framework of Ruiz et al. (2015, 2016, 2017), who already investigated how root tip geometry and soil water content affect penetration resistance. Using penetrometers with diameters of 1 mm and 2.5 mm, the study demonstrated that sharper tips (15° semi-angle) required significantly higher energy to displace soil compared to blunter tips (30° semi-angle). The results from this study aligned well with predictions from cavity expansion theory, particularly for the 15° tip. However, their experiments did not yet account for the presence of mucilage. In this chapter, I therefore extend their approach by introducing key modifications. First, a 1.5 mm diameter needle was used, bridging the gap between the sizes tested in previous work. Second, a controlled and constant penetration rate that mimics actual root growth was used to assess its influence on resistance. Third and most importantly, mucilage at different concentrations was incorporated to evaluate how soil water content, tip geometry, and mucilage concentration collectively affect penetration resistance. By comparing the results with those of Ruiz et al. (2016), the aim is to clarify how needle size and shape, and mucilage alter root-soil mechanical interactions. Specifically, it will be tested whether cavity expansion theory remains predictive

under these modified conditions and how mucilage, which can either reduce or increase penetration resistance depending on moisture levels, affects the performance of sharp versus blunt root tips. These findings will enhance our understanding of root penetration mechanics in real-world scenarios where dynamic soil properties and root exudates play a critical role.

3.2 Materials and Methods

3.2.1 Extraction of chia seed mucilage

Mucilage was obtained from chia seeds. For this, 10 g of chia seeds and 100 mL of water were mixed in a beaker and stirred continuously for 2 minutes (Ahmed et al., 2014). After this, the mixture was allowed to rest for 30 minutes. Next, a sieve with a mesh size of 500 µm was carefully placed inside a funnel on which the mucilage-water mixture was poured. A vacuum pump was used to create suction in the conical flask to increase the pace of extraction by drawing the mucilage into the flask, leaving only the seeds in the sieve. The collected chia seed mucilage was freeze-dried to obtain pure mucilage. Pure mucilage was then used to create mucilage solutions with different concentrations (0.1%, 0.3%, and 0.5% by weight) by mixing a known amount of pure mucilage with water. Mucilage solutions were stored in a refrigerator at 4º C before sample preparation.

3.2.2 Soil sample preparation

Soil samples were prepared using a silt loam soil containing 8.1% clay, 58.6% silt, and 33.3% sand obtained from an agricultural field near Karlsruhe, Germany (latitude: 49.137078º; longitude: 8.361419º). In a first step, the soil was sieved using a 600 µm sieve to remove coarse-grained particles, such as stones, roots, etc. Then, the soil was oven dried for 24 hours at 105º C. In a next step, a compaction test was performed using the mini-compaction apparatus under constant mechanical energy (Sridharan and Sivapullaiah, 2005). For this, soil was mixed with water in increments of 2% gravimetric water content and was compacted using a hammer of 1 kg falling from a height of 160 mm. Each sample was compacted into three layers with each layer receiving 33 hammer blows. The resulting compaction curve (Figure 3.1) shows the bulk density of the soil samples as a function of gravimetric water content. Based on the compaction curve, it was decided to prepare five replicate samples with water contents of 15%, 20%, 25%, and 30% and respective bulk densities (1.6, 1.7, 1.9, and 1.9 g/cm^3) to investigate the effect of water content and bulk density on the penetration resistance.

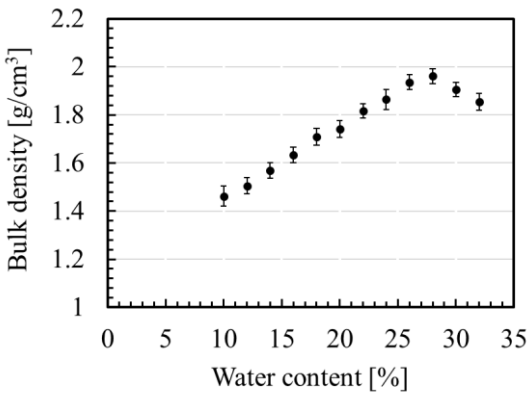

Figure 3.1 Compaction curve showing the bulk density [g/cm^3] as a function of gravimetric water content for a series of silt loam soil samples prepared with the same amount of mechanical energy.

3.2.3 Penetration resistance measurements using a rheometer

A rheometer (MCR102, Anton Paar GmbH, Germany) was used to measure the penetration resistance as function of insertion depth using two types of stainless-steel needles with a semi-apex angle of 15° (sharp) and 30° (blunt) and a diameter of 1.5 mm (as a proxy for roots). The length of the needle cones was 1.3 mm for the blunt needle and 2.8 mm for the sharp needle. A single penetration measurement was made in each of the five replicate soil samples. The insertion velocity of both types of needles was 2.5 mm min^{-1}, which is close to the velocity of 2 mm min^{-1} used in the study by Oleghe et al. (2017).

To examine the effect of the mucilage concentration on penetration resistance, experiments were conducted with varying mucilage concentrations (0%, 0.1%, 0.3%, and 0.5%). For each measurement, 100 µl of mucilage solution was applied to the surface of a soil sample and allowed to infiltrate. Before the needle was inserted in the middle of the region with the applied solution, the needle was rinsed with the respective mucilage solution. In total, the penetration resistance of 160 samples was investigated (4 water contents and associated bulk density × 4 mucilage concentrations × 2 needle types × 5 replicates).

3.2.4 Statistical analysis

To evaluate whether root tip geometry significantly affected penetration resistance, and to assess the effects and interactions of water content, mucilage concentration, and mucilage addition compared to unamended soil samples, a multi-way ANOVA was performed. For this, penetration resistance values for both needles for the same water content and mucilage concentration were grouped and analysed. To evaluate the combined effect of water content and mucilage concentration, a multi-factorial ANOVA was used. Here, the penetration

resistance values were grouped for water content and all mucilage concentrations were then compared to evaluate whether significant differences were observed for a given needle. When the ANOVA results suggested a significant difference (P value < 0.05), subsequent posthoc tests, such as the TukeyHSD and the Bonferroni approach, were used to identify between which groups the significant differences occurred. The statistical analysis was performed using the open software RStudio (RStudio Team, 2020).

3.3 Results

3.3.1 Effect of soil water content and tip geometry on predicted penetration resistance using cavity expansion models

The cavity expansion model presented in Chapter 2 showed that cohesion, elastic modulus, and the interfacial coefficient of friction of the soil determines the total penetration resistance. It is well known that these soil mechanical properties are significantly affected by soil bulk density, soil water content, and soil texture (Abbaspour-Gilandeh et al., 2018; Cokca et al., 2004; Mouazen, 2002). At high water content, the cohesion and elastic modulus (Bravo et al., 2014; Mouazen et al., 2002) as well as the interfacial friction (Abbaspour-Gilandeh et al., 2018) are significantly reduced, which will affect the penetration resistance. To illustrate how penetration resistance is affected by soil water content and different types of needles, the soil mechanical parameters in Table 3.1 were used to predict penetration resistance for blunt and sharp needles (Figure 3.2). The values in Table 3.1 represent typical values for cohesion, elastic modulus, and coefficient of friction for a silt loam soil at low and high-water contents. Figure 3.2 shows penetration resistance as a function of depth for blunt and sharp needle tips under low and high-water content conditions. The blunt needle (30º) corresponds to the spherical cavity expansion model, with a shorter cone length (l_c = 1.3 mm), while the sharp needle (15º) corresponds to the cylindrical cavity expansion model, with a longer cone length (l_c = 2.8 mm). These cone lengths mark the transition from tip penetration to shaft friction, which is reflected as a noticeable change in slope in the resistance curves.

Spherical cavity expansion models are commonly used to represent blunt needles. When a blunt needle penetrates the soil, it generates a three-dimensional, nearly isotropic stress field that radiates outward from the point of contact (Chadwick, 1959). This results in a large plastic zone and greater soil displacement, requiring higher energy for penetration. The associated stress distribution is marked by elevated radial and hoop stresses near the cavity wall, which diminish with distance (Ruiz et al., 2016). In contrast, cylindrical cavity expansion models are better suited to sharp or conical needle tips. Sharp needles concentrate stress along the

axis of penetration, producing a more directional, two-dimensional stress field that extends radially in a cylindrical pattern (Carter and Yeung, 1985). This leads to an elongated plastic zone along the shaft, where shaft friction and continuous shearing dominate the resistance mechanism. The distinction between the two models lies in how stress accumulates around the needle. Blunt needles distribute stress more uniformly across a larger area, increasing initial resistance. Sharp needles, with their pointed geometry, localize stress at the tip for easier entry, but frictional forces along the shaft become more prominent as depth increases.

The blunt needle consistently shows higher penetration resistance than the sharp needle at both water content levels, highlighting the role of tip geometry. The shorter, more abrupt shape of the blunt tip leads to greater soil displacement and resistance, especially under drier conditions. In contrast, the sharp needle with its longer cone shape causes a more gradual increase in resistance, consistent with the cylindrical expansion assumption. These results demonstrate the combined effects of water content, tip geometry, and cavity expansion model on penetration mechanics.

Penetration resistance increases with depth for all cases but is significantly reduced with increasing soil water content. This reduction applies to both tip shapes and reflects the decrease in soil strength and frictional resistance due to higher moisture. In particular, the frictional component of the resistance—visible beyond the cone length—increases more gradually under high water content, confirming the strong influence of moisture on shaft–soil interaction.

Table 3.1 Mechanical parameters for typical silt loam soil

Cohesion (N/mm^2)	*Elastic modulus* (N/mm^2)	*Co-efficient of interfacial friction*	*Description*
0.028	6	0.70	Low water content
0.010	2	0.30	High water content

Source: Obrzud and Truty (2012) and Minnesota Department of Transportation (2007).

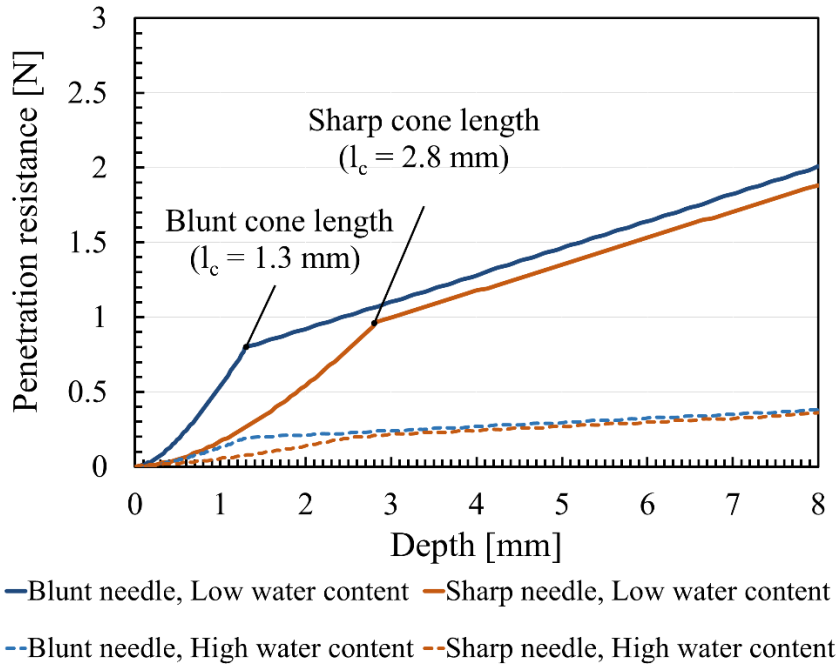

Figure 3.2 Penetration resistance for spherical cavity and cylindrical cavity model for blunt needle (30º) and sharp needle (15º) at 8 mm depth as function of high and low water content respectively.

3.3.2 Effect of water content and root tip geometry (cone shape) on the penetration resistance

Figure 3.3 shows the penetration resistance curves for both needle types for the four selected gravimetric water contents (and associated dry bulk density, see Figure 3.1). It can be seen that the penetration resistance increases sharply until the cone depth (l_c), beyond which a change in slope is observed for both needle types. As discussed in section 3.3.1, the insertion of the cone increasingly deforms the soil, which explains the initially steep increase in penetration resistance up to the cone depth. For shaft insertion depth ($Z - l_c$), the increase in penetration resistance is mainly due to frictional forces. At cone depth, the penetration resistance was significantly reduced for very high water content (30%) for both needles compared to the other water contents. In addition, the decrease of the slope during shaft insertion suggests that frictional forces were also strongly reduced at high water content for both blunt and the sharp needle. For the other three water contents, the penetration resistance for the sharp needle at total insertion of the needle up to 8 mm depth at 25% water content (bulk density 1.9 g/cm^3) was slightly higher than the penetration resistance for the samples with 15% and 20% water content (bulk densities of 1.6 and 1.7 g/cm^3, respectively). Similarly, the penetration resistance for the blunt needle at 20% water content was slightly higher than the penetration resistance of the samples with 15% and 25% water content. It can also be

observed that the effect of frictional forces on the total penetration resistance is significant at these water contents, suggesting the strong influence of soil-metal friction at lower water contents.

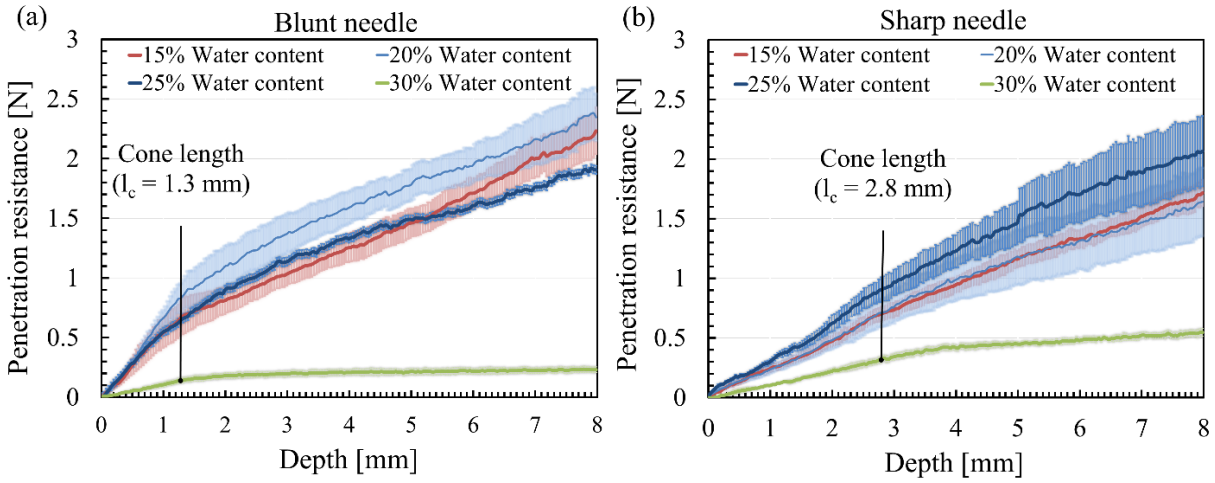

Figure 3.3 Penetration resistance for the (a) sharp (15º) and (b) blunt (30º) needle as a function of insertion depth for samples with different gravimetric water content (15%, 20%, 25%, and 30%). The shaded area represents ±1 standard deviation (SD) of five replicates.

Figure 3.4a and Figure 3.4b present the total energy required for needle insertion up to 8 mm depth (Z), and the energy required for shaft insertion depth ($Z - l_c$), for the sharp and blunt needle, respectively. At 15% and 20% water content, the ANOVA results suggest that the blunt needle required significantly higher energy than the sharp needle to reach a depth of 8 mm. For 25% water content, no significant difference in required energy was observed between the two needle types. Figure 3.4b shows that the effect of frictional forces for the blunt needle is significantly higher than the sharp needle at 15%, 20%, and 25% water content. The length of the shaft for the blunt needle (6.7 mm) is higher than the sharp needle (5.2 mm) and this has contributed to higher frictional forces. For 30% water content, the ANOVA results suggest that the sharp needle required significantly higher penetration resistance than the blunt needle for the total insertion depth of 8 mm, and the results also confirm that the sharp needle experienced significantly higher frictional forces than the blunt needle. At cone depth (l_c), the penetration resistance at 25% and 30% water content was higher for the sharp needle than for the blunt needle. These results clearly suggest that the four water contents/bulk densities used in my study affected the penetration resistance differently for both needle types. Because water content and bulk density are coupled in this experiment, it is difficult to clearly establish

the factors that determine the different behavior. Further investigation is required to clearly establish the dominant factors affecting the penetration resistance for both needle types.

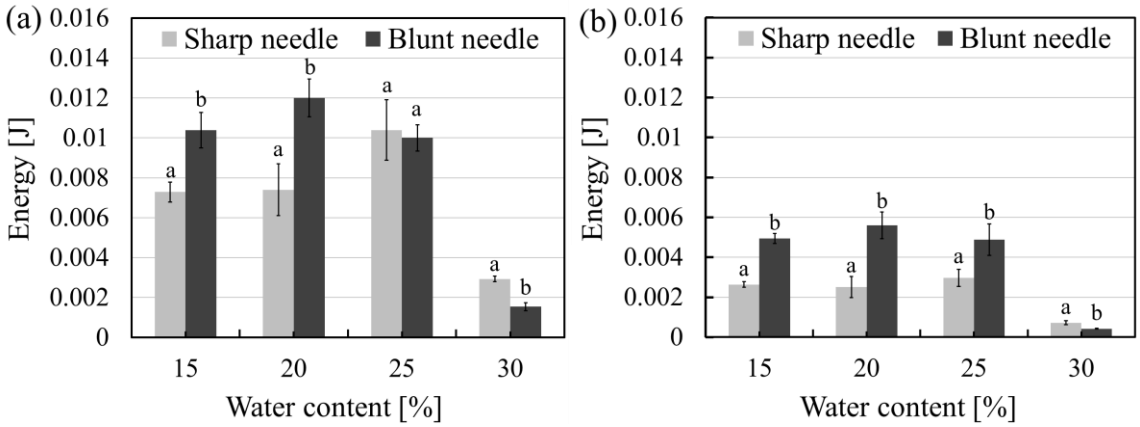

Figure 3.4 Energy required (a) total insertion depth of 8 mm and (b) shaft insertion for the sharp needle (15º) and the blunt needle (30º) needle as a function of gravimetric water content (15%, 20%, 25%, and 30%). Bars labelled with different lowercase letters (a, b) denote statistically significant differences between means of two values ($p < 0.05$).

To compare the experimental results with the cavity expansion model presented in section 2, Figure 3.5 shows a selection of experimentally obtained penetration resistance curves that can directly be compared to the modelling results presented in Figure 3.2. Although this comparison can only be made in a qualitative sense, the model captures several key features of the experimental results. At low water content, the model predicts a steep increase in penetration resistance up to cone depth (l_c) and a linear increase in frictional forces up to 8 mm depth for both needles. At very high-water content, the model predicted a significant reduction in penetration resistance at cone depth and a reduction in frictional forces for both needles. Both these features are also clearly observed in the experimental results. The model also predicted that the total penetration resistance for the blunt needle at 8 mm is higher than the penetration resistance for the sharp needle at low water content, which is also seen in the experimental results in Figure 3.5. For the high-water content, the model again predicted that the penetration resistance for the blunt needle is higher at 8 mm, which is not consistent with the experimental results. In summary, the cavity expansion model captured the behavior of the needles at low water content but showed limitations at very high water content.

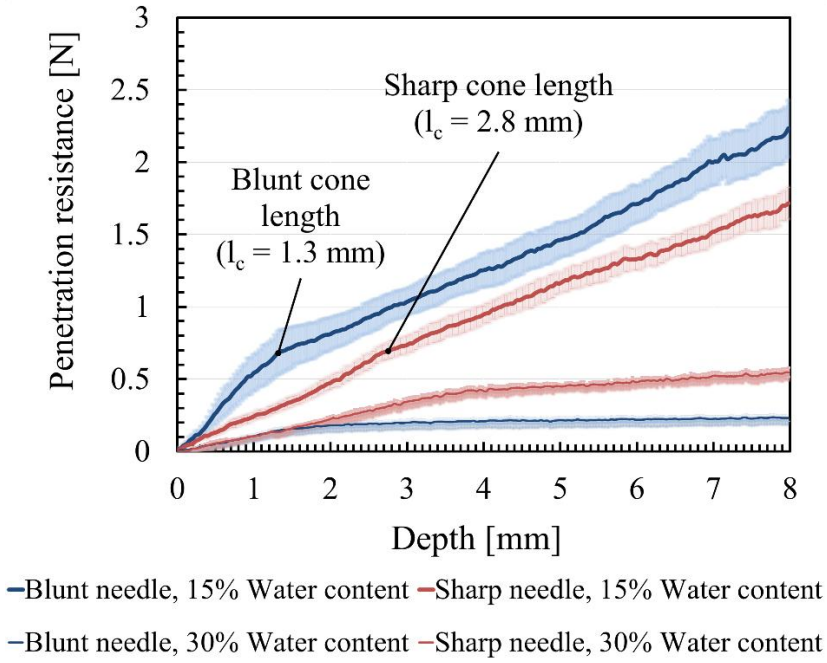

Figure 3.5 Penetration resistance for the sharp needle (15º) and the blunt needle (30º) needle as a function of insertion depth for two gravimetric gravimetric water content (15% and 30%). The shaded area represents ±1 standard deviation (SD) of five replicates.

3.3.3 Effect of addition of mucilage on penetration resistance

Figure 3.6 exemplary shows the measured penetration resistance as a function of depth for the blunt and sharp needle up to the total insertion depth of 8mm (Z) for the samples with 15% water content and different mucilage concentrations. The addition of mucilage reduced penetration resistance for both needles significantly. This significant reduction in penetration resistance is already observed at the cone depth. The reduction in slope for shaft insertion suggests that the addition of mucilage also reduced frictional forces for both needles. The penetration resistance also showed a slight increase in slope between 5-7 mm depth for both needle types. This may be related to the application method for mucilage where a droplet was applied at the surface, which may not have infiltrated beyond this depth.

Figure 3.7 shows the total energy required for needle insertion up to 8 mm (Figure 3.7a-d) and for shaft insertion (Figure 3.7e-h) for both needle types and samples with different mucilage concentrations (0, 0.1%, 0.3%, and 0.5%) and water content (15%, 20%, 25%, and 30%). Statistical analysis using ANOVA suggests a significant reduction ($p < 0.05$) in required energy for needle insertion up to 8 mm depth in samples with mucilage in case of the samples with 15%, 20%, and 25% water content for both needle types. No significant reduction in energy was observed at 30% water content. This suggests that the effect of the addition of

mucilage on penetration resistance is limited in soils with high water content. The results also suggest that it is more the presence of mucilage instead of the concentration that affects penetration resistance, since no significant differences were observed for the different concentrations, except for the penetration of the blunt needle into samples with 0.5% mucilage concentration at 15% water content.

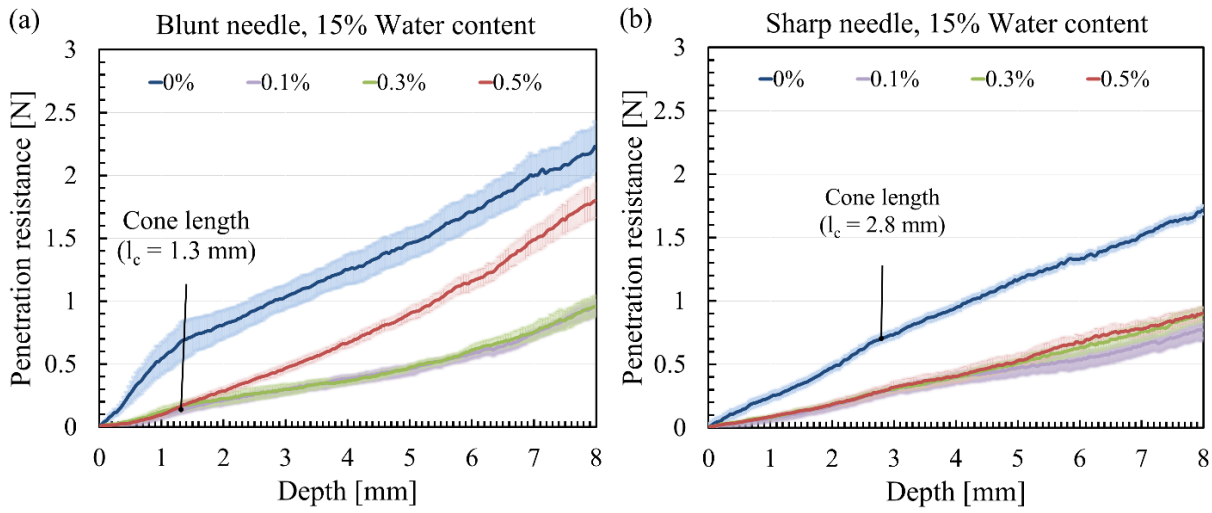

Figure 3.6 Penetration resistance as a function of insertion depth for the (a) blunt needle (30º) and (b) sharp needle (15º) for different mucilage concentrations (0%, 0.1%, 0.3%, and 0.5%) for 15% gravimetric water content. The shaded area represents ±1 standard deviation (SD) of five replicates.

The addition of mucilage also significantly reduced the energy due to shaft insertion i.e. contribution of frictional forces (Figure 3.7e-h at 15% and 20% water content for both needles). ANOVA analysis confirms that the frictional energy reduction at 25% water content was only significant for the blunt needle. The addition of mucilage did not reduce the energy required to overcome the frictional forces at 30% water content. As in the previous case, different mucilage concentrations did not significantly affect the required energy for shaft insertion, except for the blunt needle with 0.5% mucilage concentration at 15% water content. In this case, needle insertion required significantly higher energy compared to concentrations of 0.3% and 0.1% (Figure 3.7e). Interestingly, the introduction of mucilage with 0.5% concentration at 15% water content for the blunt needle did not lead to a reduction in energy for shaft insertion compared to samples without mucilage.

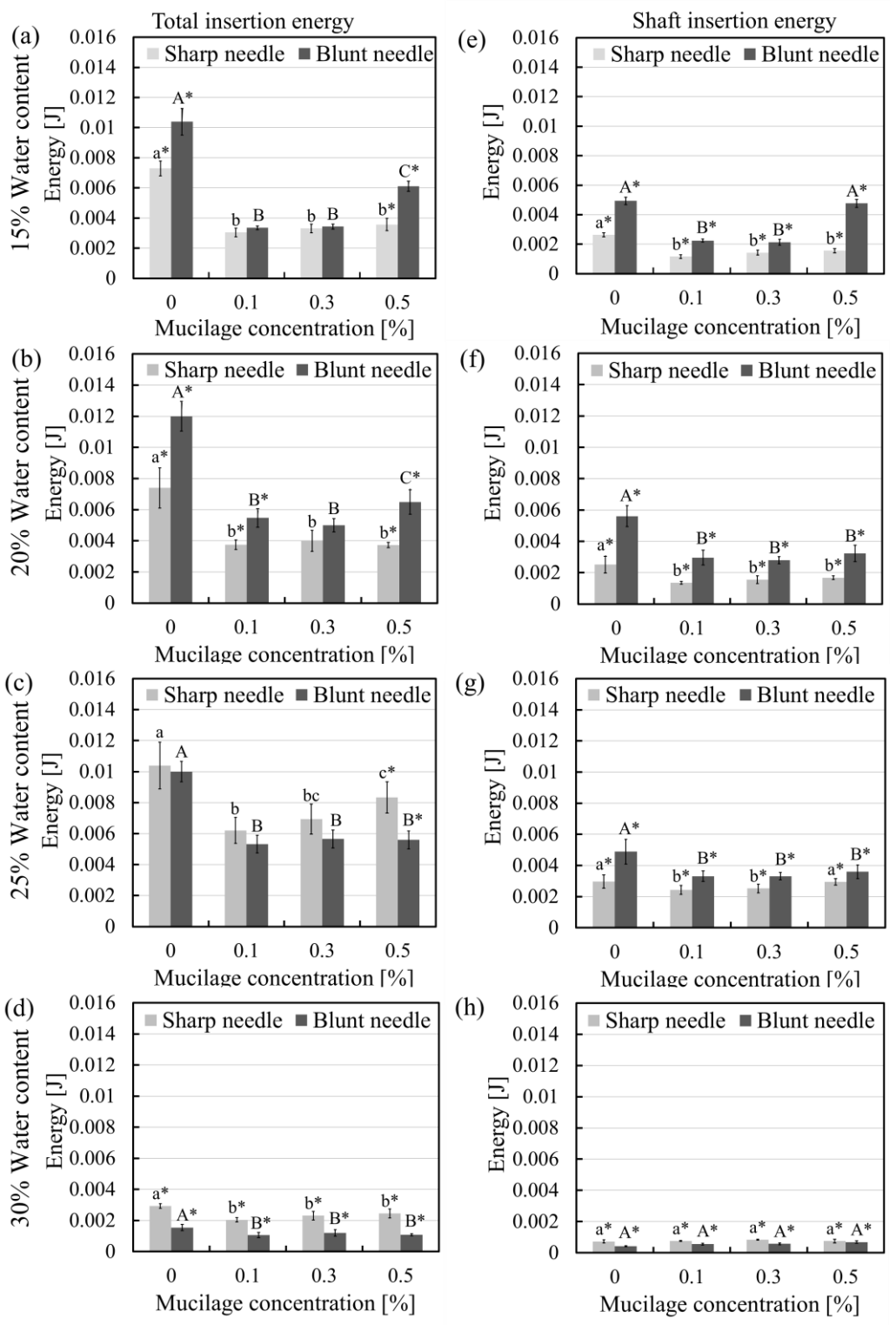

Figure 3.7a-d Total energy required to reach an insertion depth of 8 mm and 10e-h energy required shaft insertion at 15%, 20%, 25%, and 30% gravimetric water content for the blunt and sharp needles for mucilage concentrations of 0, 0.1%, 0.3%, and 0.5%, respectively. Letters above bars denote significant differences between mucilage concentrations within the same needle type (Tukey HSD, $p < 0.05$). Asterisks indicate significant differences between blunt and sharp needles at the same mucilage concentration (*$p < 0.05$). Error bars represent standard deviation of the five replicates.

The significantly higher energy that was observed at total insertion depth up to 8 mm for 0.5% mucilage concentration at 15% water content for the blunt needle is predominantly due to frictional forces. Consequently, there was significant differences in energy between mucilage concentrations at 15% water content for the shaft insertion. The significant increase in penetration resistance for 0.5% mucilage concentration at 15% water content for the blunt needle can be clearly seen after the cone depth (Figure 3.6), indicating that the significant increase is solely attributable to frictional forces. However, such behaviour was not observed for the sharp needle.

3.4 Discussion

Movement of heavy machinery on agricultural soil under varying water content can significantly affect soil density and degree of soil compaction. A subsequent decrease in water content during the dry season in a highly compacted soil layer poses a significant challenge for root growth. The experiments in my study were designed to evaluate the penetration resistance of soil samples under constant compacting energy. The compaction curve (Figure 3.1) illustrates that an increase in water content increased the bulk density up to 27% gravimetric water content (peak point on the curve). A further increase in water content decreased the bulk density significantly. This suggests that a certain amount of water in soil acts as a lubricant under compacting pressure, reducing interparticle friction and allowing for closer packing of soil particles. The excess amount of water turns soil into slurry and therefore significantly reduces soil bulk density (Gurtug and Sridharan, 2004; Mirreh and Ketcheson, 1973). The water content and bulk density in this study are inherently coupled, making it difficult to disentangle their individual effects on penetration resistance.

This study confirmed the significant effect of very high water content on reducing soil penetration resistance. A sharp decrease in penetration resistance at water contents higher than 30% was observed for both needle types. Penetration resistance for drier soil samples was significantly higher than in wet samples even with similar bulk densities (25% and 30% water content). These findings are consistent with previous studies (Rosskopf et al., 2022; Souza et al., 2021) and can be attributed to the weakening of interparticle forces at high water content, allowing soil particles to displace more easily during penetration. Although I expected a gradual decrease in penetration resistance with increasing water content for dry and moist soil, no clear trend was observed for water contents below 25% (and their respective bulk densities) for both needle types. A systematic testing of soil mechanical properties is required to disentangle the combined effects on penetration resistance.

Previous studies often evaluated results by calculating the energy required by a penetrometer to reach specific soil depths. Some studies calculated energies for the entire insertion depth of the probe, while others considered mean energies between certain depths (2 to 4 mm). I observed that all penetration resistance curves followed a clear trend along the depth of needle insertion. The slope of the penetration curves changed significantly at cone insertion depth for both needles. It is well known that root elongation in soil occurs predominantly due to the extension of the root tip, gradually displacing soil particles (Bengough et al., 2016b). Therefore, the penetration resistance experienced by the needle tip (cone) is more relevant compared to the shaft frictional forces when understanding root growth. To understand the complex interplay between needle tip geometry (cone shape) and needle shaft on penetration resistance, the energy for needle insertion up to the total depth (8 mm) and the shaft depth were separately determined. This provided insights into the influence of cone and shaft on total penetration resistance. Meanwhile, the energy required for shaft insertion reveals how needle shape influences frictional forces as it continues to penetrate the soil. This approach helped to understand some counterintuitive results and their relevance for soil-root interactions. For lower water contents (15% and 20%) at total insertion depth of 8 mm, the blunt needle required significantly higher energy than the sharp needle. No significant difference between the two was observed at 25% water content, while the sharp needle recorded higher penetration resistance than the blunt needle at very high-water content (30%). By analysing the energy components separately, it was identified whether this unexpected behaviour was due to differences in penetration resistance from cone insertion, frictional forces, or a combination of both. At 15% water content, the blunt needle recorded significantly higher energy than the sharp needle for both needle components. The opposite occurred at 30% water content. At 20% water content, cone energies for both needles were similar, while at 25% water content, the sharp cone recorded significantly higher energy than the blunt cone. This confirms that cone shape influences penetration resistance differently, depending on varying physical properties of soil. While the observed effects are significant, continued investigation into root tip geometry will provide a more comprehensive picture of its role in root-soil interactions.

Studies have shown varying results in determining penetration resistance regarding penetrometer design and soil conditions. (Bengough and Mullins 1990) used a 1 mm diameter penetrometer inserted at 1 mm min^{-1} into sandy soil and reported higher penetration resistance for blunt cones compared to sharp cones. Conversely, Ruiz et al. (2016) used 1 mm and 2.5

mm penetrometers inserted at 10 mm min^{-1} into sandy and loamy soils and found that penetration resistance was higher for sharp cones than blunt cones in both soil types. These contrasting findings highlight that penetrometer size and insertion rate significantly influenced penetration resistance, underscoring the importance of considering these parameters when interpreting results across different studies. Penetration resistance was three times higher at insertion rates of 10 mm min^{-1} compared to 3 mm min^{-1}, but no significant difference was observed between rates of 0.03 and 3 mm min^{-1} (Ruiz et al., 2017). In this study I used a 1.5 mm diameter penetrometer inserted into silt loam soil at 2.5 mm min^{-1}, I observed that the energy required for needle insertion varied significantly with soil water content. At low water content, the blunt cone required significantly more energy than the sharp needle. Increasing water content reversed this behaviour, resulting in higher energy for the sharp needle. The shape of the penetrometer cone influences soil deformation during insertion (Paniagua et al., 2015). As suggested by Greacen and Sands (1980) and Ruiz et al. (2016), soil particles tend to deform radially around sharp needles, while they accumulate and compact in front of blunt needles. Therefore, when soil particles jam due to local soil compaction around the blunt needle, this adds further resistance. This scenario could resemble compacted soil samples with lower water content, where stronger interparticle forces hold soil particles together and prevent easy deformation. Conversely, soil samples with higher water content allow easier particle movement, significantly reducing required energy.

Based on the limited studies focusing on penetration resistance models, the cavity expansion model provided promising results. The model predictions showed good qualitative agreement with the experimental results, particularly at low water contents. The model accurately predicted both the steep increase in penetration resistance at cone insertion depths and the linear increase in frictional forces. The cavity expansion model used in this study accurately predicted the behavior of both needle types for dry soil samples: the blunt needle with the spherical model and the sharp needle with the cylindrical model. The model confirmed that the cohesive and elastic properties of the soil play crucial roles in predicting penetration resistance. The Mohr-Coulomb failure criterion for purely cohesive soils that was adopted in the cavity expansion model fitted particularly well with the highly cohesive silt loam soil used in this study, effectively capturing the majority of interparticle forces between soil particles. While the model correctly predicted the significant reduction in penetration resistance at low water content for both needle types, the predictions diverged from experimental results at very high water content, especially for the blunt needle. Specifically, the model predicted higher

penetration resistance for the blunt needle at 8 mm depth for high water content, but the experimental results showed the opposite. Ruiz et al. (2016) also already noted that the accuracy of the cavity expansion model was less at high water contents in particular for blunt needles. This suggests that additional factors not accounted for in the current model or violations of the model assumptions may have influenced the diverging results at high water content.

The addition of chia seed mucilage significantly reduced penetration resistance for both needles at cone insertion depth and decreased frictional forces during shaft insertion. The findings of this study align well with the results of Oleghe et al. (2017), who reported reduced penetration resistance and enhanced root elongation in soil-mucilage mixtures. The different mucilage concentrations (0.1%, 0.3%, and 0.5%) used in my study did not significantly affect the required energy for penetration. Only, the blunt needle at 15% water content with 0.5% mucilage concentration showed significantly higher energy requirements, particularly due to increased frictional forces. The effect of mucilage on penetration resistance was limited in soils with high water content (30%). This suggests that the lubricating effect of mucilage becomes negligible close to saturation, as soil particles are already in a freely moving state offering minimal resistance to needle insertion.

I observed a slight increase in penetration resistance between 5-7 mm depth in mucilage-treated samples. This effect likely originates from my mucilage application method, where I applied a droplet at the surface, potentially limiting infiltration beyond this depth. My approach differs from previous studies (e.g., Naveed et al., 2017; Rosskopf et al., 2022), which mixed mucilage directly with soil at concentrations defined as mass of mucilage per mass of soil; instead, I defined mucilage concentration as mass of mucilage per mass of water to reflect the natural root-secreted mucilage concentration of 0.45% (Oleghe et al., 2017b). While my method more closely represents natural root exudation and growth processes, this methodological difference should be considered when comparing results across studies. The limited effect of mucilage concentration in this study contrasts with findings from Rosskopf et al. (2022), who reported that mucilage concentration could significantly increase or decrease penetration resistance depending on soil moisture content. These contrasting results likely stem from differences in mucilage concentration ranges, application methods, and energy analysis techniques. I used lower concentrations compared to Rosskopf et al. (2022) due to my surface application method. Although investigating a wider range of mucilage

concentrations could provide additional insights, my current application method may limit the use of higher concentrations due to poor soil dispersibility.

My findings have important implications for understanding root growth in varying soil conditions and how mucilage modifies soil mechanical properties. The significant reduction in penetration resistance with mucilage addition suggests that root exudates may facilitate easier root elongation, particularly in drier soils. Future research should explore a wider range of mucilage concentrations and alternative application methods to better represent root exudation processes. Additionally, studies that decouple the effects of water content and bulk density could provide clearer insights into the dominant factors affecting penetration resistance for different needle types and in the presence of mucilage.

3.5 Conclusions

This study systematically investigated how soil water content (15%, 20%, 25%, 30% gravimetric), needle tip geometry (30° blunt vs 15° sharp semi-apex angles), and chia seed mucilage addition (0.1%, 0.3%, 0.5% concentrations) influence penetration resistance relevant to root growth. The cavity expansion modeling approach - employing spherical theory for blunt needle and cylindrical theory for sharp needle - successfully predicted penetration resistance based on soil strength parameters (cohesion and elastic modulus) across moisture levels.

Experimental measurements validated these models, showing that increasing water content significantly reduces penetration resistance due to decreased soil strength parameters. While both models accurately predicted resistance in drier soils (15-25% water content), discrepancies emerged at saturation (30%), particularly for the spherical blunt-needle model which overestimated resistance compared to experimental results. This highlights the need for moisture-dependent adjustments in theoretical models.

The addition of chia seed mucilage consistently reduced penetration resistance at lower water contents (15-25%), confirming its role as an effective bio-lubricant. However, this effect diminished at 30% water content where soil particles were already highly mobile. An unexpected finding was the increased resistance for blunt needles at 15% water content with 0.5% mucilage concentration, potentially caused by uneven mucilage distribution along the penetration depth. These results demonstrate complex, non-linear interactions between soil moisture and mucilage properties that warrant further investigation.

The comprehensive analysis elucidated the critical interdependence between soil water content, needle tip geometry, and mucilage addition in governing penetration dynamics. The spherical cavity model for blunt needles and cylindrical model for sharp needles each showed distinct effectiveness depending on soil moisture conditions. While providing reliable predictions in drier soil, both models revealed limitations at saturation, particularly the spherical model's overestimation of blunt needle resistance. This suggests current theories may not fully capture soil behavior under extreme wet conditions.

The mucilage experiments demonstrated concentration-independent lubrication effects at lower water contents, though addition of mucilage itself became ineffective at 30% moisture. The anomalous behavior at 15% water content with 0.5% mucilage concentration, uneven distribution of mucilage over depth caused an increase in frictional energy thereby increasing overall energy requirements. These findings have important implications for understanding plant root growth, as they reveal how root exudates disperse in soil and facilitate penetration in drier soils while becoming less critical in saturated conditions.

My novel methodological approach of separating cone insertion energy from frictional energy provided unique insights into penetration mechanics. This distinction revealed how needle geometry differently affects initial soil deformation versus sustained penetration, with blunt tips requiring more energy for initial displacement while sharp tips faced greater frictional resistance during continued penetration. Such analysis offers valuable perspective on the shape and characteristics of penetration resistance curves.

In conclusion, this study advances our understanding of the mechanical constraints on root growth and highlights the intricate interplay between soil physical properties, root geometry, and root exudates. These findings contribute to our understanding of the mechanical constraints on root growth and underscore the need for considering multiple factors when assessing soil physical properties in relation to plant root development. The observed complexity in needle behavior across different water contents and bulk densities emphasizes the importance of context-specific assessments in soil-root interactions.

CHAPTER 4

EFFECTS OF SOIL TEXTURE, MUCILAGE TYPE AND CONCENTRATIONS ON THE PENETRATION RESISTANCE TO ROOT GROWTH

4.1 Introduction

This chapter investigates how different mucilage types and concentrations affect root penetration resistance in various soil textures and moisture conditions. In particular, chia and flax seed mucilage at 0.1% and 0.5% concentrations were examined to understand their impact on soil mechanical properties and root growth dynamics. This work builds upon previous work while introducing key methodological improvements to better simulate natural root-soil interactions. Previous research by Rosskopf et al. (2022) and Ruiz et al. (2016, 2017) established important relationships between soil properties and penetration resistance. Their comparative studies of loam and sandy soils revealed several consistent findings. First, loam consistently demonstrated higher penetration resistance than loamy sand across all tested moisture levels. Second, increasing water content reduced penetration resistance in both soil types. Third, maize and chia seed mucilage showed that mucilage can either increase or decrease penetration resistance depending on specific combinations of water content and soil texture. While these studies provided valuable insights, they relied on homogeneous mixtures of soil and mucilage. This mucilage application strategy does not accurately reflect how roots naturally exude mucilage in soil.

In this chapter, this limitation is addressed through several important innovations. First, a droplet application method is used that introduces small and controlled amounts (0.1 ml) of mucilage at specific locations, better mimicking natural root exudation. Additionally, the scope of tested mucilage types was extended by including flax seed mucilage alongside chia seed mucilage. By maintaining a consistent bulk density (1.6 g/cm^3) while varying water content (9-18%), the effects of soil texture (comparing loam vs sand) under controlled conditions can be better evaluated. The inclusion of different mucilage types and concentrations allows to identify specific patterns in how root exudates (mucilage) modify

soil physical properties. These methodological improvements are expected to provide insights into important practical applications. By better understanding how natural root exudation processes affect rhizosphere physical properties, more effective crop breeding strategies and soil management approaches can be developed.

4.2 Materials and methods

4.2.1 Extraction of mucilage

Mucilage was extracted from chia and flax seeds by mixing 10 g of seeds with 100 ml of water. The mixture was stirred for 2 minutes and left to stand for 30 minutes (Kroener et al., 2018). Due to the difficulty in separating seeds from mucilage, a vacuum pump was used to create suction in a conical flask. A funnel fitted with a 500 µm mesh sieve was placed on the neck of the flask, and the seed-mucilage mixture was poured through. The setup was sealed with parafilm to ensure efficient separation. After extraction, both mucilage types were freeze-dried to obtain pure mucilage, which was then diluted to 0.1% and 0.5% concentrations by weight with water. The prepared mucilage was stored at 4°C until soil sample preparation.

4.2.2 Soil sample preparation

To evaluate different types of soil texture, two soil types were used in this study: a loam soil from Selhausen, Germany (13% sand, 70% silt, 17% clay) and a loamy sand from Kaldenkirchen, Germany (60.3% sand, 33.2% silt, 6.4% clay). The soil was sieved using a 2 mm sieve and oven-dried at 105°C for 24 hours. They were then mixed with water to obtain samples with a gravimetric water content of 9%, 12%, 15%, and 18%. During sample preparation, samples were compacted using a mini-compaction apparatus in a mould with a 38 mm diameter and 45 mm height. Compaction was achieved using a 1 kg hammer falling from a height of 160 mm to reach a constant density of 1.6 g/cm³.

4.2.3 Penetration resistance measurements using rheometer

Penetration resistance was measured using a rheometer (MCR102, Anton Paar GmbH, Germany) equipped with a stainless-steel needle with a diameter of 1.5 mm and a semi-apex angle of 30° (cone length of 1.3 mm). The needle was pushed into the soil samples at a constant speed of 2.5 mm/min to a total insertion depth of 8 mm while continuously recording penetration resistance. To evaluate the effect of different types of mucilage, 0.1 ml of chia or flax seed mucilage with 0%, 0.1%, and 0.5% mass concentrations were applied to the soil sample surface before needle insertion. Before insertion, the needle was also rinsed with the

respective mucilage solution. In total, 144 samples were investigated (2 soil types × 4 water contents × 2 mucilage types × 3 concentrations × 3 replicates).

4.3 Results

Findings reveal significant variations in soil penetration resistance across different soil types and water contents, shedding light on the complex interplay between soil texture and water availability in the rhizosphere. Figure 4.1 provides a visual representation of these differences, illustrating the penetration resistance curves for both soil types across a range of gravimetric water contents. In loam soil, particularly at low water content the penetration resistance increased sharply with depth, reaching a maximum at the total depth ($Z = 8\,mm$). This increase was particularly pronounced during the initial insertion phase, corresponding to the 0 - cone depth (l_c). This pattern suggests that roots in loam soil may encounter rapidly increasing resistance as they attempt to penetrate deeper layers. In contrast, loamy sand displays a more gradual increase in penetration resistance for both 0 - cone and cone - 8 mm depths, indicating potentially easier root penetration in sandy soils. As anticipated, the study found that penetration resistance at 0 - cone depth significantly decreased with increasing water content for both soil types. This trend underscores the critical role of soil moisture in facilitating root growth. The reduction in the slope of the penetration resistance curve along the cone – 8 mm depth ($Z - l_c$) further emphasizes how water content contributes to reducing shaft frictional forces in both soil types. Figure 4.2 shows the energy required for needle insertion for 0 - 8 mm (U_T) and for cone – 8 mm (U_{F_R}). Statistical analysis using ANOVA (Figure 4.2a) confirms that the penetration into loam requires several times more energy than the penetration into loamy sandfor all water contents. The analysis also confirmed that the energy required for the total insertion of needle 0 - 8 mm depth decreased significantly with increasing water content for both soil types. Figure 4.2 provides crucial insights into the energy requirements for needle insertion, serving as a proxy for root penetration energy. This finding highlights the considerable challenges roots may face when growing in finer-textured soils like loam. The results also demonstrate that the energy required for the total insertion needle of 0 - 8 mm depth decreased significantly with increasing water content for both soil types, reinforcing the importance of adequate soil moisture for root growth.

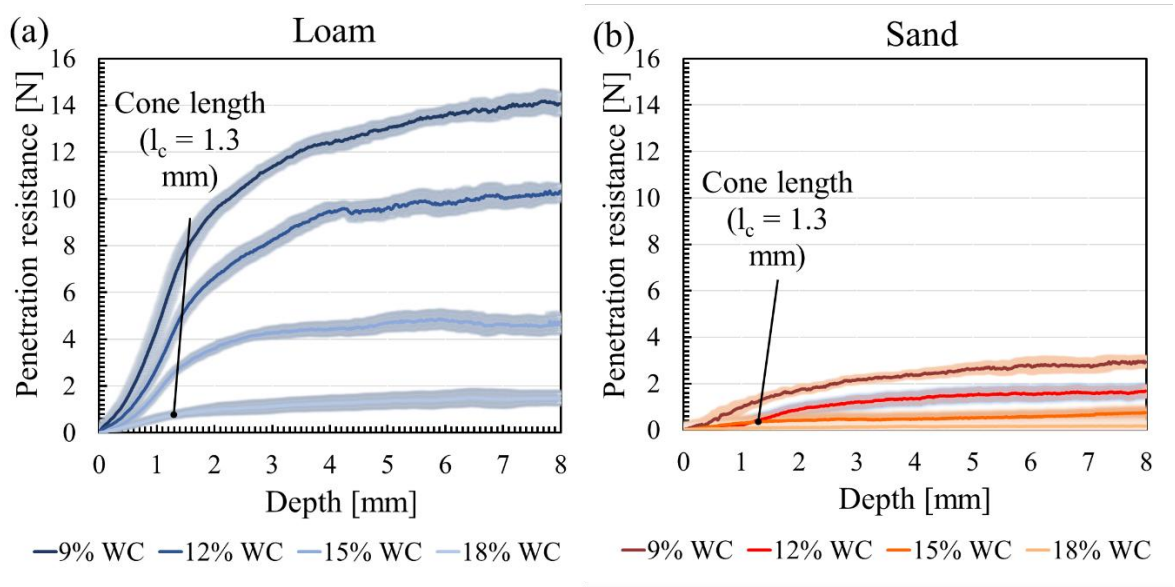

Figure 4.1 Penetration resistance for (a) loam and (b) loamy sandas a function of insertion depth for samples with different gravimetric water content (9%, 12%, 15%, and 18%). The shaded area represents ±1 standard deviation (SD) of the triplicates.

Interestingly, while the energy required for penetration in loamy sand with 18% water content was very low, but the energy needed to penetrate loam remained significantly higher at this water content. This observation suggests that even at higher moisture levels, roots in loam soils may still encounter substantial resistance. Figure 4.2b further confirms that the energy required for needle for cone - 8 mm depth (shaft insertion) plays a substantial role in determining the total required energy for both soil types, especially at lower water contents. In a next step, the impact of mucilage addition on penetration resistance across soil types and water contents is evaluated. Figures 4.3a-d present the penetration resistance curves for loamy sand with chia seed mucilage at different concentrations (0%, 0.1%, and 0.5%) and various gravimetric water contents. The addition of mucilage reduced penetration resistance at total depth (Z) for samples with water contents of 9%, 12%, and 15%. This reduction suggests that mucilage secretion by roots could play a crucial role in facilitating root penetration, particularly in drier soil conditions. However, at 18% water content, the effect of adding mucilage was negligible, indicating that the benefits of mucilage may diminish in well-hydrated soils. Figures 4a-d also suggest there is minimal mucilage impact in reducing penetration resistance for cone - 8 mm depth ($Z - l_c$) for both mucilage concentrations. This observation indicates that mucilage only aided initial penetration but didn't reduce frictional forces.

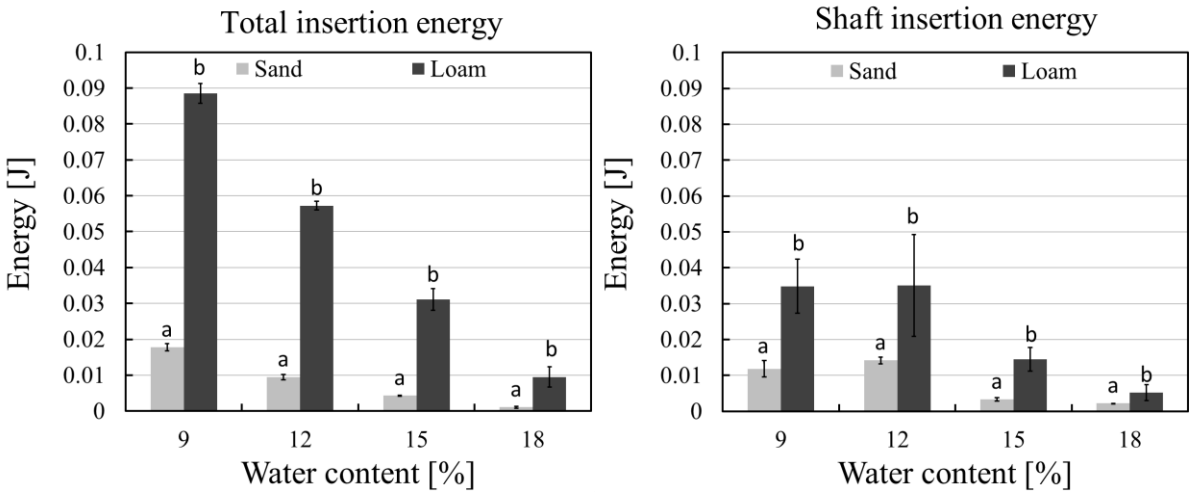

Figure 4.2 Energy required for penetration into loam and loamy sand for (a) the total insertion of needle 0 - 8 mm depth and (b) cone - 8 mm depth (shaft) for samples with different gravimetric water contents (9%, 12%, 15%, and 18%). Bars labelled with different lowercase letters (a, b) denote statistically significant differences between means of two values ($p < 0.05$).

The ANOVA results for the energy requirements (Figures 4.4a and 4.4b) support the observed trends in penetration resistance, showing a statistically significant reduction in total energy (U_T) for total depth 0 - 8 mm (Z) at 9% water content (Figure 4.4a). However, only a marginal variation in shaft frictional energy (U_{F_R}) was noted for cone - 8 mm depth (Figure 4.4b), further indicating that chia mucilage's primary effect is on easing initial penetration rather than overcoming frictional forces during deeper insertion. Figure 4.4b shows that mucilage addition only slightly reduced the energy required for cone - 8 mm depth at this water content, suggesting that mucilage primarily reduced the initial penetration resistance rather than the total insertion depth.

Figure 4.3b and 4.3c show that for the samples with 12% and 15% water content, mucilage addition reduced the penetration resistance for 0 - cone depth. However, for cone - 8 mm depth, the penetration resistance seems to gradually increase, overlapping with the curve for samples without mucilage condition. Particularly, the penetration resistance curve for 0.5% mucilage concentration with 12% gravimetric water content rises above the curve without mucilage.

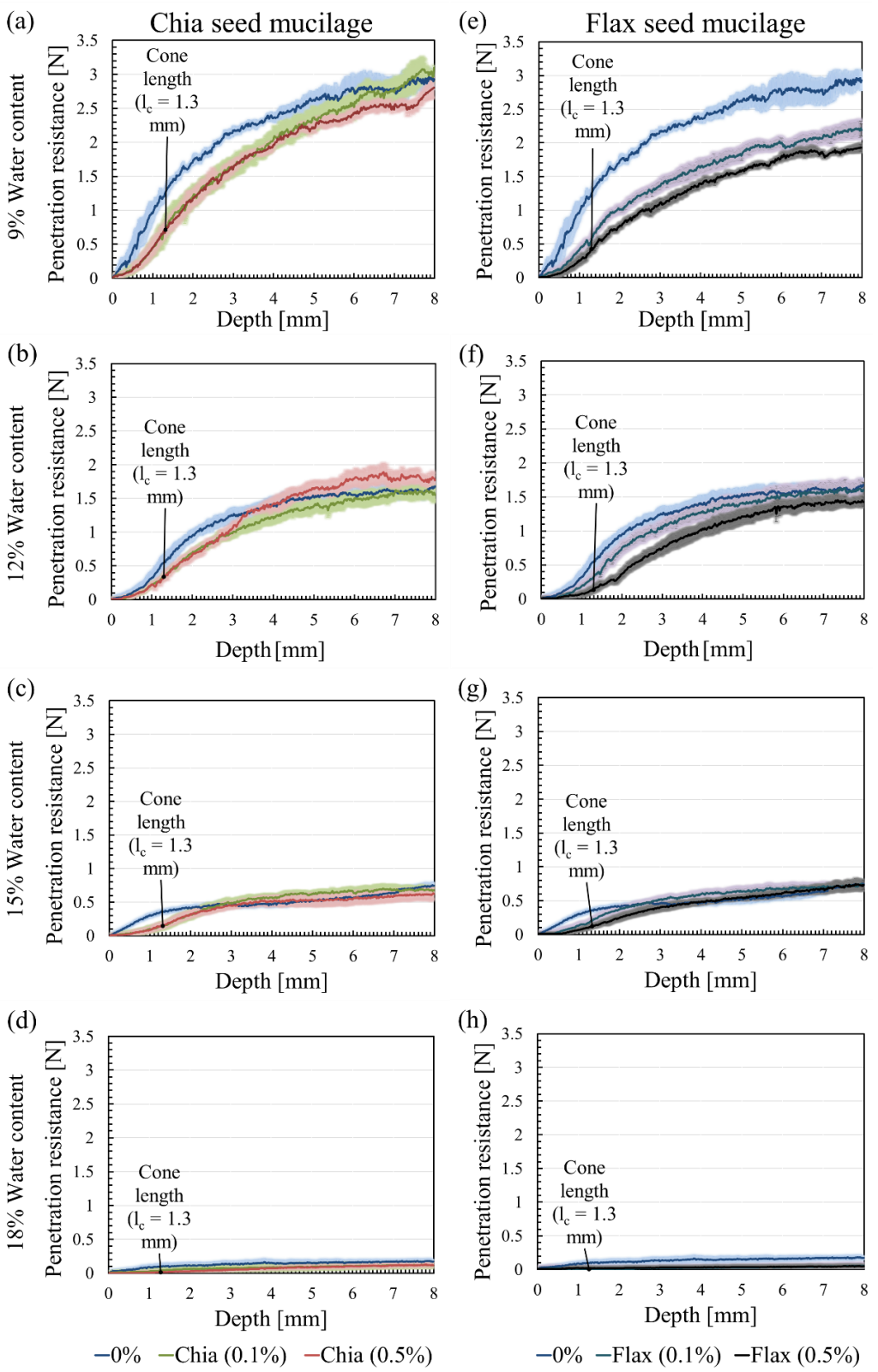

Figure 4.3 Penetration resistance as a function of insertion depth for loamy sand with the addition of (a-d) chia seed mucilage and (e-h) flax seed mucilage with concentrations 0%, 0.1%, and 0.5% for gravimetric water contents of (a,e) 9%, (b,f) 12%, (c,g) 15%, and (d-h) 18%, respectively. The shaded area represents ±1 standard deviation (SD) of the triplicates.

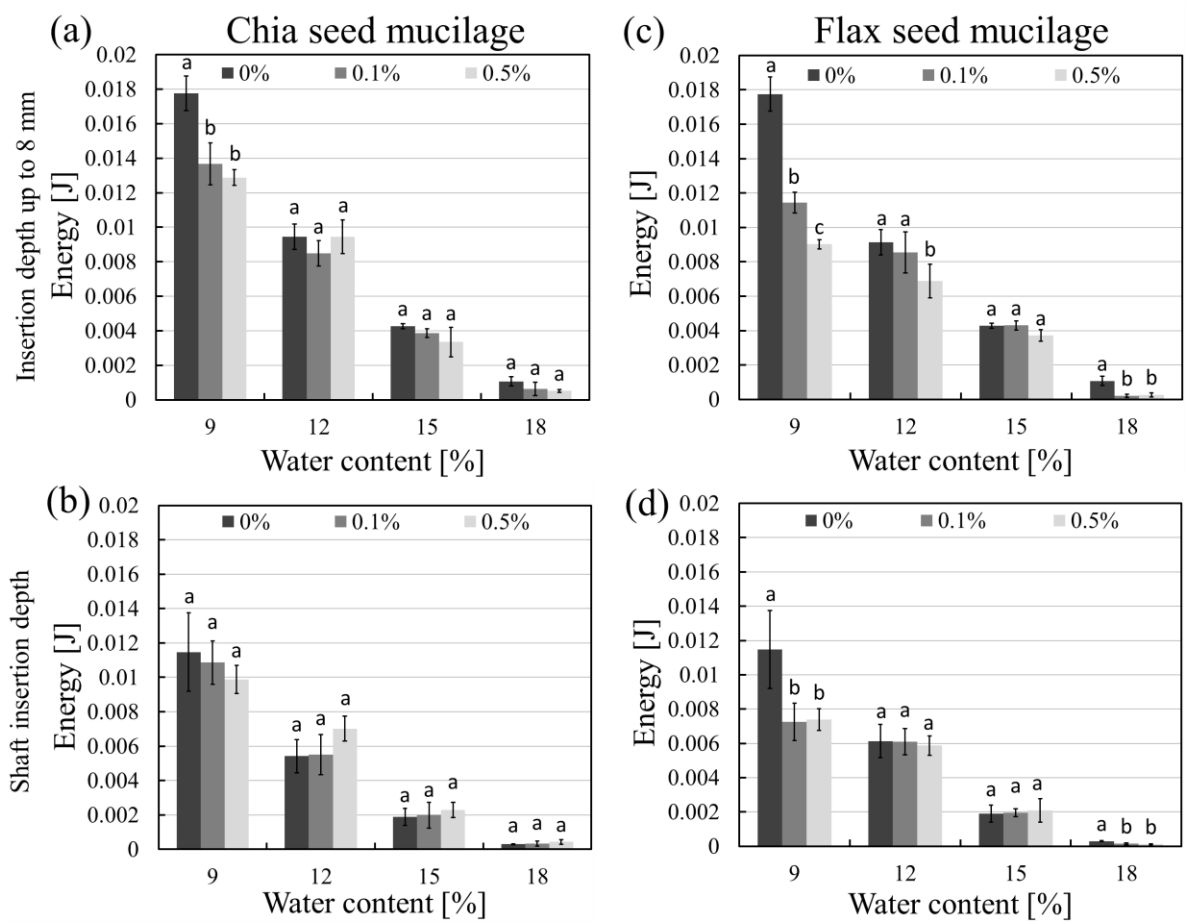

Figure 4.4 Required energy for insertion into loamy sand sample with the addition of (a,b) chia seed and (c, d) flax seed mucilage at the (a,c) full insertion depth of 8 mm and (b,d) beyond the full cone insertion depth for mucilage concentrations of 0%, 0.1% and 0.5% and gravimetric water contents of 9%, 12%, 15%, and 18%. Bars labelled with different lowercase letters (a, b) denote statistically significant differences between means of two values ($p < 0.05$).

Figures 4.4a and 4.4b indicate that mucilage has no significant effect on the energy required for total insertion depth and shaft insertion depth in soil samples with gravimetric water contents of 12%, 15%, and 18%. However, ANOVA analysis confirms a significant reduction in energy for cone penetration (0 - cone depth) at 12% and 15% water content. The increased frictional resistance observed in Figures 4.3b and 4.2c, particularly at depths of 3 - 6 mm for 12% and 15% water content appears to mask mucilage's influence on the total energy requirement. Finally, the results in Figures 4.3 and 4.4 show that while chia seed mucilage significantly reduces penetration resistance at a 9% water content in loamy sand for both total and shaft frictional energies.

Comparative analysis using flax seed mucilage (Figures 4.3e-h) reveals both similarities and differences with chia seed mucilage. Like chia seed mucilage, flax seed mucilage reduces penetration resistance at cone insertion depth (l_c) for water contents of 9%, 12%, and 15%. However, the reduction in penetration resistance is more pronounced in flax seed, especially at gravimetric water contents of 9% and 12%. Unlike with chia seed mucilage, a substantial difference in penetration resistance between the concentrations of flax mucilage is also noticed at these water contents. Samples with 0.5% concentration showed a more substantial reduction in resistance compared to samples with a 0.1% concentration at 0 - cone depth (Figures 4.3e and 4.3f). Figures 4.4c and 4.4d illustrate the corresponding energy requirements for needle insertion in the presence of flax seed mucilage. The results confirm a significant reduction in energy due to the addition of flax seed mucilage for both the 0 - 8 mm and cone - 8 mm depth. The ANOVA results confirm that the presence of 0.5% mucilage concentration results in significantly lower energy than a concentration of 0.1% for 9% and 12% water content for 0 - 8 mm depth. Figures 4.3g and 4.3h indicate that mucilage addition only slightly reduces penetration resistance at cone insertion depth for 15% water content and shows no reduction at 18% water content. Consistent with this, the ANOVA results (Figures 4.4c and 4.4d) suggest that mucilage addition does not significantly reduce the energy for either the total insertion depth range or for the shaft insertion depth range at these water contents for both flax seed mucilage concentrations.

The results for loam soil with chia seed mucilage reveal intriguing patterns that differ from those observed in loamy sand. Figures 4.5a-d show a reduction in penetration resistance at both 0 - cone (l_c) and cone – 8 mm depth ($Z - l_c$) for water contents of 9%, 12%, and 15% in loam. This contrasts with the behaviour seen in loamy sand soil, suggesting that the effect of chia seed mucilage is more pronounced in loam. Figure 4.6 illustrates the energy requirements for loam for 0 - 8 mm and cone - 8 mm depth, with varying concentrations of chia seed mucilage (0%, 0.1%, and 0.5%) across different water contents. The ANOVA results confirm that the reduction in energy for loam is statistically significant for 0 - 8 mm depth at water contents of 9%, 12%, and 15%. This is a notable difference from loamy sand, where significant reduction was only observed at 9% water content. Furthermore, the energy required for cone - 8 mm depth range in loam significantly decreased at a water content of 9% and 12%, whereas in loamy sand, chia seed mucilage did not reduce frictional energy (cone – 8 mm depth) requirements at any investigated water content. These findings indicate that chia mucilage more effectively reduces both total energy (U_T) and frictional energy along

the shaft (U_{F_R}) in loam soil. Interestingly, chia seed mucilage showed no significant effect on penetration resistance in loam (and associated energy requirements) at 18% water content, as was also observed for loamy sand soil (Figures 4.5d, 4.6a, and 4.6b). This suggests that above a certain moisture threshold, the lubricating effect of mucilage becomes negligible, possibly due to soil saturation reducing friction and making additional lubrication redundant. Moreover, in loam, there is no significant effect of mucilage concentration on penetration resistance at any water content, mirroring the observations in loamy sand that also suggested that the presence of mucilage is more important than the concentration.

The results for flax seed mucilage in loam soil (Figure 4.5e-h) show similar trends to those observed with chia seed mucilage. There is a reduction in penetration resistance at the both 0 -cone depth (l_c) and for cone - 8 mm depth range ($Z - l_c$) for gravimetric water contents of 9%, 12%, and 15%. Figures 4.6c-d and the associated ANOVA results confirm that the energy required for penetration in loam significantly reduced at 9%, 12%, and 15% water content for 0 - 8 mm depth range. Significant reduction was also observed at 9% and 12% water content for the shaft frictional forces, mirroring the results seen with chia seed mucilage. When comparing the effects in loamy sand and loam, the impact of flax seed mucilage is more pronounced in loam, similar to the observations for chia seed mucilage. In loam, flax seed mucilage significantly reduced required energy for 0 – 8 mm depth range at 9%, 12%, and 15% water contents, whereas in loamy sand significant reduction was only observed at 9% water content. The trend for shaft frictional energy (U_{F_R}) is also similar to that of chia seed mucilage, with flax seed showing no impact in loamy sand but a significant reduction at a water content of 9% and 12% in loam. An interesting observation is that in loam soil, a concentration of 0.1% flax seed mucilage reduced the required energy for penetration more effectively than a concentration of 0.5% at gravimetric water contents of 9%, 12%, and 15%. This concentration dependent effect was not observed in loamy sand soil for either mucilage type, highlighting the complex interactions between soil type, mucilage concentration, and water content in determining penetration resistance and energy requirements. Overall, these findings emphasize the importance of considering soil type when evaluating the effects of mucilage on soil penetration resistance. The more pronounced effects observed in loam soil suggest that the benefits of mucilage addition may be particularly relevant in finer textured soils, potentially offering greater advantages for root growth and soil exploration in these environments.

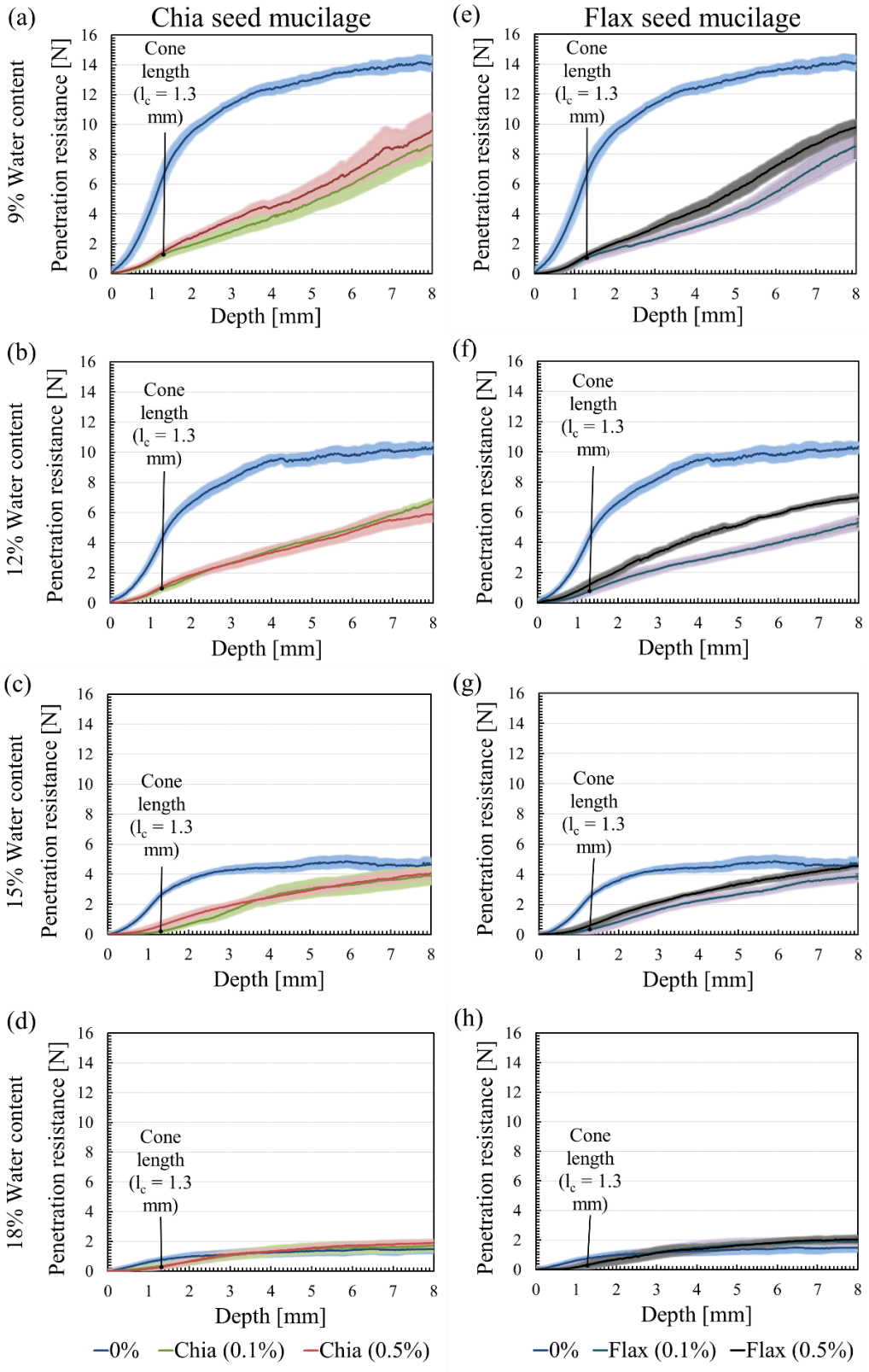

Figure 4.5 Penetration resistance as a function of insertion depth for loam with the addition of (a-d) chia seed mucilage and (e-h) flax seed mucilage with concentrations 0%, 0.1%, and 0.5% for gravimetric water contents of (a,e) 9%, (b,f) 12%, (c,g) 15%, and (d-h) 18%, respectively. The shaded area represents ±1 standard deviation (SD) of the triplicates.

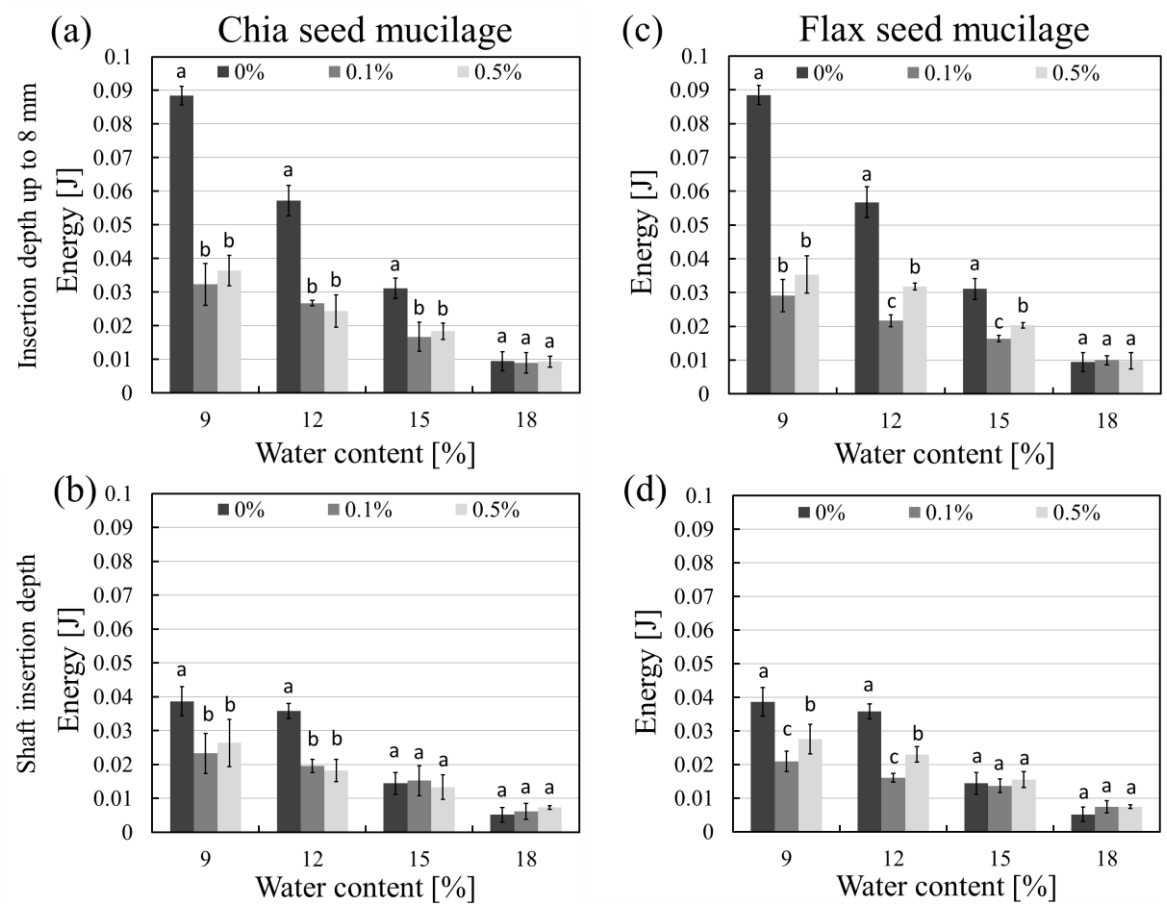

Figure 4.6. Required energy for insertion into loam samples with the addition of (a,b) chia seed and (c, d) flax seed mucilage at the (a,c) full insertion depth of 8 mm and (b,d) beyond the full cone insertion depth for mucilage concentrations of 0%, 0.1% and 0.5% and gravimetric water contents of 9%, 12%, 15%, and 18%. Bars labelled with different lowercase letters (a, b) denote statistically significant differences between means of two values ($p < 0.05$).

4.4 Discussion

The present study investigated the effects of soil texture, water content, and type as well as concentration of mucilage on soil penetration resistance and associated energy requirements. By analyzing two distinct soil (loam and loamy sand) and mucilage (chia and flax seeds) types for a range of water contents and concentrations, complex interactions between these factors were found. The results demonstrated significant differences in penetration resistance and energy requirements between loam and loamy sand, which can be attributed to their distinct physical characteristics. Loam consistently exhibited higher penetration resistance and energy requirements compared to loamy sand, particularly at lower water contents (Figure 4.1 and 4.2). This observation aligns with previous studies and can be attributed to variations in particle size distribution and clay content in the soils used. In loamy soil, smaller particles and

higher clay content (over 15%) enhance interparticle cohesion and binding capacity (Le Bissonnais, 1996), leading to greater mechanical strength compared to loamy sand and subsequently higher penetration resistance (Rosskopf et al., 2022).

The influence of water content on penetration resistance was evident for both soil types, with resistance decreasing as water content increased. This phenomenon is well known and can be attributed to the lubricating effect of water, which reduces friction between soil particles. The reduction in matric suction with higher water content leads to a decreased effective stress between particles, facilitating easier penetration (Lu et al., 2010). Increased water content likely also weakens the electrostatic and van der Waals forces between soil particles (Ding et al., 2019; Or and Ghezzehei, 2002), further reducing soil strength. These findings are consistent with previous research highlighting the critical role of water content in modifying soil mechanical properties (Abbaspour-Gilandeh et al., 2018; Abdalla et al., 1969; Cokca et al., 2004; Rosskopf et al., 2022). The effect was particularly pronounced in sand, especially at higher water contents. Interestingly, the contribution of the frictional energy to the total energy was more significant in loamy sand than in loam. This finding suggests that while the strength of loam is primarily derived from particle cohesion, the penetration resistance of sand is more dependent on inter-particle friction, which is more readily influenced by water content.

The addition of seed mucilage significantly affected the penetration resistance for both loamy sand and loam, with effects varying based on soil type, water content, and mucilage concentration. These findings contribute to available understanding from several studies that investigated the role of plant exudates in modifying soil structure and stability (Benard et al., 2018; Zhong et al., 2021). My results show that mucilage addition reduced penetration resistance and energy requirements, particularly at low water contents (Figures 4.3-4.6). This effect was more pronounced in loam than in sand, which aligns with some previous studies (Rosskopf et al., 2022) but contrasts with others (Oleghe et al., 2017). These discrepancies may be attributed to differences in mucilage application methods, sample preparation techniques, and the specific properties of the soils and mucilage used across studies (Naveed et al., 2017).

The differential effects of mucilage in soil with different grain distributions can be partly explained by the interaction between mucilage and the soil pore size distribution. Smaller soil particles, as found in loam, result in increased micropores (Benard et al., 2018), which have been shown to enhance soil aggregation by absorbing mucilage more effectively than the

larger pores created by larger soil particles (Morel et al., 1991). This interaction likely contributes to the more significant reduction in penetration resistance observed in loam compared to loamy sand upon mucilage addition. This study also revealed differences in the effectiveness of chia and flax seed mucilage, particularly in loamy sand (Figure 4.4) at low water contents. In particular, flax seed mucilage showed a more substantial reduction in penetration resistance compared to chia seed mucilage. This observation highlights the importance of mucilage composition in determining its effects on soil mechanical properties, as noted by Rosskopf et al. (2022). The chemical and biological composition of different mucilage can either glue soil particles together and thus increase aggregate stability, or disperse soil particles reducing interparticle bonding (Naveed et al., 2017; Oleghe et al., 2019; Zhong et al., 2021).

Concentration-dependent effects of mucilage were observed in some cases, particularly with flax seed mucilage in loamy sand at 9% water content. However, the impact of concentration was not consistently significant across all conditions, suggesting that even less concentrated mucilage can induce measurable changes in soil mechanical properties. This finding has important implications for understanding the potential impacts of plant exudates on soil structure in rhizosphere, where exudate concentrations may vary widely. It is important to note that while this study focused on the immediate effects of mucilage addition on soil mechanical properties, previous research has shown that plant exudates can also influence soil structure and stability over longer time scales, particularly when subjected to wetting and drying cycles (Oleghe et al., 2017). Future studies could explore these temporal dynamics to provide a more comprehensive understanding of how mucilage affects soil properties in field condition.

4.5 Conclusions

This study investigated the interplay between soil texture, water content, and the type and concentration of seed mucilage in determining soil penetration resistance and associated energy requirements. By examining two soil types (loam and sand) and two mucilage types (chia and flax seeds) across a range of water contents and concentrations, I uncovered complex interactions that shape soil mechanical behaviour.

Loam consistently exhibited higher penetration resistance and energy requirements compared to sand, particularly at lower water contents. This can be attributed to the finer particle size in loam, which enhances interparticle cohesion and binding capacity. In contrast, the penetration

resistance of loamy sandwas lower and more influenced by interparticle friction than cohesion, making it more sensitive to changes in water content. As water content increased, penetration resistance decreased in both soils, highlighting the lubricating effects of water and its role in reducing soil strength through weakening interparticle forces.

The addition of seed mucilage demonstrated a significant influence on soil penetration resistance, with the effects varying by soil type, water content, and mucilage concentration. Mucilage addition was particularly effective in reducing penetration resistance in loam at low water contents, likely due to the enhanced interaction of mucilage with the smaller pores in loamy soil. In sand, mucilage effects were less pronounced but varied by type, with flax seed mucilage showing greater effectiveness in reducing penetration resistance than chia seed mucilage. This difference underscores the importance of mucilage composition in determining its interaction with soil. Concentration-dependent effects of mucilage were limited. This suggests that even low concentrations of mucilage can induce measurable changes in soil mechanical properties, which is relevant for understanding the role of plant exudates in the rhizosphere.

While the focus of this study was on immediate effects of mucilage application, future research could explore how mucilage impacts soil penetration resistance over time, especially under cycles of wetting and drying. Overall, these findings provide valuable insights into the complex relationships between soil texture, water content, and biophysical amendments, with implications for sustainable soil management and agricultural practices.

CHAPTER 5

EFFECT OF DIFFERENT MUCILAGE APPLICATION METHODS ON PENETRATION RESISTANCE TO ROOT GROWTH

5.1 Introduction

Root penetration resistance is a critical factor influencing plant root growth, and mucilage exudation plays a significant role in modulating soil mechanical properties to facilitate penetration. However, nearly all previous studies, including those by Naveed et al. (2018), Oleghe et al. (2017), and Rosskopf et al. (2022b, 2022a) have exclusively used a mixing approach, in which mucilage is thoroughly blended with soil before performing penetration resistance tests. These studies reported that penetration resistance varies depending on mucilage type, concentration, soil texture, and water content. Some observed that mucilage reduces penetration resistance by lubricating the soil-root interface and enhancing soil aggregation, while others found that mucilage can increase penetration resistance, particularly under dry conditions where it forms strong hydrophobic films. Despite these valuable insights, the mixing method does not accurately represent natural conditions, as roots exude mucilage locally at the growing root tip, creating distinct spatial gradients in the rhizosphere rather than distributing it uniformly throughout the soil. This key limitation means that previous findings may not fully capture the true role of mucilage in root-soil interactions.

Recognizing this gap, the droplet method was introduced in the previous chapters, which is an application technique that better simulates localized mucilage secretion at the root tip. Using this application approach, it was found that the spatial distribution of mucilage significantly alters its effects on soil mechanical properties. This realization raised fundamental questions about how mucilage application determines penetration resistance and led me to systematically investigate different mucilage application methods. In this study, I expand upon my previous work by introducing the injection method, which represents an even more realistic approach to mimic root exudation by continuously releasing mucilage along the penetration path.

To systematically assess how mucilage application methods influence root penetration resistance, three distinct techniques are compared in this chapter: the mixing method, the droplet method, and the injection method. These methods are applied using two types of plant-derived mucilage (from chia and flax seeds) at two concentrations (0.1% and 0.5%) under controlled soil conditions with sandy soil, two gravimetric water contents (9% and 12%), and a constant bulk density of 1.6 g/cm³. By employing these different application techniques, the aim is to determine how mucilage spatial distribution affects penetration resistance and whether previous findings based on the mixing method fully capture the role of mucilage in root-soil interactions. This study provides crucial insights into the mechanics of root penetration in the rhizosphere and contributes to the refinement of experimental approaches that more accurately reflect natural root exudation processes.

5.2 Materials and methods

5.2.1 Extraction of chia and flax seed mucilage

Mucilage was extracted from chia and flax seeds using the procedure suggested by Kroener et al. (2018). First, 10 g of seeds were mixed with 100 ml of water in a beaker and stirred continuously for 2 minutes. The mixture was then allowed to rest for 30 minutes. Subsequently, a sieve with a 500 µm mesh size was carefully positioned inside a funnel, and the mucilage-water mixture was poured through it. A vacuum pump was employed to create suction in the conical flask, accelerating the extraction process by drawing the mucilage into the flask while retaining the seeds in the sieve. The collected mucilage was freeze-dried to obtain pure mucilage. Pure mucilage was then used to create mucilage solutions with different concentrations (0.1% and 0.5% by weight) by mixing a known amount of pure mucilage with water. The prepared mucilage solutions were stored at 4°C prior to soil sample preparation.

5.2.2 Soil sample preparation

Soil samples were prepared using loamy sand obtained from Kaldenkirchen, Germany. This soil consists of 60.35% sand, 33.25% silt, and 6.4% clay. The soil was first sieved using a 2 mm sieve and then oven-dried at 105°C for 24 hours. Subsequently, the soil was mixed with water to achieve gravimetric water contents of 9% and 12%. To achieve the same bulk density, samples were compacted with a mini-compaction apparatus using a mould with a 38 mm diameter and 45 mm height using a 1 kg hammer falling from a height of 160 mm. All soil samples were compacted to a constant dry bulk density of 1.6 g/cm³.

5.2.3 Penetration resistance measurements using rheometer

A rheometer (MCR102, Anton Paar GmbH, Germany) was used to measure the penetration resistance as function of insertion depth using a stainless-steel hollow needle (Figure 5.2) with a semi-apex angle of 30° (cone length of 1.3 mm) and a diameter of 1.5 mm (as a proxy for roots). The hollow needle was developed at the Institute of Technology and Engineering (Forschungszentrum Jülich GmbH). We sourced the stainless-steel tubing externally and then designed and engineered the needle. The needle was pushed at a constant speed of 2.5 mm min^{-1} to a total insertion depth of 8 mm. In total, 96 samples were investigated (1 soil type × 2 water contents × 2 mucilage types × 2 concentrations × 3 replicates × 4 types of mucilage application).

5.2.4 Methods of mucilage application

In this chapter, different mucilage application methods are developed and applied to investigate their impact on root penetration resistance. Three distinct mucilage application methods were used for this study, along with a control where no mucilage was applied. As in the previous chapters, a 0.1 ml volume of mucilage was applied locally onto the soil surface at the point of needle penetration for the droplet method. To achieve an equivalent volumetric mucilage concentration across methods, I first defined the target concentration based on the droplet application method. 0.1 ml droplet of mucilage formed a circular area roughly 1 cm in diameter upon contact with the soil. Assuming full penetration to a depth of 0.8 cm, this droplet would occupy a cylindrical volume of 0.64 cm^3. To obtain an appropriate application amount for the mixing method, the sample volume (51 cm^3) was used to scale the mucilage volume. This resulted in an application amount of 7.9 ml. Crucially, this mucilage volume was considered in the gravimetric water content by reducing the applied amount of water by the mucilage volume. This differs slightly from the standard mixing method used in previous studies (e.g. Naveed et al., 2017), where mucilage concentration is defined solely as a mass fraction of freeze-dried mucilage to dry soil mass (e.g., 0.5% concentration = 0.005 g mucilage per 1 g dry soil). Next, the predetermined mucilage amount was added to the dry soil and mixed thoroughly with a spatula for 5 minutes to ensure a homogeneous distribution for the mixing method. Finally, the soil-mucilage mixture is compacted to the target bulk density, ensuring uniformity and replicability across all samples. Although the total mucilage solution volume in my approach differs from standard methods from other studies, this strategy maintains flexibility for cross-study comparison while enabling direct evaluation of different application methods in this study.

The injection method involved the exudation of the same 0.1 ml volume of mucilage through the needle tip at a controlled rate of 0.03 ml/min for 200 seconds, ensuring that the amount of mucilage released over the entire insertion period was consistent with the other methods. The injection method employed a specially designed needle to achieve precise mucilage application (Figure 5.2). This needle was engineered to exude mucilage continuously through the tip of the needle. The controlled rate ensured uniform release throughout the entire application process, matching the consistency achieved by the droplet and mixing methods. The innovative design of the needle is central to this method. The needle features a tapered tip with a precision micro-opening, which minimizes variability in mucilage flow and prevents clogging during extended use. The flow rate was regulated using a syringe pump calibrated for accuracy. This setup ensured that the mucilage delivery adhered to the specified parameters without deviation.

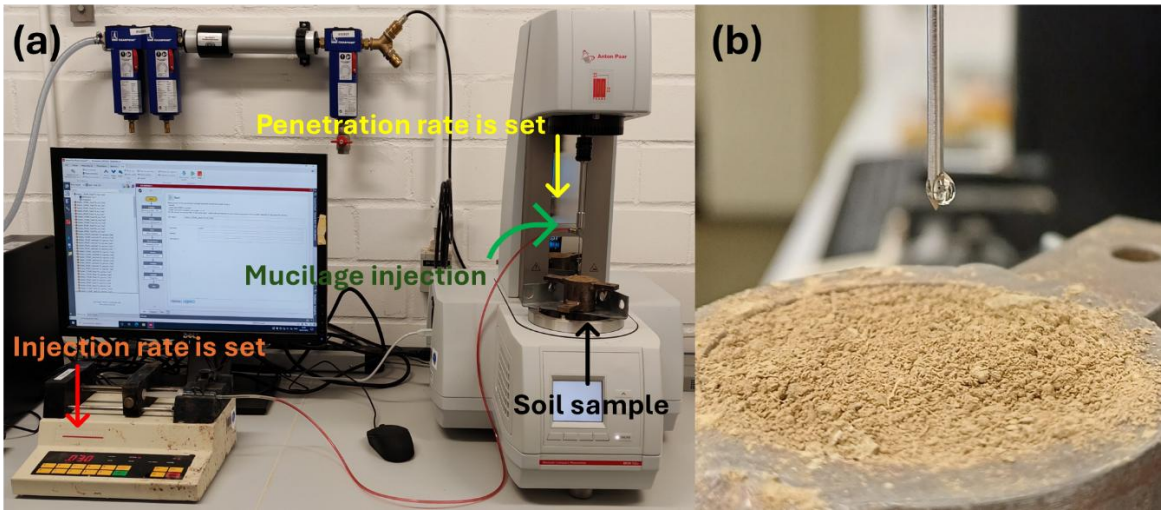

Figure 5.1 Experimental setup for mucilage injection into soil and injection process, (a) injection setup, and (b) mucilage exudation at tip.

By standardizing the volume of mucilage for all three methods, it was ensured that each method provided a comparable volume of mucilage, with the droplet method representing local exudation, the mixing method achieving even distribution throughout the sample, and the injection method simulating continuous release during needle insertion. To evaluate the effect of mucilage and mucilage application strategy, the penetration resistance tests were conducted by applying chia and flax seed mucilage with 0.1% and 0.5% concentration with control, droplet, mixing, and injection application methods.

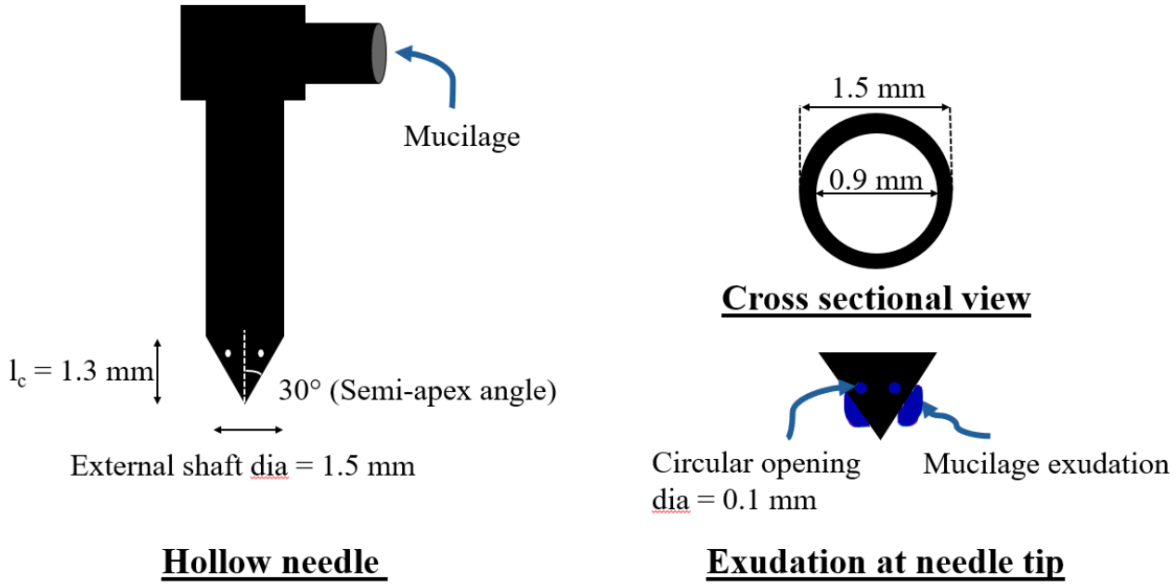

Figure 5.2 Sketch of hollow needle, cross sectional view of hollow shaft, and mucilage exudation at tip.

5.3 Results

Figure 5.3 presents the penetration resistance curves and energies for chia seed mucilage at 0.1% and 0.5% concentrations obtained using different application methods at gravimetric water contents of 9% and 12% for loamy sand. Figure 5.4 provides the required energy for insertion both for 0 - 8 mm (Z) and the cone - 8 mm ($Z - l_c$) depth range. It can be seen that the injection method consistently resulted in lower penetration resistance compared to other methods. The reduction was evident both from 0 - cone depth (l_c) and from cone depth to 8 mm depth ($Z - l_c$). The penetration resistance curve for the injection method exhibited a distinctive pattern: a rapid increase until full cone insertion, followed by a gradual increase due to shaft frictional forces, eventually reaching a plateau. This plateau suggests that the shaft frictional forces stabilize with continued needle insertion, potentially indicating a zone of influence created by the injected mucilage. Figure 5.4 confirms a significant reduction in energy for both total energy (U_T) from 0 - 8mm depth (Z) and shaft frictional energy (U_{F_R}) for cone to 8 mm depth ($Z - l_c$), confirming that the injection method most effectively reduced penetration resistance.

The mixing method consistently showed higher penetration resistance than the injection method. This difference was apparent from 0 - cone depth (l_c) and became even more

pronounced from cone - 8 mm depth ($Z - l_c$) for both gravimetric water contents. Unlike the injection method, the penetration resistance curves obtained with the mixing method showed a continuous rise after reaching the cone depth due to shaft frictional forces without reaching a plateau. This distinct pattern suggests a significant difference in soil-mucilage interaction associated with the more uniform distribution of mucilage throughout the soil matrix.

The droplet method demonstrated a significant decrease in penetration resistance compared to the control method from 0 - cone depth. However, for cone - 8 mm depth, the resistance observed in the droplet method surpassed that of the control measurement. This counterintuitive observation may suggest that higher frictional forces are acting along the shaft during deeper penetration. A similar trend was also observed in the previous chapter for chia seed mucilage in loamy sand for both 0.1% and 0.5% concentrations. The increased friction in the droplet method may be attributed to the spatial distribution and interaction of the mucilage with the surrounding medium. Unlike the control sample, the droplet method introduces mucilage that may form localized regions of adhesion at the shaft surface. Understanding the role of the rheological properties of mucilage (e.g., viscosity) and how they change under pressure is crucial to explaining this behavior. Further investigation into the interface dynamics could provide a clearer insight into why the droplet method results in higher friction at these depths compared to the reference sample.

Statistical analysis using ANOVA provides further support for these observations. The results reveal that the energy required for insertion into the samples prepared with the mixing approach is significantly lower than that with the droplet method across all tested gravimetric water contents and mucilage concentrations. This finding aligns with the earlier observation of lower penetration resistance in the mixing method, indicating that the uniform distribution of mucilage throughout the soil substantially reduces frictional energy compared to the more localized exudation simulated by the droplet method. Importantly, the ANOVA results also highlight the limited effectiveness of the droplet method in reducing the shaft frictional energy (U_{F_R}), further emphasizing that different interactions resulted due to difference in mucilage application methods.

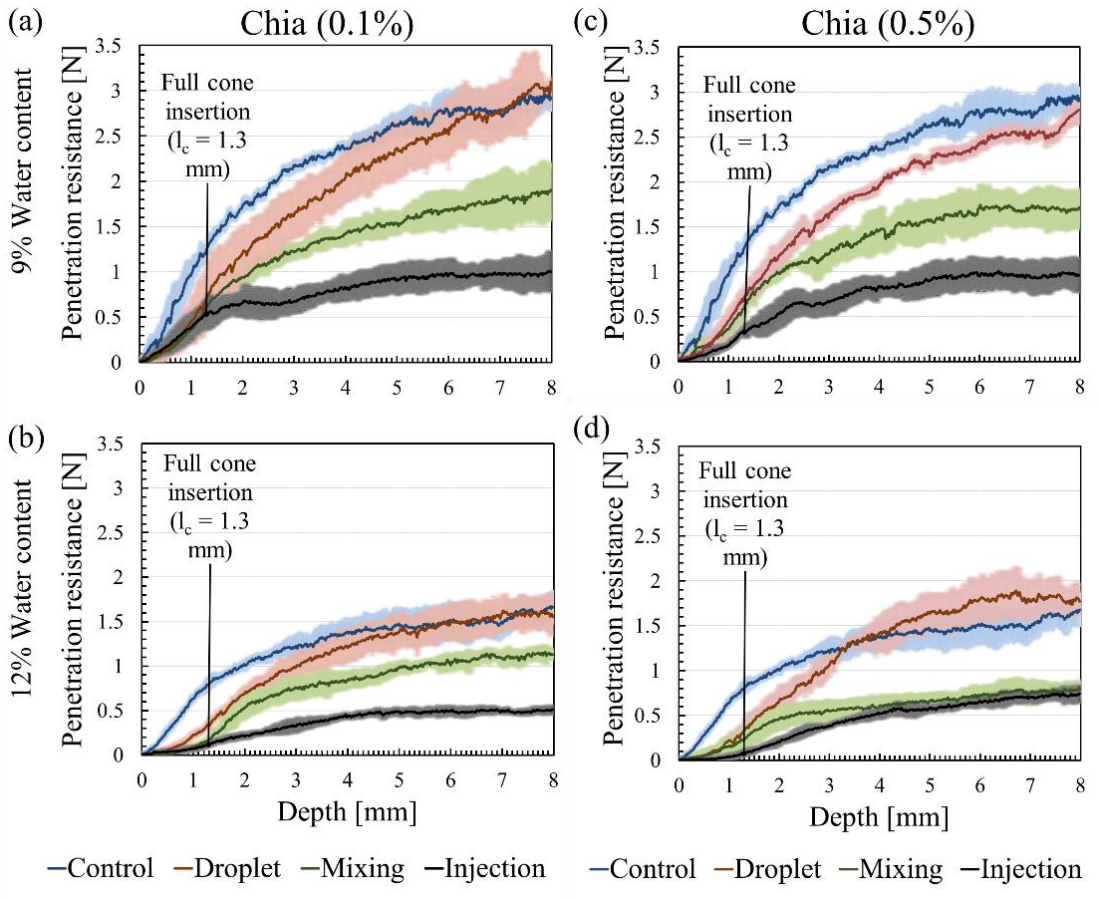

Figure 5.3 Penetration resistance curves for control, droplet, mixing, and injection application methods for chia seed mucilage in sand with an insertion depth up to 8 mm. (a) and (b) represent 0.1% concentration and (c) and (d) represent 0.5% concentration for gravimetric water contents of 9% and 12%. The shaded area represents ±1 standard deviation (SD) of the triplicates.

Figure 5.4 also suggests that water content and chia mucilage concentration play a critical role in determining soil penetration resistance and the energy required. Their complex interactions influence the effectiveness of different mucilage application methods. Statistical analysis of the total energy for insertion shows that at 0.1% mucilage concentration, the droplet method shows a significant reduction at 9% water content compared to the control ($p = 0.004$). However, no significant reduction is observed at 12% ($p = 0.4$). Similarly, the mixing approach shows a stronger effect at 9% ($p = 0.00005$) than at 12% ($p = 0.0002$). The injection approach also showed strong and statistically significant reductions at both water contents ($p = 0.000002$ at 9%; $p = 0.000001$ at 12%).

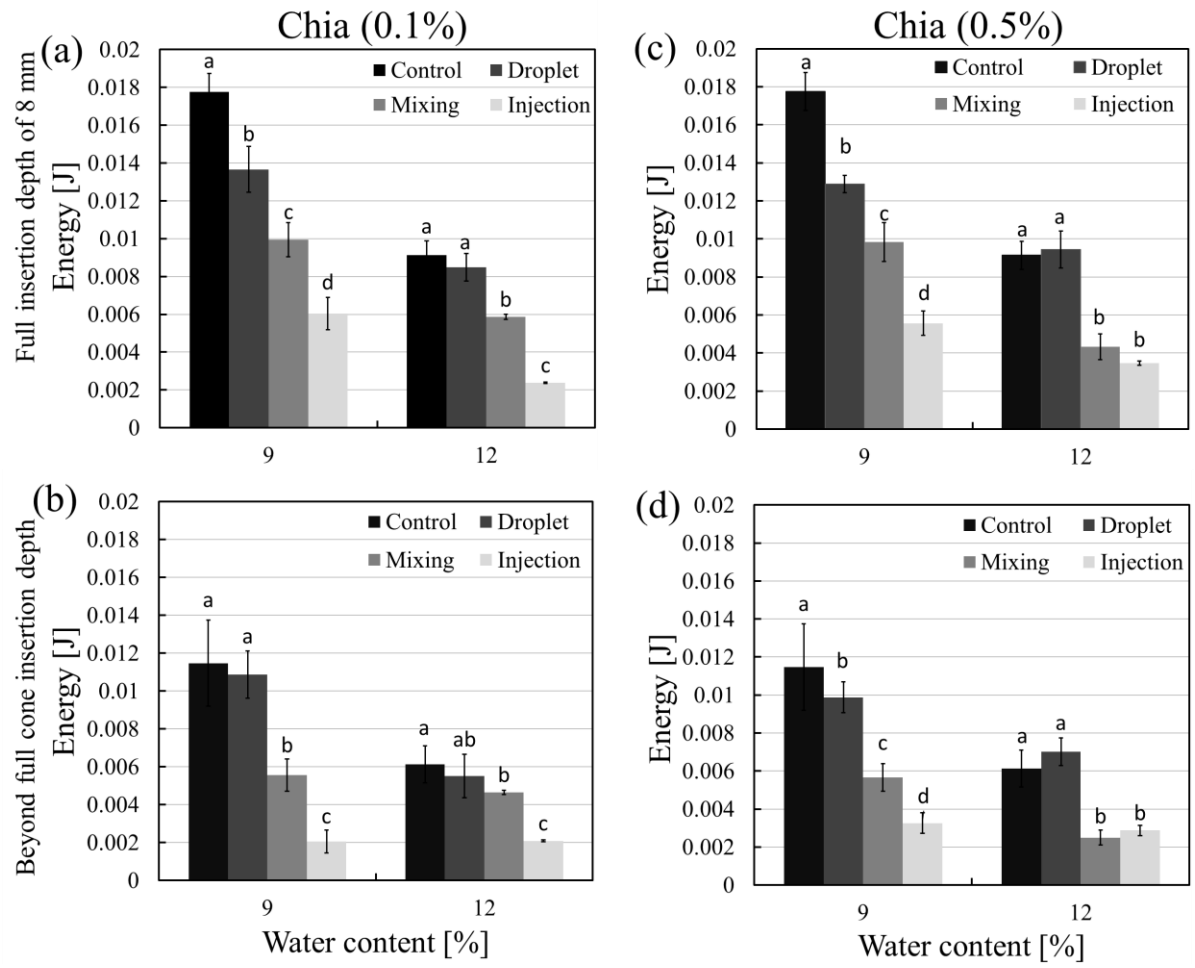

Figure 5.4 Energy for control, droplet, mixing, and injection exudation methods for chia seed mucilage in sand. (a) and (b) represent 0.1% concentration and (c) and (d) represent 0.5% concentration for insertion depth of 8 mm and shaft insertion depth for gravimetric water contents of 9% and 12%. Bars labelled with different lowercase letters (a, b) denote statistically significant differences between means of two values ($p < 0.05$).

For 0.5% mucilage concentration, the droplet method again shows a significant reduction of total penetration energy at 9% water content compared to the control ($p = 0.0003$), but no significant difference at 12% ($p = 0.9$). For the mixing method, reductions are significant for both water contents, with a stronger effect at 9% ($p = 0.00001$) compared to 12% ($p = 0.0001$). The injection method also showed a significant reductions at both water contents, with a more pronounced effect at 9% ($p = 0.0000004$) than at 12% ($p = 0.00003$). These patterns also extend to the frictional energy, reinforcing the conclusion that both water content and chia mucilage concentration strongly influence the effectiveness of mucilage application methods in reducing soil penetration resistance.

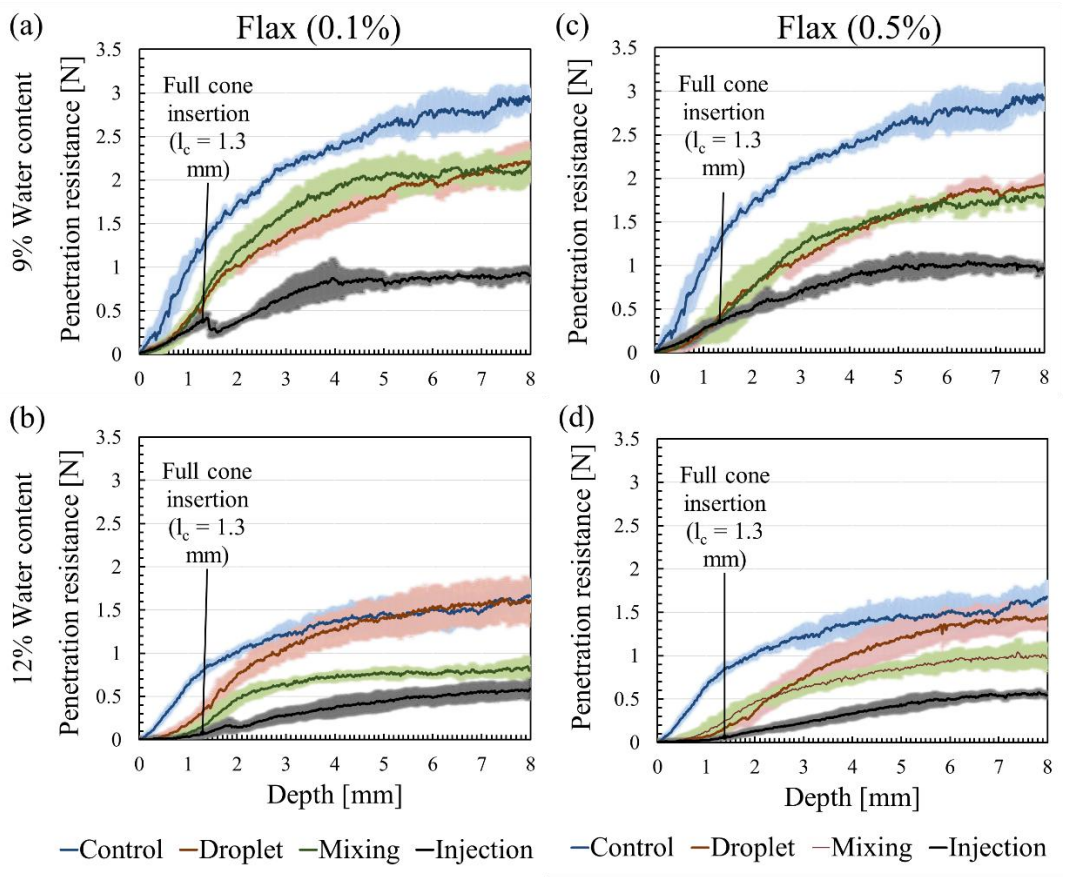

Figure 5.5 Penetration resistance for control, droplet, mixing, and injection exudation methods for flax seed mucilage in sand with an insertion depth of 8 mm. (a) and (b) represent 0.1% concentration and (c) and (d) represent 0.5% concentration as a function of gravimetric water contents of 9% and 12%. The shaded area represents ±1 standard deviation (SD) of the triplicates.

In summary, for both mucilage concentrations (0.1% and 0.5%), the droplet method did not significantly reduce penetration resistance at 12% water content, while it showed significant reduction at 9%. The mixing method showed significant effects at both water contents, though consistently stronger at 9%. The injection method remained effective across all conditions, but with slightly more pronounced reductions at lower water content (9%) for 0.5% mucilage concentration. These findings highlight that higher mucilage concentration (0.5%) generally enhanced the effectiveness of most application methods—particularly for the droplet and mixing method in dry soil—while the injection method remained robust regardless of conditions.

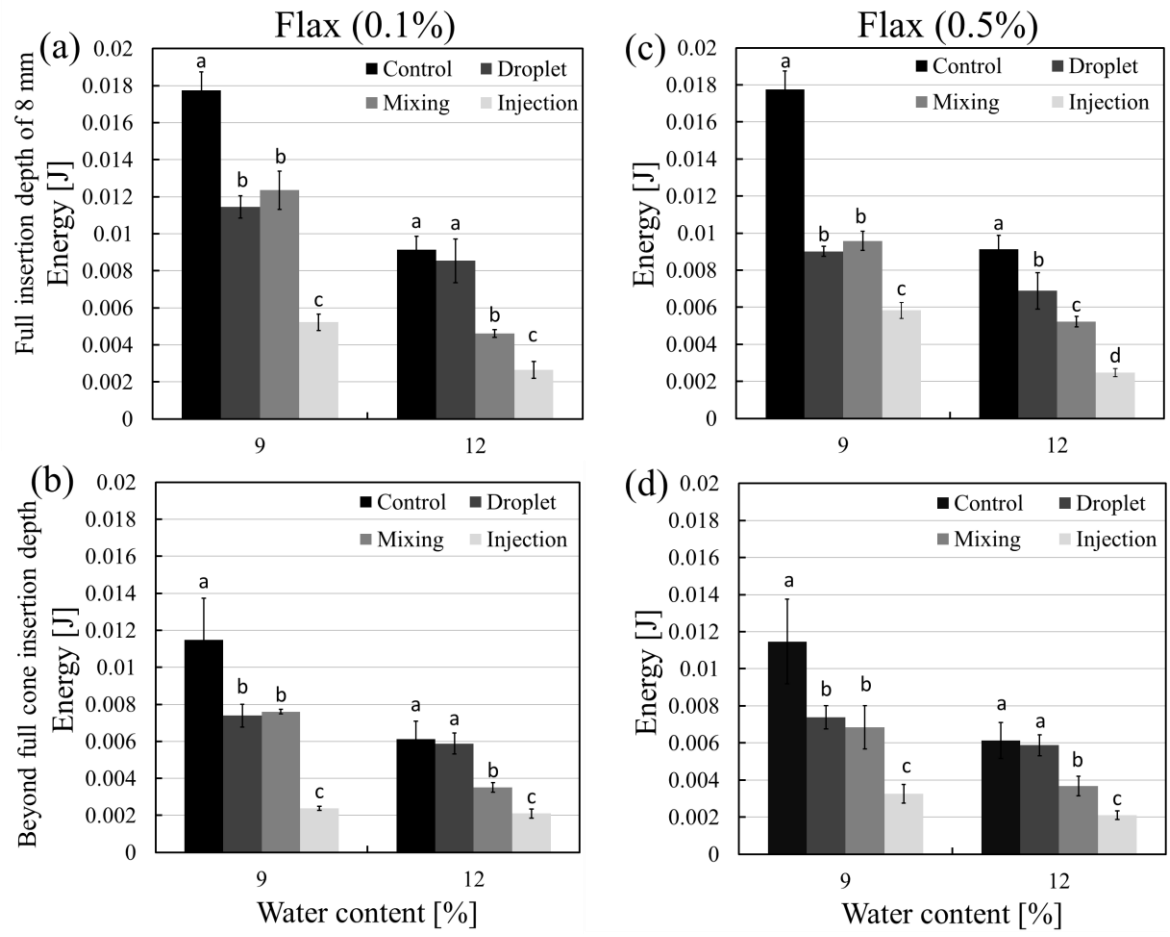

Figure 5.6 Required energy for penetration using the control, droplet, mixing, and injection exudation methods for flax seed mucilage in sand. (a) and (b) represent 0.1% concentration and (c) and (d) represent 0.5% concentration for insertion depth of 8 mm and shaft insertion depth as a function of gravimetric water contents of 9% and 12%. Bars labelled with different lowercase letters (a, b) denote statistically significant differences between means of two values ($p < 0.05$).

Figures 5.5 and 5.6 present the penetration resistance curves and associated energy requirements for flax seed mucilage at 0.1% and 0.5% concentrations for gravimetric water contents of 9% and 12%. Consistent with the behavior observed for chia seed mucilage, the injection method was the most effective in reducing both penetration resistance and the energy required for needle insertion from 0 - 8 mm depth (Z) and from cone - 8 mm depth ($Z - l_c$). For flax seed mucilage at 9% water content, penetration resistance curves for the mixing and droplet methods are similar, and statistical analysis using ANOVA confirms that no significant differences are observed in total energy (U_T) or shaft frictional energy (U_{F_R}). In contrast, for chia seed mucilage, the mixing method consistently demonstrated lower resistance and required significantly less energy at this water content.

At 12% water content, flax seed mucilage exhibited greater variation in penetration resistance between the mixing and droplet methods, with the mixing method showing lower resistance and energy requirements. This aligns with the trend observed for chia seed mucilage, where the uniform distribution of mucilage achieved through mixing becomes increasingly important at higher water content. These results highlight the interplay between mucilage type, application method, and water content in influencing both penetration resistance and the associated energy requirements.

When comparing the effects of mucilage and water content on penetration resistance and energy requirements across application methods, the results demonstrated complex interactions for both chia and flax seed mucilage with changes in mucilage concentration and increase in water content. Like in the case of chia seed mucilage, the energy reductions for flax seed mucilage were statistically significant at both water contents and mucilage concentrations. For 0.5% mucilage concentration, the reduction in total energy is more significant than for 0.1% concentration for the droplet method and the mixing methods at both water contents (Figure 5.6). Interestingly, the injection method for flax seed mucilage showed no strong difference in total energy between the two concentrations at both water contents. Although the differences in required energy for the injection method across water content and mucilage concentration are not significant for flax seed mucilage, the combined results of chia and flax highlight that the interactions due to mucilage concentration are influenced by a combination of factors.

In summary, measurements with flax and chia seed mucilage showed that the injection method exhibited the lowest penetration resistance and energy requirements. Notable differences between the mixing and droplet methods were observed for chia mucilage across water contents and mucilage concentrations. Flax seed mucilage showed more variability between the different application methods, also depending on water content, while chia seed mucilage showed a relatively more consistent behavior. Overall, these findings suggest that the type of mucilage, mucilage concentrations, and the specific soil water content significantly influence the penetration resistance energies of mucilage application methods.

5.4 Discussion

This study provides critical insights into the effects of different mucilage application methods on soil penetration resistance, a significant factor for root growth. The results demonstrate that the method of mucilage application significantly influences the penetration resistance and

energy required for root growth, with implications for our understanding of root-soil interactions in the rhizosphere. The most striking finding of this study is the consistently lower penetration resistance observed with the injection method compared to mixing, droplet, and control methods for both chia and flax seed mucilage. This result highlights the crucial role that the manner of mucilage introduction into the soil plays in determining its effects on penetration resistance. The injection method best mimics the natural exudation of mucilage from roots, making its results the most relevant in this study (Figure 5.1).

The distinct behavior observed between application methods suggests important implications for understanding the role of mucilage in root-soil interactions. In the droplet method, mucilage was concentrated in a localized area, and once the needle moved below the depth of droplet infiltration, the soil around the tip likely contained little to no mucilage. Consequently, the penetration resistance at larger depths for the droplet method closely resembled those of the control experiment. In contrast, the mixing method, while resulting in uniform mucilage concentrations due to distribution within the entire soil volume, ensured that mucilage was present around the needle tip at all insertion depths. This consistent presence of mucilage led to lower resistance compared to the droplet method.

The lower penetration resistance observed with the injection method suggests that as roots grow and exude mucilage, they create localized zones of reduced mechanical impedance. This mechanism facilitates easier root penetration and elongation, particularly in compacted or dense soils. Moreover, the spatial distribution of mucilage achieved through injection may better represent the gradients of mucilage distribution that occur around growing roots in natural conditions.

The results revealed a complex interplay between mucilage application method, mucilage concentration, and soil water content, highlighting the distinct differences between chia and flax seed mucilage. Chia seed mucilage exhibited complex interactions between mucilage concentrations and water content, particularly for the mixing and injection methods (Figure 5.4). The differences in energy requirements between the 0.1% and 0.5% mucilage concentrations in these cases were significant. For flax seed mucilage, these interactions were particularly pronounced in the mixing and droplet application methods across water content (Figure 5.6). While both methods recorded significantly different energy requirements at 12% water content, the difference was statistically insignificant at 9% water content. These observations align with previous studies, which also suggested that the behavior of mucilage in soil significantly depends on water content (e.g. Rosskopf et al., 2022b). This differential

response to water content between chia and flax seed mucilage signifies the importance of considering mucilage concentration and soil moisture when evaluating the effects of mucilage application methods on penetration resistance. The results also point to the importance of considering the chemical and biological composition of mucilage. The distinct differences observed between chia and flax seed mucilage align with the results of Rosskopf et al. (2022a) and Oleghe et al. (2019), who also emphasized that the source of mucilage, whether seed derived or root derived, can significantly influence its impact on soil physical properties. Despite methodological differences in application, all approaches consistently demonstrated that mucilage reduces penetration resistance, thus confirming qualitative conclusions of previous studies while highlighting that effect magnitude depends critically on application method.

Careful assessment of the complex interplay between all the factors, which significantly influences soil penetration dynamics, is crucial for understanding its relevance to natural root elongation in the rhizosphere. The interactions observed in the study may reflect authentic responses specific to certain controlled conditions; however, they could also emerge from experimental designs that do not accurately mimic real conditions. Therefore, it is essential to critically evaluate whether these interactions genuinely represent natural processes or arise due to inappropriate experimental approaches. It requires validating findings against field measurements, redesigning experiments to isolate artifacts, and replicating results across scaled systems like lab-to-field transitions.

These observations highlight the critical importance of the mucilage application method in determining experimental outcomes. The strong variations in mucilage distribution around the needle tip across different application methods raises questions about the relevance of the applied mucilage treatments. These findings suggest that while the droplet method provides valuable initial insights, it may require complementary approaches when assessing the impact of mucilage on root penetration resistance, as it presents challenges in ensuring consistent mucilage influence throughout the insertion process. Previous studies utilizing soil-mucilage mixing strategies have demonstrated that mucilage uniformly dispersed within the soil matrix can increase particle contact surfaces and bonding forces under specific conditions (Naveed et al., 2017). Critically, this strengthening effect is highly dependent on conditioning factors like compressive pressure and wetting-drying cycles, where samples mixed with mucilage consistently lead to increased penetration resistance compared to unamended soil, particularly at high mucilage concentrations under high compressive pressure (Oleghe et al., 2017a).

However, this study – conducted without compressive pressure or wet-dry cycles – revealed that mixing weakened interparticle bonding relative to the droplet method, especially for chia seed mucilage. This is evidenced by significantly lower frictional energy in mixed samples as compared with the droplet application method (Figure 5.4). For flax seed mucilage, method-dependent differences were only significant at 12% water content (Figure 5.6), highlighting the complex interactions also noted by Rosskopf et al. (2022), where conditioning protocols critically determine whether uniform dispersion strengthens or weakens the soil matrix. In stark contrast, the injection method deposits mucilage in localized pockets along the insertion path, creating discrete weak planes where concentrated mucilage lubricates particle contacts – confirming that penetration energy depends fundamentally on mucilage distribution patterns, not just the total amount present. This signifies the importance of considering the spatial distribution of mucilage in the rhizosphere when studying its effects on soil properties and root growth. Future studies should carefully consider the application method to ensure that it accurately represents the natural dynamics of mucilage exudation and distribution in the rhizosphere.

While this study provides valuable insights into the impact of mucilage application methods on root penetration resistance, several limitations should be acknowledged. The experiments were conducted under controlled laboratory settings, which not fully represent the complexity of natural soil environments. The heterogeneity of soil structure, organic matter content, and microbial activity in field conditions could influence mucilage behavior and its effects on penetration resistance. The rigid needles used in this study to mimic roots do not fully capture the flexibility and adaptive growth patterns of real plant roots. These limitation may affect the interpretation of penetration resistance measurements, as actual roots can navigate soil pores and adjust their growth in response to mechanical impedance. In addition, I relied on seed-derived mucilage, which has been shown to have different properties than root-exuded mucilage in terms of viscosity, adhesion, and chemical composition (Naveed et al., 2017).

5.5 Conclusions

This study reveals the critical role of the mucilage application method in assessing root penetration resistance, with the injection method as the most representative of natural root-soil interactions. I demonstrate that the injection method consistently results in lower penetration resistance compared to mixing, droplet, and control methods for both chia and flax seed mucilage. This suggests that the spatial distribution of mucilage in the rhizosphere plays a crucial role in modifying soil physical properties to facilitate root growth. This

challenges the conventional mixing application approach used in many previous studies and highlights the need for more meticulous experimental designs for investigating root elongation in rhizosphere research.

This research findings suggest a complex interplay between soil-root-mucilage interactions based on application methods. These results align with previous studies that discussed the complex interactions observed between mucilage type, concentration, soil water content, and point to the multifaceted nature of mucilage effects on soil physical properties (Oleghe et al., 2017; Rosskopf et al., 2022b, 2022a; Traore et al., 2000). Both chia and flax seed mucilage demonstrated significant effects on penetration resistance and associated energy requirements, with notable differences in their responses to varying conditions. For instance, flax seed mucilage showed a complex response at lower water content, whereas the response of chia seed mucilage was more complex at higher water content, particularly when comparing different concentrations.

The presented findings raise critical questions about the relevance of experimental conditions to natural rhizosphere processes. Much of the complex interactions reported in prior research, predominantly relying on mixing methods, may stem from application techniques that inadequately mimic natural root exudation. While the droplet and mixing methods introduce artificial spatial distributions, my results demonstrate that the injection method closely replicates the localized, dynamic release of mucilage by roots. This disparity underscores both the limitations of conventional approaches and the necessity for experimental designs that accurately reflect rhizosphere dynamics. Consequently, this multi-method approach provides a more ecologically relevant framework for understanding mucilage's impact on soil physical properties, emphasizing that conclusions drawn solely from mixing strategies require careful evaluation to establish their true significance in Rhizosphere system.

While this study has limitations, including the use of seed-derived mucilage and simplified root models, it opens new avenues for research in plant-soil interactions. Future work should validate these findings under more diverse natural conditions, incorporate root-derived mucilage, and integrate results with broader rhizosphere processes. By addressing these gaps through refined experimental approaches, I can gain deeper insights into rhizosphere dynamics governing root elongation. This progression will enable more accurate modeling of root-soil-mucilage interactions and ultimately inform innovative strategies to enhance root growth in natural environments.

CHAPTER 6

CONCLUSIONS AND OUTLOOK

In this chapter, the conclusions of this thesis will be presented and possible directions for future research will be discussed.

6.1 Conclusions

Understanding the mechanical interactions between plant roots and soil is critical for advancing agricultural practices, improving soil management, and enhancing crop resilience in challenging environments. Root growth is fundamentally constrained by soil mechanical impedance, which is influenced by a complex interplay of soil physical properties, root morphology, and biological factors such as mucilage exudation. This thesis addressed these interactions through a series of experiments designed to quantify the effects of soil water content, bulk density, soil texture, root tip geometry, as well as mucilage type and concentration on penetration resistance. By integrating theoretical frameworks like cavity expansion theory, this research provides novel insights into the mechanisms governing root-soil interactions.

In Chapter 3, the role of soil mechanical properties, such as water content and bulk density, on penetration resistance was investigated. Unlike previous studies by Bengough et al. (2005) and Ruiz et al. (2019), which often maintained constant bulk density across varying water contents, a constant compaction energy approach was considered in this chapter. This method more accurately reflects real-world scenarios, where heavy machinery or natural processes (e.g., seasonal changes, irrigation) lead to varying bulk densities at different water contents along the soil profile. The results revealed a non-linear relationship between water content and penetration resistance, with maximum resistance occurring at intermediate moisture levels. This aligns with Ruiz et al. (2019), who reported similar trends in loamy soils. However, the study extends prior work by demonstrating that bulk density, which varied naturally under constant compaction energy, might play a critical role in shaping penetration resistance. This approach captures the dynamic interplay between water content and bulk density, providing a more realistic representation of field conditions. Additionally, this

chapter highlights the significant influence of root tip geometry (sharp vs. blunt) on penetration resistance. While sharper tips generally reduce penetration resistance in dry soils, blunt tips more easily penetrated in wet soils. This challenges the assumption that sharper tips always facilitate root growth. This finding underscores the importance of context-specific assessments and aligns with the work of Kirby and Bengough (2002), who emphasized the role of root morphology in overcoming soil impedance.

The novel energy requirement analysis strategy employed in this study allows to separate cone insertion energy from the required energy to overcome frictional resistance and thus provides a more detailed understanding of the penetration process and the characteristics of penetration resistance curves. The energy analysis method revealed significant differences in the energy requirements for sharp and blunt needles across varying water contents and bulk densities. Specifically, the behaviour of the needle tips (cones) changed markedly with water content, highlighting the relevance of root tip geometry for root penetration during growth. For instance, at low water content, the blunt needle exhibited higher penetration resistance than the sharp needle due to localized compaction and soil particle jamming at the needle tip (Ruiz et al., 2016). However, as water content increased, the jamming effect diminished, and the penetration resistance became more dependent on the cone contact surface area. This explains why the sharp needle, with its larger surface area, showed higher penetration resistance at high water contents. These findings are supported by cavity expansion theory, which emphasizes the critical role of soil cohesion in determining penetration resistance. At low water contents, higher cohesion leads to greater resistance, particularly for blunt needles, due to soil particle jamming at the needle tip (Ruiz et al., 2016). However, as water content increases, cohesion decreases, reducing the jamming effect and shifting the resistance dynamics to depend more on the cone geometry. This behaviour aligns with the theoretical predictions of Yu (2000) and Salgado (2008), who highlighted the importance of soil failure mechanisms in cavity expansion processes.

In addition to evaluating soil mechanical properties and root tip geometry, Chapter 3 also investigated the effect of mucilage on penetration resistance. I employed a droplet application method, which is more realistic and better simulates field conditions compared to the conventional mixing method used in previous studies. By allowing mucilage to infiltrate naturally into the soil, I observed that chia seed mucilage at concentrations of 0.1%, 0.3%, and 0.5% significantly reduced penetration resistance and associated energy requirements. This reduction was particularly pronounced for the energy required for cone insertion, which

is highly relevant for root growth. The penetration resistance curves clearly demonstrated that mucilage addition lowered resistance, especially at low water contents, where soil cohesion is typically higher. This finding aligns with the work of Colombi et al. (2017), who reported that mucilage reduces soil strength by acting as a lubricant and altering soil particle interactions. However, my study advances this understanding by showing that even low concentrations of mucilage (0.1%) can significantly reduce penetration resistance, highlighting the efficiency of root exudates in facilitating root elongation.

Building on the fundamentals established in Chapter 3, Chapter 4 investigates how soil texture, mucilage type, and concentration affect penetration resistance. Using a droplet application method that better simulates natural root exudation, I found that mucilage consistently reduced penetration resistance in both loam and loamy sand—regardless of concentration or type. These finding challenges earlier assumptions from studies that introduced mucilage via bulk mixing with soil (by mass ratio), which suggested higher concentrations increase mechanical impedance. Thus, the method of application critically determines mucilage's effects on soil resistance. The texture-specific response was particularly revealing in loam, which inherently exhibits higher penetration resistance due to the higher clay content and more cohesive nature (Bengough and Mullins, 1990). In loam, the addition of mucilage resulted in the most pronounced reduction in penetration resistance, especially at low water contents where particle bonding dominates. This aligns with the findings of Naveed et al. (2017), who emphasized the ability of mucilage to disrupt clay-particle interactions. In contrast, loamy sand showed smaller albeit still significant reductions in penetration resistance. Here, it was also found that flax seed mucilage proved more effective than chia seed mucilage in reducing penetration resistance, a novel finding that was not previously reported.

These results refined the broader understanding of how mucilage affects penetration resistance. While prior mixing-based studies suggested mucilage could increase soil strength at high concentrations, my approach that is more representative of actual root-soil interactions showed that mucilage consistently acts as a bio-lubricant, easing root penetration across soil types. The texture-dependent responses suggest that in loam, mucilage primarily disrupts cohesive bonds, while in loamy sand, it modifies interparticle friction. This distinction has important implications for managing soil compaction and facilitating root growth in different soil types. By bridging the gap between laboratory mixing methods and real-world root

exudate dynamics, this research advances our understanding of how mucilage modifies soil mechanical behaviour.

The results in Chapter 3 and 4 raised concerns about the impact of different mucilage application methods on the reported penetration resistances. While prior studies have predominantly relied on mixing methods (Oleghe et al., 2019; Naveed et al., 2013) or droplet application, I recognized the need to develop more biologically realistic application approaches that better simulate natural root exudation patterns. This methodological advancement is crucial for understanding true rhizosphere dynamics, as conventional approaches may not adequately capture the spatial complexity of root-soil interactions. Therefore, Chapter 5 directly addresses this critical gap. It builds upon the insights gained using the droplet method (which better simulates localized secretion) by introducing and evaluating an even more realistic injection method that continuously releases mucilage along the penetration path. This chapter systematically compares these three distinct application techniques – the conventional mixing method, the droplet method, and the novel injection method – to determine how mucilage spatial distribution fundamentally affects penetration resistance and critically assesses whether findings based solely on the mixing method capture the true role of mucilage in root-soil interactions. Comparative analysis of these application methods revealed fundamentally different penetration resistance behaviours across application methods. The conventional mixing approach produced penetration resistance curves that increased linearly with insertion depth - a pattern characteristic of bulk-amended soils where mucilage is distributed uniformly. The droplet method, while representing an improvement in spatial specificity, still showed gradual resistance increases with depth. Most remarkably, the injection method – designed to precisely mimic continuous mucilage exudation at the root tip – produced nearly flat resistance curves after cone insertion, maintaining consistently low resistance throughout the penetration depth. This striking difference signifies a strong reduction in frictional forces along the soil-metal interface. Crucially, these results demonstrate that the spatial organization of mucilage deposition plays a determining role in the soil's mechanical response, with localized, continuous exudation providing higher lubrication compared to bulk mixing or discrete droplet application.

These findings challenge several established assumptions in rhizosphere mechanics research. First, they reveal that the linear resistance profiles commonly reported in mixed systems may represent methodological artifacts rather than true root-experienced conditions. The sustained low resistance observed in the injection treatments provides experimental support for

theoretical models proposed by (Barré and Hallett, 2009), suggesting that roots may employ tip-focused exudation as an active penetration strategy. This depth-dependent effect implies that roots do not simply encounter uniform resistance but rather may manipulate their immediate soil environment to facilitate growth - a concept with important implications for understanding root biomechanics (Bengough, 2012; Carminati et al., 2017).

The implications of these findings are both methodological and conceptual. On a practical level, these results caution against overinterpreting mixing method-based studies for real root growth scenarios, as they may systematically overestimate mechanical impedance. More fundamentally, the injection method suggests an evolutionary advantage to root tip-focused exudation strategies, providing new insights into how roots navigate soil environments. Methodologically, this work advances the field by introducing a novel application technique that better captures rhizosphere physics, while providing the first quantitative comparison of method-dependent penetration resistance profiles.

These insights establish a new foundation for studying root penetration mechanics and suggest promising directions for bio-inspired soil management strategies. Ultimately, these findings underscore that both the biological reality of exudation patterns and the physical consequences of their spatial distribution must be considered to truly understand and potentially enhance root penetration in soil with higher mechanical impedance. This represents a significant step toward more ecologically relevant studies of root-soil interactions.

6.2 Outlook

While my study has advanced the understanding of mucilage and soil mechanical properties mediated root-soil interactions, several important challenges and research avenues remain that could further bridge the gap between laboratory measurements and real root growth dynamics. The limitations of current penetrometer approaches present a key area for improvement. Although the use of needle-sized penetrometers represents an advancement over conventional large probes, there remain fundamental differences between penetrometer measurements and actual root growth. Roots are flexible biological structures that actively navigate paths of least resistance, while laboratory tests typically assume homogenous soil strength conditions.

My application of cavity expansion theory for validation, while providing valuable insights, is most appropriate for purely cohesive soils where plastic flow dominates deformation. However, this theory struggles to fully capture the behaviour of frictional soils (e.g., sand,

loam, and etc), where penetration resistance arises significantly from dilatancy, particle interlocking, and shear-induced volume changes. In such soils, root growth may involve localized fracture and crack propagation rather than uniform cavity expansion—a process better described by fracture mechanics principles. Yet, both approaches face limitations: cavity expansion theory inadequately models the mixed cohesive-frictional behaviour typical of agricultural soils, while classical fracture mechanics often overlooks the pressure-dependent shear strength and compressibility of granular materials.

To address this gap for cohesive-frictional soils, future work should develop integrated constitutive frameworks that unify critical state soil mechanics with elastic-plastic fracture mechanics (EPFM) and advanced cavity expansion theory. This approach would leverage modified cavity expansion theory – incorporating friction, dilation, and critical state principles – to model the plastic deformation zone around root tips in cohesive phases, while employing EPFM to govern crack propagation through frictional domains where particle bonds fracture. The integration hinges on transition criteria (e.g., clay-to-sand ratio, confining pressure) that determine whether deformation follows plastic flow (cohesive-dominant soils), brittle fracture (friction-dominant soils), or a coupled hybrid response. For mixed soils, EPFM would define crack advancement using pressure-dependent yield surfaces (e.g., Drucker-Prager failure criteria) and dilatancy rules within the fracture process zone, while cavity expansion quantifies the surrounding plastic envelope's resistance. Discrete Element Methods (DEM) can validate this framework by explicitly simulating bond breakage (cohesion) and grain rearrangement (friction) during root penetration, with parameterization requiring concurrent measurement of fracture toughness and critical state parameters across soil textures. This dual-mechanism model captures the competition between plastic flow and brittle fracture, significantly improving root penetration resistance predictions across the soil textural spectrum.

The methodological and analytical refinements needed in this field are substantial. The results clearly demonstrate how experimental design and analysis strategies critically influence penetration resistance measurements, yet systematic validation is still required to determine how accurately laboratory conditions replicate true rhizosphere dynamics. Root growth in nature involves continuous exudation, dynamic soil restructuring, and complex microbial interactions - factors that are rarely incorporated in current mechanical testing protocols. Future investigations should particularly focus on time-dependent rheological effects, as the viscoelastic properties of mucilage suggest that penetration resistance may vary significantly

with loading rate, while most existing studies (including my own) have relied on quasi-static measurements.

Bridging the gap between mechanical measurements and real root growth behaviour will require innovative approaches. To better mimic biological reality, future experiments should incorporate penetrometers that can replicate root buckling. Advanced imaging techniques such as x-ray computed tomography or synchrotron-based imaging could provide crucial insights into mucilage distribution and its real-time interaction with soil particles during actual root growth. Furthermore, since mucilage degradation by soil microbes significantly alters its mechanical properties, there is a pressing need for studies that combine biomechanical approaches with microbial ecology.

Developing predictive models of root penetration represents another critical frontier. Current modelling approaches often oversimplify the complex interactions between roots, soil, and mucilage. Future modelling efforts should incorporate multi-phase mechanics to better represent the interactions between solid soil particles, liquid mucilage, and water in unsaturated soil conditions. There is also great potential in integrating root growth algorithms with advanced soil failure criteria to simulate how roots navigate heterogeneous soil environments.

Several key unanswered questions also emerged from this work. The temporal dynamics of mucilage properties remain poorly understood - how does mucilage aging through processes like degradation or repeated drying-rewetting cycles alter its mechanical influence over time? At the biological level, do root cap cells possess the ability to actively sense local soil strength and modify their exudation patterns accordingly? From a technological perspective, can it be possible to develop field-deployable sensors capable of measuring rhizosphere mechanical properties in real time under natural growing conditions?

Could following approaches answer the questions mentioned above? : First, I recommend to simulate degradation by treating mucilage with root-relevant enzymes (e.g., pectinase) and soil microbes under repeated drying-rewetting cycles. Synchronized rheometry and microfluidic adhesion tests will quantify mechanical changes, with biological validation comparing root growth in soils amended with fresh versus aged mucilage using needle-sized penetrometers. Second, for root cap sensing mechanisms, I recommend cultivating Arabidopsis mutants (e.g., msl10 knockouts) in transparent microfluidic devices with controlled soil strength gradients. Live calcium imaging will detect mechanosensitive

responses, while micro-capillary sampling of root exudates followed by metabolomics will identify strength-dependent mucilage components. Third, to enable field-deployable sensing, I propose to implement two technologies: 1) wireless hydrogel-based sensors embedded in rhizotrons to monitor soil rigidity changes, and 2) commercial micro-penetrometers (200 μm tips) mapping localized soil resistance. Both systems will be validated against x-ray computed tomography root imaging across soil textures to correlate mechanical data with actual root growth patterns. This work directly links mucilage mechanics, root responses, and field monitoring to predict root-soil interactions.

While my work has demonstrated the critical role of mucilage application methods in determining penetration resistance, the next phase of research should focus on integrating biomechanics, advanced imaging, and microbiology to fully unravel the complexity of root-soil interactions. Addressing these challenges will not only advance our fundamental understanding of plant-soil relationships but could also inform practical strategies to enhance crop resilience in compacted soils. Future studies should prioritize the development of more biologically realistic experimental systems while leveraging cutting-edge imaging and modelling approaches to bridge the persistent gap between controlled laboratory studies and actual root growth in field conditions.

REFERENCES

Abbaspour-Gilandeh, Y., Hasankhani-Ghavam, F., Shahgoli, G., Shrabian, V. R., & Abbaspour-Gilandeh, M. (2018). Investigation of the effect of soil moisture content, contact surface material and soil sexture on soil friction and soil adhesion coefficients. Acta Technologica Agriculturae, 21(2), 44–50. https://doi.org/10.2478/ata-2018-0009

Abdalla, A. M., Hettiaratchi, D. R. P., & Reece, A. R. (1969). The mechanics of root growth in granular media. Journal of Agricultural Engineering Research, 14(3), 236–248. https://doi.org/10.1016/0021-8634(69)90126-7

Ahmed, M. A., Kroener, E., Holz, M., Zarebanadkouki, M., & Carminati, A. (2014). Mucilage exudation facilitates root water uptake in dry soils. Functional Plant Biology, 41(11), 1129. https://doi.org/10.1071/FP13330

Anderson, V., Clinton, J., Gibson, D., & Kirsten, O. (1972). Instrumenting RUM for in situ subsea soil surveys. ASTM International. https://doi.org/10.1016/0022-4898(73)90139-0

Barré, P., & Hallett, P. D. (2009). Rheological stabilization of wet soils by model root and fungal exudates depends on clay mineralogy. European Journal of Soil Science, 60(4), 525–538. https://doi.org/10.1111/j.1365-2389.2009.01151.x

Benard, P., Zarebanadkouki, M., Hedwig, C., Holz, M., Ahmed, M. A., & Carminati, A. (2018). Pore-scale distribution of mucilage affecting water repellency in the rhizosphere. Vadose Zone Journal, 17(1), 1–9. https://doi.org/10.2136/vzj2017.01.0013

Bengough, A. G. (1997). Modelling rooting depth and soil strength in a drying soil profile. Journal of Theoretical Biology, 186(3), 327–338. https://doi.org/10.1006/jtbi.1996.0367

Bengough, A. G., Bransby, M. F., Hans, J., McKenna, S. J., Roberts, T. J., & Valentine, T. A. (2005). Root responses to soil physical conditions; growth dynamics from field to cell. Journal of Experimental Botany, 57(2), 437–447. https://doi.org/10.1093/jxb/erj003

Bengough, A. G., Campbell, D. J., & O'Sullivan, M. F. (2000). Penetrometer techniques in relation to soil compaction and root growth. In Soil and environmental analysis (pp. 389–416). CRC Press. https://doi.org/10.1201/9780203908600

Bengough, A. G., Loades, K., & McKenzie, B. M. (2016a). Root hairs aid soil penetration by anchoring the root surface to pore walls. Journal of Experimental Botany, 67(4), 1071–1078. https://doi.org/10.1093/jxb/erv560

Bengough, A. G., Loades, K., & McKenzie, B. M. (2016b). Root hairs aid soil penetration by anchoring the root surface to pore walls. Journal of Experimental Botany, 67(4), 1071–1078. https://doi.org/10.1093/jxb/erv560

Bengough, A. G., McKenzie, B. M., Hallett, P. D., & Valentine, T. A. (2011). Root elongation, water stress, and mechanical impedance: A review of limiting stresses and beneficial root tip traits. Journal of Experimental Botany, 62(1), 59–68. https://doi.org/10.1093/jxb/erq350

Bengough, A. G., & Mullins, C. E. (1990). Mechanical impedance to root growth: A review of experimental techniques and root growth responses. Journal of Soil Science, 41(3), 341–358. https://doi.org/10.1111/j.1365-2389.1990.tb00070.x

Bigoni, D., & Laudiero, F. (1989). The quasi-static finite cavity expansion in a non-standard elasto-plastic medium. International Journal of Mechanical Sciences, 31(11–12), 825–837. https://doi.org/10.1016/0020-7403(89)90027-1

Bishop, R. F., Hill, R., & Mott, N. F. (1945). The theory of indentation and hardness tests. Proceedings of the Physical Society, 57(3), 147–159. https://doi.org/10.1088/0959-5309/57/3/301

Bravo, E. L., Tijskens, E., Suárez, M. H., Gonzalez Cueto, O., & Ramon, H. (2014). Prediction model for non-inversion soil tillage implemented on discrete element method. Computers and Electronics in Agriculture, 106, 120–127. https://doi.org/10.1016/j.compag.2014.05.007

Brown, L. K., George, T. S., Neugebauer, K., & White, P. J. (2017). The rhizosheath – a potential trait for future agricultural sustainability occurs in orders throughout the angiosperms. Plant and Soil, 418(1–2), 115–128. https://doi.org/10.1007/s11104-017-3220-2

Carminati, A., & Javaux, M. (2020). Soil rather than xylem vulnerability controls stomatal response to drought. Trends in Plant Science, 25(9), 868–880. https://doi.org/10.1016/j.tplants.2020.04.003

Carminati, A., Moradi, A. B., Vetterlein, D., Vontobel, P., Lehmann, E., Weller, U., Vogel, H.-J., & Oswald, S. E. (2010). Dynamics of soil water content in the rhizosphere. Plant and Soil, 332(1–2), 163–176. https://doi.org/10.1007/s11104-010-0283-8

Carminati, A., & Vetterlein, D. (2013). Plasticity of rhizosphere hydraulic properties as a key for efficient utilization of scarce resources. Annals of Botany, 112(2), 277–290. https://doi.org/10.1093/aob/mcs262

Carminati, A., Zarebanadkouki, M., Kroener, E., Ahmed, M. A., & Holz, M. (2016a). Biophysical rhizosphere processes affecting root water uptake. Annals of Botany, 118(4), 561–571. https://doi.org/10.1093/aob/mcw113

Carminati, A., Zarebanadkouki, M., Kroener, E., Ahmed, M. A., & Holz, M. (2016b). Biophysical rhizosphere processes affecting root water uptake. Annals of Botany, 118(4), 561–571. https://doi.org/10.1093/aob/mcw113

Carter, J. P., Booker, J. R., & Yeung, S. K. (1986). Cavity expansion in cohesive frictional soils. https://doi.org/10.1680/geot.1986.36.3.349

Carter, J. P., & Yeung, S. K. (1985). Analysis of cylindrical cavity expansion in a strain weakening material. Computers and Geotechnics, 1(3), 161–180. https://doi.org/10.1016/0266-352X(85)90021-7

Carvalhais, L. C., Dennis, P. G., Fedoseyenko, D., Hajirezaei, M., Borriss, R., & Von Wirén, N. (2011). Root exudation of sugars, amino acids, and organic acids by maize as affected by nitrogen, phosphorus, potassium, and iron deficiency. Journal of Plant Nutrition and Soil Science, 174(1), 3–11. https://doi.org/10.1002/jpln.201000085

Chadwick, P. (1959). The quasi-static expansion of a spherical cavity in metals and ideal soils. The Quarterly Journal of Mechanics and Applied Mathematics, 12(1), 52–71. https://doi.org/10.1093/qjmam/12.1.52

Chen, Z. C., & Liao, H. (2016). Organic acid anions: An effective defensive weapon for plants against aluminum toxicity and phosphorus deficiency in acidic soils. Journal of Genetics and Genomics, 43(11), 631–638. https://doi.org/10.1016/j.jgg.2016.11.003

Clark, L. J., Whalley, W. R., & Barraclough, P. B. (2002). How do roots penetrate strong soil? https://ui.adsabs.harvard.edu/link_gateway/2003PlSoi.255...93C/doi:10.1023/A:1026140122848

Cokca, E., Erol, O., & Armangil, F. (2004). Effects of compaction moisture content on the shear strength of an unsaturated clay. Geotechnical and Geological Engineering, 22(2), 285–297. https://doi.org/10.1023/B:GEGE.0000018349.40866.3e

Colombi, T., Braun, S., Keller, T., & Walter, A. (2017). Artificial macropores attract crop roots and enhance plant productivity on compacted soils. Science of The Total Environment, 574, 1283–1293. https://doi.org/10.1016/j.scitotenv.2016.07.194

Colombi, T., Chakrawal, A., & Herrmann, A. M. (2022). Carbon supply–consumption balance in plant roots: Effects of carbon use efficiency and root anatomical plasticity. New Phytologist, 233(4), 1542–1547. https://doi.org/10.1111/nph.17598

Colombi, T., Torres, L. C., Walter, A., & Keller, T. (2018). Feedbacks between soil penetration resistance, root architecture and water uptake limit water accessibility and crop growth – A vicious circle. Science of The Total Environment, 626, 1026–1035. https://doi.org/10.1016/j.scitotenv.2018.01.129

Correa, J., Postma, J. A., Watt, M., & Wojciechowski, T. (2019). Soil compaction and the architectural plasticity of root systems. Journal of Experimental Botany, 70(21), 6019–6034. https://doi.org/10.1093/jxb/erz383

Coyago-Cruz, E., Salazar, I., Guachamin, A., Alomoto, M., Cerna, M., Mendez, G., Heredia-Moya, J., & Vera, E. (2025). Bioactive compounds, antioxidant, and antimicrobial activity of seeds and mucilage of non-Traditional cocoas. Antioxidants, 14(3), 299. https://doi.org/10.3390/antiox14030299

Dakora, F. D., & Sinclair, T. R. (2002). Genetic approaches for manipulating crop plants to enhance root exudation and access low nutrients in the rhizosphere. In J. J. Adu-Gyamfi (Ed.), Food Security in Nutrient-Stressed Environments: Exploiting Plants Genetic Capabilities (pp. 261–265). Springer Netherlands. https://doi.org/10.1007/978-94-017-1570-6_28

Delory, B. M., Weidlich, E. W., van Duijnen, R., Pagès, L., & Temperton, V. M. (2018). Measuring plant root traits under controlled and field conditions: Step-by-step procedures. Root Development: Methods and Protocols, 3–22. https://doi.org/10.1007/978-1-4939-7747-5_1

Dennis, P. G., Miller, A. J., & Hirsch, P. R. (2010). Are root exudates more important than other sources of rhizodeposits in structuring rhizosphere bacterial communities?: Root

exudates and rhizosphere bacteria. FEMS Microbiology Ecology, 72(3), 313–327. https://doi.org/10.1111/j.1574-6941.2010.00860.x

Dexter, A. R. (1987). Mechanics of root growth. Plant and Soil, 98(3), 303–312. https://doi.org/10.1007/BF02378351

Ding, W., Liu, X., Hu, F., Zhu, H., Luo, Y., Li, S., & Li, H. (2019). How the particle interaction forces determine soil water infiltration: Specific ion effects. Journal of Hydrology, 568, 492–500. https://doi.org/10.1016/j.jhydrol.2018.11.017

Fan, C C, & Su, C.-F. (2009). Effect of soil moisture content on the deformation behaviour of root-reinforced soils subjected to shear. Plant and Soil, 324(1), 57–69. http://dx.doi.org/10.1007/s11104-008-9856-1

Garcia E Silva, L. L., Alves Bastos, R., Souza Lima, G. V., De Souza Soares, L., Selia Dos Reis Coimbra, J., Arêdes Martins, M., & De Castro Santana, R. (2022). Stabilizing properties of chia seed mucilage on dispersions and emulsions at different pHs. Food Biophysics, 17(4), 568–574. https://doi.org/10.1007/s11483-022-09742-x

Ghezelbash, E., Mohammadi, M. H., & Shorafa, M. (2025). Investigating soil–root interactions and mucilage secretion under varying soil mechanical resistance in maize cultivars. Plant and Soil. https://doi.org/10.1007/s11104-025-07263-3

Greacen, E., Farrell, D., & Cock-roft, B. (1968). Soil resistance to metal probes and plant roots. https://eurekamag.com/research/014/669/014669002.php

Greacen, E., & Sands, R. (1980). Compaction of forest soils. A review. Soil Research, 18(2), 163. https://doi.org/10.1071/SR9800163

Gregory, P. J. (2006). Roots, rhizosphere and soil: The route to a better understanding of soil science? European Journal of Soil Science, 57(1), 2–12. https://doi.org/10.1111/j.1365-2389.2005.00778.x

Gurtug, Y., & Sridharan, A. (2004). Compaction behaviour and prediction of its characteristics of fine grained soils with particular reference to compaction energy. Soils and Foundations, 44(5), 27–36. https://doi.org/10.3208/sandf.44.5_27

Hallett, P. D., Marin, M., Bending, G. D., George, T. S., Collins, C. D., & Otten, W. (2022). Building soil sustainability from root–soil interface traits. Trends in Plant Science, 27(7), 688–698. https://doi.org/10.1016/j.tplants.2022.01.010

Hamza, M. A., & Anderson, W. K. (2005). Soil compaction in cropping systems. Soil and Tillage Research, 82(2), 121–145. https://doi.org/10.1016/j.still.2004.08.009

Herrick, J. E., & Jones, T. L. (2002). A dynamic cone penetrometer for measuring soil penetration resistance. Soil Science Society of America Journal, 66(4), 1320. https://doi.org/10.2136/sssaj2002.1320

Hill, R. (1950). C. A theory of the plastic bulging of a metal diaphragm by lateral pressure. The London, Edinburgh, and Dublin Philosophical Magazine and Journal of Science, 41(322), 1133–1142. http://dx.doi.org/10.1093/oso/9780198503675.001.0001

Holz, M., Zarebanadkouki, M., Kuzyakov, Y., Pausch, J., & Carminati, A. (2018). Root hairs increase rhizosphere extension and carbon input to soil. Annals of Botany, 121(1), 61–69. https://doi.org/10.1093/aob/mcx127

Houlsby, G. T., Clarke, B. G., & Wroth, C. P. (1986). Analysis of the unloading of a pressuremeter in sand. 245–262. http://dx.doi.org/10.1520/STP19290S

Houlsby, G. T., & Withers, N. J. (1988). Analysis of the cone pressuremeter test in clay. Geotechnique, 38(4), 575–587. https://doi.org/10.1680/geot.1988.38.4.575

Houlsby, G. T., & Wroth, C. P. (1984). Calculation of stresses on shallow penetrometers and footings. In B. Denness (Ed.), Seabed Mechanics (pp. 107–112). Springer Netherlands. https://doi.org/10.1007/978-94-009-4958-4_12

Jones, D. L., Nguyen, C., & Finlay, R. D. (2009). Carbon flow in the rhizosphere: Carbon trading at the soil–root interface. Plant and Soil, 321(1–2), 5–33. https://doi.org/10.1007/s11104-009-9925-0

Kirby, J. M., & Bengough, A. G. (2002). Influence of soil strength on root growth: Experiments and analysis using a critical-state model. European Journal of Soil Science, 53(1), 119–127. https://doi.org/10.1046/j.1365-2389.2002.00429.x

Koebernick, N., Daly, K. R., Keyes, S. D., Bengough, A. G., Brown, L. K., Cooper, L. J., George, T. S., Hallett, P. D., Naveed, M., & Raffan, A. (2019). Imaging microstructure of the barley rhizosphere: Particle packing and root hair influences. New Phytologist, 221(4), 1878–1889. https://doi.org/10.1111/nph.15516

Koebernick, N., Daly, K. R., Keyes, S. D., George, T. S., Brown, L. K., Raffan, A., Cooper, L. J., Naveed, M., Bengough, A. G., Sinclair, I., & others. (2017). High-resolution synchrotron imaging shows that root hairs influence rhizosphere soil structure formation. New Phytologist, 216(1), 124–135. https://doi.org/10.1111/nph.14705

Koebernick, N., Weller, U., Huber, K., Schlüter, S., Vogel, H.-J., Jahn, R., Vereecken, H., & Vetterlein, D. (2014). In situ visualization and quantification of three-dimensional root

system architecture and growth using X-Ray computed tomography. Vadose Zone Journal, 13(8), 0. https://doi.org/10.2136/vzj2014.03.0024

Kolb, E., Legué, V., & Bogeat-Triboulot, M.-B. (2017). Physical root–soil interactions. Physical Biology, 14(6), 065004. https://doi.org/10.1088/1478-3975/aa90dd

Kolb, E., Quiros, M., Meijer, G. J., Bogeat-Triboulot, M.-B., Carminati, A., Andò, E., Sibille, L., & Anselmucci, F. (2022). Root–soil interaction. https://doi.org/10.1039/9781839161162-00165

Kroener, E., Holz, M., Zarebanadkouki, M., Ahmed, M., & Carminati, A. (2018). Effects of mucilage on rhizosphere hydraulic functions depend on soil particle size. Vadose Zone Journal, 17(1), 0. https://doi.org/10.2136/vzj2017.03.0056

Le Bissonnais, Y. (1996). Aggregate stability and assessment of soil crustability and erodibility: Theory and methodology. European Journal of Soil Science, 47(4), 425–437. https://doi.org/10.1111/j.1365-2389.1996.tb01843.x

Lee, M.-H., Comas, L. H., & Callahan, H. S. (2013). Experimentally reduced root–microbe interactions reveal limited plasticity in functional root traits in Acer and Quercus. Annals of Botany, 113(3), 513–521. https://doi.org/10.1093/aob/mct276

Lehmann, J., Hansel, C. M., Kaiser, C., Kleber, M., Maher, K., Manzoni, S., Nunan, N., Reichstein, M., Schimel, J. P., Torn, M. S., Wieder, W. R., & Kögel-Knabner, I. (2020). Persistence of soil organic carbon caused by functional complexity. Nature Geoscience, 13(8), 529–534. https://doi.org/10.1038/s41561-020-0612-3

Lu, N., Godt, J. W., & Wu, D. T. (2010). A closed-form equation for effective stress in unsaturated soil. Water Resources Research, 46(5), 2009WR008646. https://doi.org/10.1029/2009WR008646

Lucas, M., Santiago, J. P., Chen, J., Guber, A., & Kravchenko, A. (2023). The soil pore structure encountered by roots affects plant-derived carbon inputs and fate. New Phytologist, 240(2), 515–528. https://doi.org/10.1111/nph.19159

Lucas, M., Schlüter, S., Vogel, H.-J., & Vetterlein, D. (2019). Soil structure formation along an agricultural chronosequence. Geoderma, 350, 61–72. https://doi.org/10.1016/j.geoderma.2019.04.041

Lynch, J. P. (2013). Steep, cheap and deep: An ideotype to optimize water and N acquisition by maize root systems. Annals of Botany, 112(2), 347–357. https://doi.org/10.1093/aob/mcs293

Mckenzie, B. M., Mullins, C. E., Tisdall, J. M., & Bengough, A. G. (2013). Root–soil friction: Quantification provides evidence for measurable benefits for manipulation of root-tip traits. Plant, Cell & Environment, 36(6), 1085–1092. https://doi.org/10.1111/pce.12037

Mirreh, H. F., & Ketcheson, J. W. (1973). Influence of soil water matric potential and resistance to penetration on corn root elongation. Canadian Journal of Soil Science, 53(4), 383–388. https://doi.org/10.4141/cjss73-055

Mooney, H. A., & Drake, J. A. (2012). Ecology of biological invasions of North America and Hawaii (Vol. 58). Springer Science & Business Media.

Morel, J. L., Habib, L., Plantureux, S., & Guckert, A. (1991). Influence of maize root mucilage on soil aggregate stability. Plant and Soil, 136(1), 111–119. https://doi.org/10.1007/BF02465226

Mouazen, A. M. et al. (2002). Effects of bulk density and moisture content on selected mechanical properties of sandy loam soil. https://doi.org/10.1006/bioe.2002.0103

Naveed, M., Brown, L. K., Raffan, A. C., George, T. S., Bengough, A. G., Roose, T., Sinclair, I., Koebernick, N., Cooper, L., Hackett, C. A., & Hallett, P. D. (2017). Plant exudates may stabilize or weaken soil depending on species, origin and time: Effect of plant exudates on rhizosphere formation. European Journal of Soil Science, 68(6), 806–816. https://doi.org/10.1111/ejss.12487

Naveed, M., Brown, L. K., Raffan, A. C., George, T. S., Bengough, A. G., Roose, T., Sinclair, I., Koebernick, N., Cooper, L., & Hallett, P. D. (2018a). Rhizosphere-scale quantification of hydraulic and mechanical properties of soil impacted by root and seed exudates. Vadose Zone Journal, 17(1), 0. https://doi.org/10.2136/vzj2017.04.0083

Naveed, M., Brown, L. K., Raffan, A. C., George, T. S., Bengough, A. G., Roose, T., Sinclair, I., Koebernick, N., Cooper, L., & Hallett, P. D. (2018b). Rhizosphere-scale quantification of hydraulic and mechanical properties of soil impacted by root and seed exudates. Vadose Zone Journal, 17(1), 0. https://doi.org/10.2136/vzj2017.04.0083

Nazari, M., Bickel, S., Benard, P., Mason-Jones, K., Carminati, A., & Dippold, M. A. (2022). Biogels in soils: plant mucilage as a biofilm matrix that shapes the rhizosphere microbial habitat. Frontiers in Plant Science, 12, 798992. https://doi.org/10.3389/fpls.2021.798992

Obrzud, R. F., & Truty, A. (2010). The hardening soil model - A practical guidebook.

Oburger, E., Dell‘mour, M., Hann, S., Wieshammer, G., Puschenreiter, M., & Wenzel, W. W. (2013). Evaluation of a novel tool for sampling root exudates from soil-grown plants

compared to conventional techniques. Environmental and Experimental Botany, 87, 235–247. https://doi.org/10.1016/j.envexpbot.2012.11.007

Oleghe, E., Naveed, M., Baggs, E. M., & Hallett, P. D. (2017a). Plant exudates improve the mechanical conditions for root penetration through compacted soils. Plant and Soil, 421(1–2), 19–30. https://doi.org/10.1007/s11104-017-3424-5

Oleghe, E., Naveed, M., Baggs, E. M., & Hallett, P. D. (2017b). Plant exudates improve the mechanical conditions for root penetration through compacted soils. Plant and Soil, 421(1–2), 19–30. https://doi.org/10.1007/s11104-017-3424-5

Oleghe, E., Naveed, M., Baggs, E. M., & Hallett, P. D. (2019). Residues with varying decomposability interact differently with seed or root exudate compounds to affect the biophysical behaviour of soil. Geoderma, 343, 50–59. https://doi.org/10.1016/j.geoderma.2019.02.023

Or, D., & Ghezzehei, T. A. (2002). Modeling post-tillage soil structural dynamics: A review. Soil and Tillage Research, 64(1–2), 41–59. https://doi.org/10.1016/S0167-1987(01)00256-2

Oswald, S. E., Menon, M., Carminati, A., Vontobel, P., Lehmann, E., & Schulin, R. (2008). Quantitative imaging of infiltration, root growth, and root water uptake via neutron radiography. Vadose Zone Journal, 7(3), 1035. https://doi.org/10.2136/vzj2007.0156

Palmer, A. (1972). Undrained plane-strain expansion of a cylindrical cavity in clay: A simple interpretation of the pressuremeter test. Geotechnique, 22(3), 451–457. https://doi.org/10.1680/geot.1972.22.3.451

Paniagua, D. P., Fonseca, D. J., Gylland, D. A. S., & Nordal, S. (n.d.). Microstructural study of the deformation zones during cone penetration in silt at variable penetration rates. http://dx.doi.org/10.1139/cgj-2014-0498

Peng, H., Li, S., Shangguan, L., Zhang, H., & Zhao, D. (2023). Research on the rheological characteristics of wind power grease based on rheological parameters. Lubricants, 11(7), 299. https://doi.org/10.3390/lubricants11070299

Philippot, L., Raaijmakers, J. M., Lemanceau, P., & Van Der Putten, W. H. (2013). Going back to the roots: The microbial ecology of the rhizosphere. Nature Reviews Microbiology, 11(11), 789–799. https://doi.org/10.1038/nrmicro3109

Plant–Soil Modelling. (2021). In S. Ruiz, D. M. Fletcher, K. Williams, & T. Roose, Annual Plant Reviews online (1st ed., pp. 127–198). Wiley. https://doi.org/10.1002/9781119312994.apr0755

Prosser, J. I., & Martiny, J. B. H. (2020). Conceptual challenges in microbial community ecology. Philosophical Transactions of the Royal Society B: Biological Sciences, 375(1798), 20190241. https://doi.org/10.1098/rstb.2019.0241

Randolph, M. F., & Houlsby, G. T. (1986). Discussion: The limiting pressure on a circular pile loaded laterally in cohesive soil. Géotechnique, 36(3), 457–457. https://doi.org/10.1680/geot.1986.36.3.457

Rosskopf, U., Uteau, D., & Peth, S. (2022a). Development of mechanical soil stability in an initial homogeneous loam and sand planted with two maize (Zea mays L.) genotypes with contrasting root hair attributes under in-situ field conditions. Plant and Soil, 478(1–2), 143–162. https://doi.org/10.1007/s11104-022-05572-5

Rosskopf, U., Uteau, D., & Peth, S. (2022b). Effects of mucilage concentration at different water contents on mechanical stability and elasticity in a loamy and a sandy soil. European Journal of Soil Science, 73(1). https://doi.org/10.1111/ejss.13189

Rosskopf, U., Uteau, D., & Peth, S. (2022c). Effects of mucilage concentration at different water contents on mechanical stability and elasticity in a loamy and a sandy soil. European Journal of Soil Science, 73(1). https://doi.org/10.1111/ejss.13189

Rüger, L., Ganther, M., Freudenthal, J., Jansa, J., Heintz-Buschart, A., Tarkka, M. T., & Bonkowski, M. (2023). Root cap is an important determinant of rhizosphere microbiome assembly. New Phytologist, 239(4), 1434–1448. https://doi.org/10.1111/nph.19002

Ruiz, S., Or, D., & Schymanski, S. J. (2015). Soil penetration by earthworms and plant roots—mechanical energetics of bioturbation of compacted soils. PLOS ONE, 10(6), e0128914. https://doi.org/10.1371/journal.pone.0128914

Ruiz, S., Schymanski, S. J., & Or, D. (2017). Mechanics and energetics of soil penetration by earthworms and plant roots: higher rates cost more. Vadose Zone Journal, 16(8), 1–16. https://doi.org/10.2136/vzj2017.01.0021

Ruiz, S., Straub, I., Schymanski, S. J., & Or, D. (2016). Experimental evaluation of earthworm and plant root soil penetration–cavity expansion models using cone penetrometer analogs. Vadose Zone Journal, 15(3), 0. https://doi.org/10.2136/vzj2015.09.0126

Sagaseta, C. (1987). Analysis of undrained soil deformation due to ground loss. Géotechnique, 37(3), 301–320. https://doi.org/10.1680/geot.1987.37.3.301

Sher, Y., Baker, N. R., Herman, D., Fossum, C., Hale, L., Zhang, X., Nuccio, E., Saha, M., Zhou, J., Pett-Ridge, J., & Firestone, M. (2020). Corrigendum to "Microbial extracellular polysaccharide production and aggregate stability controlled by Switchgrass (Panicum virgatum) root biomass and soil water potential" [Soil Biology and Biochemistry 143 (2020) 107741]. Soil Biology and Biochemistry, 148, 107907. https://doi.org/10.1016/j.soilbio.2020.107907

Souza, R., Hartzell, S., Freire Ferraz, A. P., De Almeida, A. Q., De Sousa Lima, J. R., Dantas Antonino, A. C., & De Souza, E. S. (2021). Dynamics of soil penetration resistance in water-controlled environments. Soil and Tillage Research, 205, 104768. https://doi.org/10.1016/j.still.2020.104768

Traore, O., Groleau-Renaud, V., Plantureux, S., Tubeileh, A., & Boeuf-Tremblay, V. (2000). Effect of root mucilage and modelled root exudates on soil structure. European Journal of Soil Science, 51(4), 575–581. https://doi.org/10.1046/j.1365-2389.2000.00348.x

Vacheron, J., Desbrosses, G., Bouffaud, M.-L., Touraine, B., Moënne-Loccoz, Y., Muller, D., Legendre, L., Wisniewski-Dyé, F., & Prigent-Combaret, C. (2013). Plant growth-promoting rhizobacteria and root system functioning. Frontiers in Plant Science, 4. https://doi.org/10.3389/fpls.2013.00356

Valentine, T. A., Hallett, P. D., Binnie, K., Young, M. W., Squire, G. R., Hawes, C., & Bengough, A. G. (2012). Soil strength and macropore volume limit root elongation rates in many UK agricultural soils. Annals of Botany, 110(2), 259–270. https://doi.org/10.1093/aob/mcs118

Vesić, A. S. (1972). Expansion of cavities in infinite soil mass. Journal of the Soil Mechanics and Foundations Division, 98(3), 265–290. https://doi.org/10.1061/JSFEAQ.0001740

Wang, Z., Timlin, D., Li, S., Fleisher, D., Dathe, A., Luo, C., Dong, L., Reddy, V. R., & Tully, K. (2021). A diffusive model of maize root growth in maizsim and its applications in ridge-furrow rainfall harvesting. Agricultural Water Management, 254, 106966. https://doi.org/10.1016/j.agwat.2021.106966

Watt, M., McCully, M. E., & Canny, M. J. (1994). Formation and stabilization of rhizosheaths of zea mays. http://dx.doi.org/10.1104/pp.106.1.179

White, R. G., & Kirkegaard, J. A. (2010). The distribution and abundance of wheat roots in a dense, structured subsoil – implications for water uptake. Plant, Cell & Environment, 33(2), 133–148. https://doi.org/10.1111/j.1365-3040.2009.02059.x

Yu, H. S., & Houlsby, G. T. (1991). Finite cavity expansion in dilatant soils: Loading analysis. Géotechnique, 41(2), 173–183. https://doi.org/10.1680/geot.1991.41.2.173

Yu, H.-S. (2000). Cavity expansion methods in geomechanics. Springer Netherlands. https://doi.org/10.1007/978-94-015-9596-4

Zhang, X., Dippold, M. A., Kuzyakov, Y., & Razavi, B. S. (2019). Spatial pattern of enzyme activities depends on root exudate composition. Soil Biology and Biochemistry, 133, 83–93. https://doi.org/10.1016/j.soilbio.2019.02.010

Zhong, X., Li, J., Naveed, M., Raffan, A., & Hallett, P. D. (2021). A laboratory study to disentangle hydrological, mechanical and structural mechanisms of soil stabilization by plant mucilage between eroding and depositional zones of a slope. European Journal of Soil Science, 72(1), 125–140. https://doi.org/10.1111/ejss.12955

Zickenrott, I., Woche, S. K., Bachmann, J., Ahmed, M. A., & Vetterlein, D. (2016). An efficient method for the collection of root mucilage from different plant species—A case study on the effect of mucilage on soil water repellency. Journal of Plant Nutrition and Soil Science, 179(2), 294–302. https://doi.org/10.1002/jpln.201500511